Investigation of an Innovative Solar-Driven Solid Desiccant Evaporative Cooler for Hot and Humid Climates

Nima Khosravi

Submitted to the
Institute of Graduate Studies and Research
in partial fulfillment of the requirements for the degree of

Doctor of Philosophy
in
Mechanical Engineering

Eastern Mediterranean University
February 2021
Gazimağusa, North Cyprus

Approval of the Institute of Graduate Studies and Research

Prof. Dr. Ali Hakan Ulusoy
Director

I certify that this thesis satisfies the requirements as a thesis for the degree of Doctor of Philosophy in Mechanical Engineering.

Prof. Dr. Hasan Hacişevki
Chair, Department of Mechanical Engineering

We certify that we have read this thesis and that in our opinion it is fully adequate in Scope and quality as a thesis for the degree of Doctor of Philosophy in Mechanical Engineering.

Asst. Prof. Dr. Devrim Aydın
Supervisor

Examining Committee

1. Prof. Dr. Hasan Hacişevki
2. Prof. Dr. Arif Hepbaşlı
3. Prof. Dr. Zafer Utlu
4. Assoc. Prof. Dr. Hüseyin Çamur
5. Asst. Prof. Dr. Devrim Aydın

ABSTRACT

In the last decade, desiccant assisted evaporative cooling (DAEC) has emerged as an alternative air conditioning (A/C) method to conventional vapor compression (VC) systems due to its lower operating costs and environmental impacts. However, for enabling wider usage of DAEC systems, new low cost, natural and locally available desiccant materials and evaporative cooling pad materials (ECPMs) need to be sought. Moreover, development of novel DAEC processes and their integration with solar energy are essential.

In that regard, the primary objective of the study was to develop a fixed bed DAEC system integrated with solar energy, that uses novel composite sorbent to be utilized as a coolth storage in hot-humid climate. To achieve this objective, initially, different natural ECPMs in a fixed-bed solid DAEC system, containing a novel desiccant material (Vmc-$CaCl_2$), were experimented in laboratory environment. During the tests, consecutive cycles with different operating conditions were performed for comprehensive performance evaluation of each candidate material. Additionally, DAEC and evaporative cooling (EC) processes were comparatively investigated with the use of different ECPMs. Results showed that the DAEC provides between 17-62% higher cooling rates than EC.

In the second part of the study, a solar-driven DAEC system was developed and tested under real climatic conditions of North Cyprus (NC). Average thermal coefficient of performance (COP_{th}) and wet bulb effectiveness (ε_{wb}) of the system were found 0.60 and 121.6% with the use of Vmc-$CaCl_2$/WoC as the working materials.

Furthermore, a numerical analysis using Transient System Simulation software (TRNSYS) was performed to assess the cyclic performance of solar assisted DAEC system. Simulation results showed that, system using silica gel/WoC couple can provide average COP_{th} and ε_{wb} of 0.32 and 104.2%, respectively.

In addition, economic analysis and life cycle assessment (LCA) were performed to investigate the feasibility of the proposed solar-driven DAEC system in comparison with a typical A/C split unit under the climatic conditions of NC. According to the performed economic analysis, SIR = 3, IRR = 31% and SPP = 3 years were obtained. Moreover, based on the performed LCA, the developed system produces 0.23 kg/year CO_2, which shows that it is environmentally friendly and economically feasible for using in residential buildings in NC.

Keywords: desiccant assisted evaporative cooling, evaporation materials, solar energy, experimental analysis, cooling effectiveness

ÖZ

Son yıllarda, desikant destekli evaporatif soğutma (DESS) sistemleri, çalışma giderleri ve çevresel etkilerinin daha düşük olması sebebiyle, buhar sıkıştırmalı (BS) soğutma sistemlerine alternatif bir iklimlendirme metodu olarak gelişmektedir. Ancak, DESS sistemlerinin daha yaygın kullanımını sağlayabilmek için düşük maaliyetli, doğal ve kolay erişilebilir yeni desikant malzemelerin (DeM) ve evaporatif soğutma ped malzemelerinin (ESPM) araştırılması gerekmektedir. Bunun yanında, yenilikçi DESS proseslerinin geliştirilmesi ve güneş enerjili teknolojiler ile entegrasyonu önem arz etmektedir.

Bu bağlamda, çalışmanın birincil amacı, güneş enerjisi kaynaklı, yenilikçi kompozit sorbent kullanan, sabit yataklı, soğutma enerjisi depolamak için kullanılabilecek bir DESS sistemi geliştirmektir. Bu amaca ulaşmak için, ilk olarak, yenilikçi kompozit bir sorbentin (Vmc-$CaCl_2$) kullanıldığı sabit yataklı laboratuvar ölçekli DESS sisteminde farklı ESPM'nin testleri gerçekleştirilmiştir. Deneyler sırasında, malzemelerin detaylı analizini yapabilmek için farklı çalışma koşulları altında tekrar eden çevrimler uygulanmıştır. Ayrıca DESS sistemi performansı evaporatif soğutma (ES) sistemi ile karşılaştırmalı olarak incelenmiştir. Çalışma sonuçları DESS sisteminin direkt ES sistemine göre 17-62% daha yüksek soğutma kapasitesine sahip olduğunu göstermiştir.

Çalışmanın ikinci kısmında, güneş enerjili bir DESS sistemi, geliştirilmiş ve Kuzey Kıbrıs iklim koşulları altında test edilmiştir. Malzeme çifti olarak Vmc-$CaCl_2$/WoC

kullanılan çalışmada, ortalama ısıl performans katsayısı (COP_{th}) ve yaş termometre etkinliği (ε_{wb}) 0.60 ve 121.6% olarak bulunmuştur.

Ayrıca, güneş enerjili DESS sisteminin çevrimsel performansını değerlendirmek için Zamana Bağlı Simülasyon programı (TRNSYS) kullanılarak sayısal bir analiz gerçekleştirilmiştir. Sonuçlara göre, silika jel / WoC malzemeleri kullanılan sistemin COP_{th} ve ε_{wb} değerleri 0.32 ve 104.2% olarak elde edilmiştir.

Çalışmanın son bölümünde, önerilen güneş enerjili DESS sisteminin Kuzey Kıbrıs iklim koşulları altında kullanımının ekonomik fizibilitesi ve yaşam döngüsü değerlendirmesi tipik bir A/C split ünitesi ile karşılaştırmalı olarak incelenmiştir. Bu kapsamda, gerçekleştirilen ekonomik analizlere göre; SIR = 3, IRR =% 31 ve SPP = 3 yıl olarak bulunmuştur. Ayrıca gerçekleştirilen yaşam döngüsü değerlendirmesi, system yıllık CO_2 salınımının 0.23 kg olduğunu göstermiştir. Sonuçlar, bu çalışmada geliştirilen güneş enerjili DESS sisteminin Kuzey Kıbrıs'taki konutlarda kullanım için ekonomik ve çevresel olarak uygun olduğunu göstermektedir.

Anahtar Kelimeler: desikant destekli evaporatif soğutma, evaporatif malzemeler, güneş enerjisi, deneysel analiz, soğutma etkinliği

DEDICATION

To My Lovely Family

ACKNOWLEDGMENT

First of all, I would like to thank my supervisor Asst. Prof. Dr. Devrim Aydın for his consistent support and guidance during the running of this study. He continuously provided encouragement, and was always willing, and enthusiastic to assist in any way he could throughout this research project. I am also thankful to the department of mechanical engineering and its entire member's staff for all the considerate guidance during this long journey. To conclude, I cannot forget to thank my family and friends for all the unconditional support in this very intense academic period.

TABLE OF CONTENTS

LIST OF TABLES

LIST OF FIGURES

LIST OF SYMBOLS

a	Air
c	Cooling
c_p	Specific Heat (kJ/kg. K)
cr	Charging
d	Dew-Point
dc	Discharging
e	Electrical
H	Heating
h	Enthalpy (kJ/kg)
hyg	Hygro-Cyclic
i	Inlet
$\dot{m}$	Mass Flow Rate (kg/s)
o	Outlet
$\dot{Q}$	Heat Transfer Rate (kW)
reg	Regeneration
solar,ava	Available Solar
solar,g	Solar Gain
T	Temperature (°C)
t	Total
th	Thermal
trans,des	Transferred to Desiccant
useful,Hx	Useful Heat-Exchanger
w	Water

W	Experimental Uncertainty (%)
$\dot{W}$	Work (kW)
wb	Wet-bulb
z	Sensor Position
Δ	Difference (-)
ε	Effectiveness (%)
ω	Absolute Humidity (g/kg)

LIST OF ABBREVIATIONS

A/C	Air Conditioning
ACOP	Average Coefficient of Performance
$CaCl_2$	Calcium Chloride
COP	Coefficient of Performance
DAEC	Desiccant Assisted Evaporative Cooling
DEC	Direct Evaporative Cooling
DW	Desiccant Wheel
EC	Evaporative Cooling
ECPM	Evaporative Cooling Pad Material
EuF	Eucalyptus Fibres
HVAC	Heating, Ventilation and Air-Conditioning
IEC	Indirect Evaporative Cooling
IRR	Internal Rate of Return
IWT	Incipient Wetness Technique
LCA	Life Cycle Assessment
LiBr	Lithium Bromide
LiCl	Lithium Chloride
NC	Northern Cyprus
NPV	Net Present Value
PCM	Phase Change Material
Pmc	Pumice
PSP	Precision Spectral Pyranometer
RH	Relative Humidity

SIR	Saving to Investment Ratio
SPP	Simple Payback Period
TRNSYS	Transient System Simulation
VC	Vapor Compression
Vmc	Vermiculite
Vmc-$CaCl_2$	Vermiculite – Calcium Chloride
VSS	Vapor Sorption Systems
WoC	Wood Chips
YeS	Yellow Stone

Chapter 1

INTRODUCTION

1.1 Background and Problem Description

Studies have shown that human beings are much more comfort in an environment with indoor air quality opposed to their performance in a workplace without change. Convenience standards for people are met as long as the temperature and humidity of individual areas are preserved. The human comfort is subject to both temperature and relative humidity varying from 20 ℃ to 26 ℃ and humidity between 30 % and 60 % [1]. It greatly raises necessity of air conditioning, both for industrial and residential usage.

Cooling systems typically use circulated air to improve indoor air quality. For direct air entering air temperature and humidity, particularly in hot and wet areas, these must be controlled. The dehumidification of condensation is normally performed by conventional A/C systems, which cools air to the dew point and then heats it to the proper temperature [2]. But this kind of system has various drawbacks including high cost and environmental hazards. These reasons lead to developments of new cooling methods especially heat driven systems. As a result, desiccant dehumidification systems have been widely upgraded in previous years where the difference in vapor pressure between air and desiccants can change air moisture content. Moreover, the desiccants can be charged with solar energy and waste heat resources which means a cost effective system [3]. Dehumidification of the desiccant becomes sustainable and

low cost in contrast to condensation dehumidification thus, it is applicable in hot and humid areas [4]. The DAEC method is a feasible solution to address challenges and the growing demands of traditional A/C systems [5].

1.2 Desiccant Enhanced Evaporative Cooling Approach

Desiccant has a high moisture absorption capability, and it decreases the air humidity content and improves the evaporative cooling efficiency. Desiccant content can be regenerated by using solar energy or waste heat so that it can be reused in this process. The processed air enters the EC phase, directed beyond the dehumidification period to decrease the processed air temperature and meets the desired comfort conditions. DAEC is an effective and cost-effective method to meet the desired temperature and moisture comfort requirements as a concurrent solution for delivering energy efficient, safe and environmentally friendly cooling results. However, more technological advances are required to commercially implement the DAEC system [6]. The desiccant dehumidifier is composed of a desiccant material which removes moisture from the air by the process of dehumidification. Different desiccant materials absorb the moisture from the air at different capacities. The desiccant materials can be solid as well as liquid which will be described in the next section [7].

1.2.1 Classification of Desiccant Materials

Desiccant materials may be liquid or solid. Each type has its advantages and disadvantages in which the best desiccant material can be regenerated at low temperatures with the highest adsorption potential in all ranges of relative humidity. Selection of the type of desiccant depends on the desired application. Solid desiccants minimize the pressure drop in the processed air as they flow through the desiccant materials, but the desiccant device configuration can remove or decrease it by optimization. Using liquid desiccant in a dryer is usually more complicated than using

solid desiccant, as it is easier to handle solid desiccant content. For packaging desiccant products, solid desiccant systems are typically in the form of stationary or rotating wheel beds [8]. One of the drawbacks of the liquid desiccant is that, it can be transmitted by air during the dehumidification and regeneration process. Nevertheless, this issue can be minimized or eliminated by a proper dehumidifier and regenerator. The use of liquid desiccants to create a dryer is usually more difficult than solid desiccants. A liquid desiccant based device is therefore versatile and can place the regeneration zone far from the dehumidifying zone that localized dehumidification is possible [9].

Desiccant performance plays a crucial role in the entire system's overall efficiency, particularly in terms of dehumidifying and regenerating ability. The analysis of solid desiccants with high adsorption potential, good regeneration capacity and availability in local market is desirable [10]. Thus, a solid desiccant material was selected to be used in this study.

1.3 Aim and Objectives of the Study

This study focuses on the analysis of the efficiency of DAEC systems to determine the enhancement of the EC system capacity by the use of desiccant material. In addition, the comparative work was carried out between EC and DAEC system, important outcomes were achieved on the effect of using novel desiccant in hot and humid climates to enhance EC efficiency. Furthermore, a solar-driven DAEC system was designed, developed and tested under real climatic conditions of NC to analyses the cyclic performance of the system and assessing the feasibility of the developed system compared to the A/C split unit. Finally, a solar assisted DAEC system was modeled and simulated in TRNSYS software for comparison with the achieved experimental

results in real climate condition. The aim of this study is to develop a fixed bed DAEC system that uses novel composite sorbets that could be used as a coolth storage in hot-humid climate.

The main objectives of the presented work are:

- To Synthesize of novel desiccant materials to be employed in the developed system.
- To design and develop a desiccant enhanced evaporative cooling system.
- To select and investigate different organic evaporation materials in the developed system.
- To select the best desiccant-evaporation materials to be used in the DAEC process.
- To perform outdoor experiments with the use of solar collector for solar driven cooling application.
- To perform numerical analysis of the purposed DAEC process by using TRNSYS software.
- To carry out the economic analysis on the developed solar driven DAEC cooling process for evaluating feasibility of it.

1.4 Novelty of the Study

In this study, novel composite desiccant material was synthesized while investigating the new organic evaporation materials like, Wood Chips (WoC), Yellow Stone (YeS), Pumice (Pmc), Eucalyptus Fibres (EuF) and Vmc. Moreover, proposed desiccant cooling process took advantage of internal heat recovery by an air to water heat exchanger that reduces the temperature of the outlet desiccant material. Finally, the comparative performance analyses between EC and DAEC were carried out. Based on

the nominated materials, solar-driven DAEC system developed and examined under real life conditions. At the end, the extensive numerical analysis was performed to compare the developed system and simulated unit. The main novelties and contributions of this study are; (i) development of a novel composite desiccant, (ii) investigation of the novel EC materials, (iii) develop and testing the fixed bed DAEC unit with solar energy under real life conditions, (iv) performing simulation on the process, and (v) developing the fixed bed coolth storage.

1.5 Organization of the Thesis

The introduction, state of the system, and aims are presented in the Chapter 1. The literature review related to DAEC and desiccant materials is provided in the Chapter 2. The Chapter 3 includes the designing and modeling of the lab scaled system as well as the synthesizing, testing and performance analysis of the composite material. An experimental investigation of the solar-driven DAEC system is presented in Chapter 4. Chapter 4 is the experimental study part, and the obtained results are fully explained with relevant graphs needed for the explanation and the comparison of the performed tests. Moreover, in Chapter 5, the extensive numerical analysis on the proposed system using TRNSYS software was carried out. Based on the results obtained, the economic feasibility analysis, for applying the DAEC system in the residential building, was performed by simulations using the DesignBuilder software package. The conclusions of the present work, discussions, and recommendations for future work are presented in Chapter 6.

Chapter 2

LITERATURE REVIEW

2.1 Overview

As the economy and society grow rapidly, modern life and industry consume a lot of cooling energy. According to the latest data, an estimated 45% of all civil and industrial buildings consumed by air conditioning [11]. Furthermore, in recent decades, the depletion of fossil fuels and the danger of global warming have forced the air conditioning industries to develop new cooling technologies to help or even replace traditional VC systems. Some alternative cooling technology have been built to replace traditional VC systems and one of them is DAEC. Desiccant materials play key role in DAEC units because their properties like adsorption isotherms and regeneration temperatures significantly affect the efficiency of the systems [12]. In solid DAEC systems silica gels and zeolites are commonly used. Recently, many new forms of solid desiccants have been developed and studied with the advancement of material science. In the meantime, some of ongoing studies have concentrated on synthesizing advanced materials with enhanced water adsorption, regeneration capability and long-term stability [13]. In this study, novel Vmc-$CaCl_2$ is used as a solid desiccant material.

2.2 Conventional Evaporative Cooling Systems

Evaporative cooling utilizes forced heat and mass transfer methods, in which water and air are functional fluids. In particular, it consists of water evaporation caused by an airflow passage, thus reducing the air temperature. The modern evaporative cooling systems are categorized in the direct and indirect modes.

2.2.1 Direct Evaporative Cooling System

If water evaporates into the air to be cooled and moisturized at the same time, this is known as a direct evaporative cooling (DEC), while the thermal process is adiabatic saturation [14]. DEC is the oldest, easiest and most common form of air conditioning for evaporation. This device normally uses a fan to draw hot air outdoors through a porous wetted medium. Water absorbs heat when evaporating from the porous wetting matrix, leaving the DEC at a lower temperature. In fact, the air's dry bulb temperature decreases as it is humidified in the phase of adiabatic [15]. The underlying principle of DEC is to turn active heat into latent heat. The wetted medium may be a porous moistened pad made up of fibers, cellulose papers or a water spray [16]. The working principle scheme of the DEC equipment and a simplified flow scheme were presented in Figure 1.

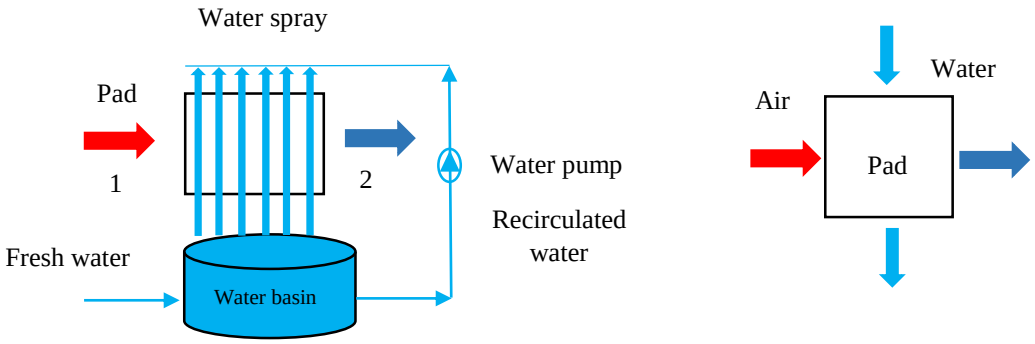

Figure 1: Working principle scheme of the DEC (Adapted from [17])

2.2.2 Indirect Evaporative Cooling System

When the cooling air is isolated from the evaporation cycle and thus moisturized during cooling, it is called indirect evaporative cooling (IEC). The key benefit of this technique is when the temperature is higher it is more efficient, i.e. more cooling is needed for thermal comfort. It has the additional benefit of low energy consumption and fast maintenance. Through the use of a full airflow replacement, the recirculation

stream and the growth of fungi and bacteria are removed, which is a chronic issue in traditional air conditioners.

IEC can be categorized into two types based on heat transfer as follows [18]:

Type (A) – IEC dry surface: Secondary air is cooled with EC prior to entering indirect heat exchangers. The cooling is achieved by DEC. This evaporative secondary air cools primary air by thermal transfer in a conventional air to air heat exchanger.

Type (B) – IEC wet surface: A wet surface heat exchanger for non-adiabatic evaporation is used in this kind. Two air streams are used in this method, respectively alternate wet and dry channels, which are isolated from each other. In dry passages, primary air is cooled isolated from the moist passages from which the secondary air and water circulate. Evaporation takes place in moist spaces, with heat lost in the impermeable dividing wall from primary air and evaporated into the secondary air. Therefore, the simultaneous and virtually indissoluble heat and mass transfer due to evaporation on wet passages and heat loss on dry passages. The air that enters the cooler's dry side has a lower wet bulb temperature than the atmosphere. It is also desirable, instead of using ambient air, to remove some of this cooled air and transfer it on the wet-side of the heat exchanger. This cooler form is known as the indirect regenerative evaporative cooler. The schematic of IEC system is shown in Figure 2.

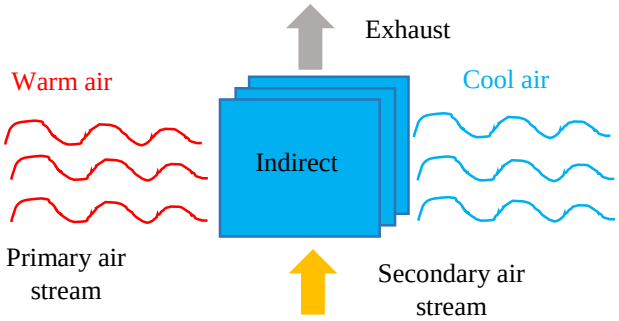

Figure 2: Working principle scheme of the IEC (Adapted from [19])

2.2.3 Classification of Evaporative Materials

The ECPM plays a crucial role in increasing the EC system's cooling capacity. The ideal evaporation content should also be high in water, moderate porosity, wide surface area, low weight, high thermal conductivity, low cost, non-corrosive and widely available. Work has been in progress over the past decade to create new pad materials to increase the performance and cooling ability of EC systems. The most studied materials for EC systems are metal, wood, plastic, ceramics, CELdek pads, cellulose pads, aspen and a rigid medium pad [20].

Manufacturers often use cellulose-based pads of paper or plastic fibers to achieve an EC device which is more suitable for extreme climatic conditions and for different applications. While these materials are effective, they are difficult to produce because of the production and processing costs. Therefore, alternative options for the EC method can be found on locally produced materials [21]. Because local products in most places are easy to find and available, they may be used in less advanced, hot countries at low cost. A new direction of work on EC technologies could be environmental-friendly porous organic materials, such as natural stones and porous agricultural materials, with strong water keeping capacity and long life, to achieve

efficient cooling in buildings [22]. In Figure 3, previously investigated EC materials are shown.

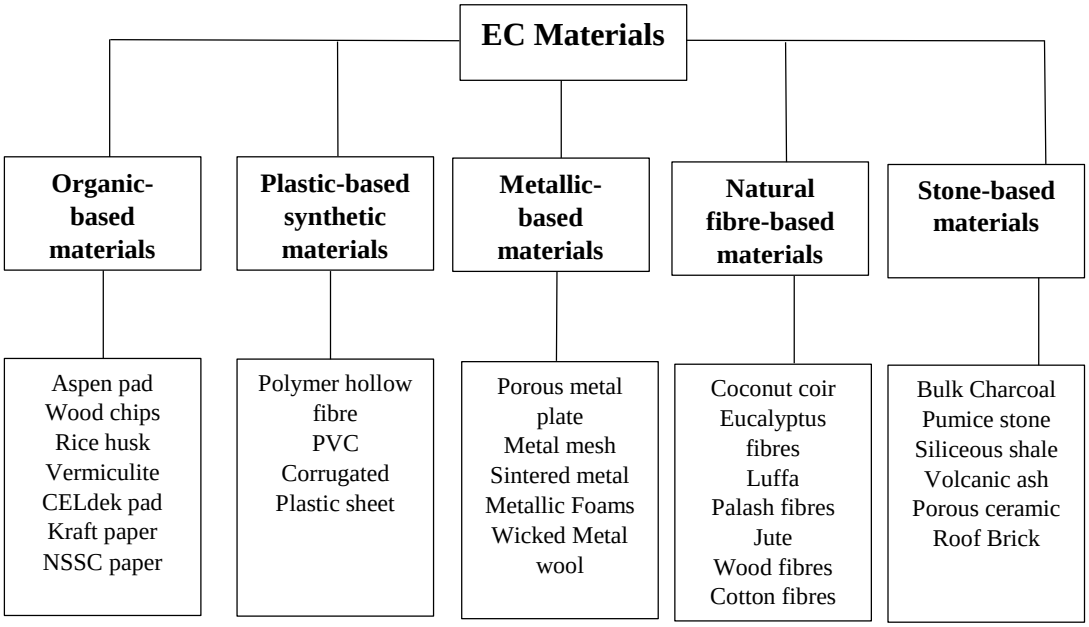

Figure 3: Classification of the EC materials (Adapted from [22])

Evaporation materials list used in the current study is given in Table 1.

Table 1: Evaporation materials used in the study [22]

Material	**Symbol**	**Density (kg/m^3)**	**Thermal Conductivity (W/(m°C))**	**Water absorption capacity (g/g)**
Wood chips	WoC	380	0.08-0.14	1.3-1.5
Yellow Stone	YeS	2880	0.6-2.5	0.024-0.0916
Pumice	Pmc	250	0.186-0.433	0.20-0.35
Eucalyptus fibres	EuF	495	0.0374-0.0368	4.3
Vermiculite	Vmc	172	0.1040-0.1530	3.5-5.9

2.3 Desiccant Assisted Evaporative Cooling

Desiccant cooling system employs a desiccant unit to dehumidify the air and to sensibly cool the air well below ambient temperature conditions in the form of EC process. To make the system working continuously, water vapor adsorbed/absorbed must be driven out of the desiccant material so that it can be dried enough to adsorb water vapor in the next cycle. This is done by heating the desiccant material to its temperature of regeneration which is dependent upon the nature of the desiccant used. A desiccant cooling system, therefore, comprises principally three components, namely the regeneration heat source, the dehumidifier (desiccant material), and the cooling unit.

2.3.1 The Concept of Desiccant Cooling

Desiccant cooling systems are heat-driven cooling devices that are alternatives to traditional cooling systems for VC and absorption [23]. These systems are largely dependent on the used desiccant material. The desiccants are natural or synthetic substances capable of absorbing or adsorbing water vapor due to the difference of water vapor pressure between the surrounding air and the desiccant surface. They are encountered in both liquid and solid states. Each of liquid and solid desiccant system has its own advantages and shortcomings [24] as described in the following section.

The desiccant dehumidifier can be of different configurations which are shown in Figure 4.

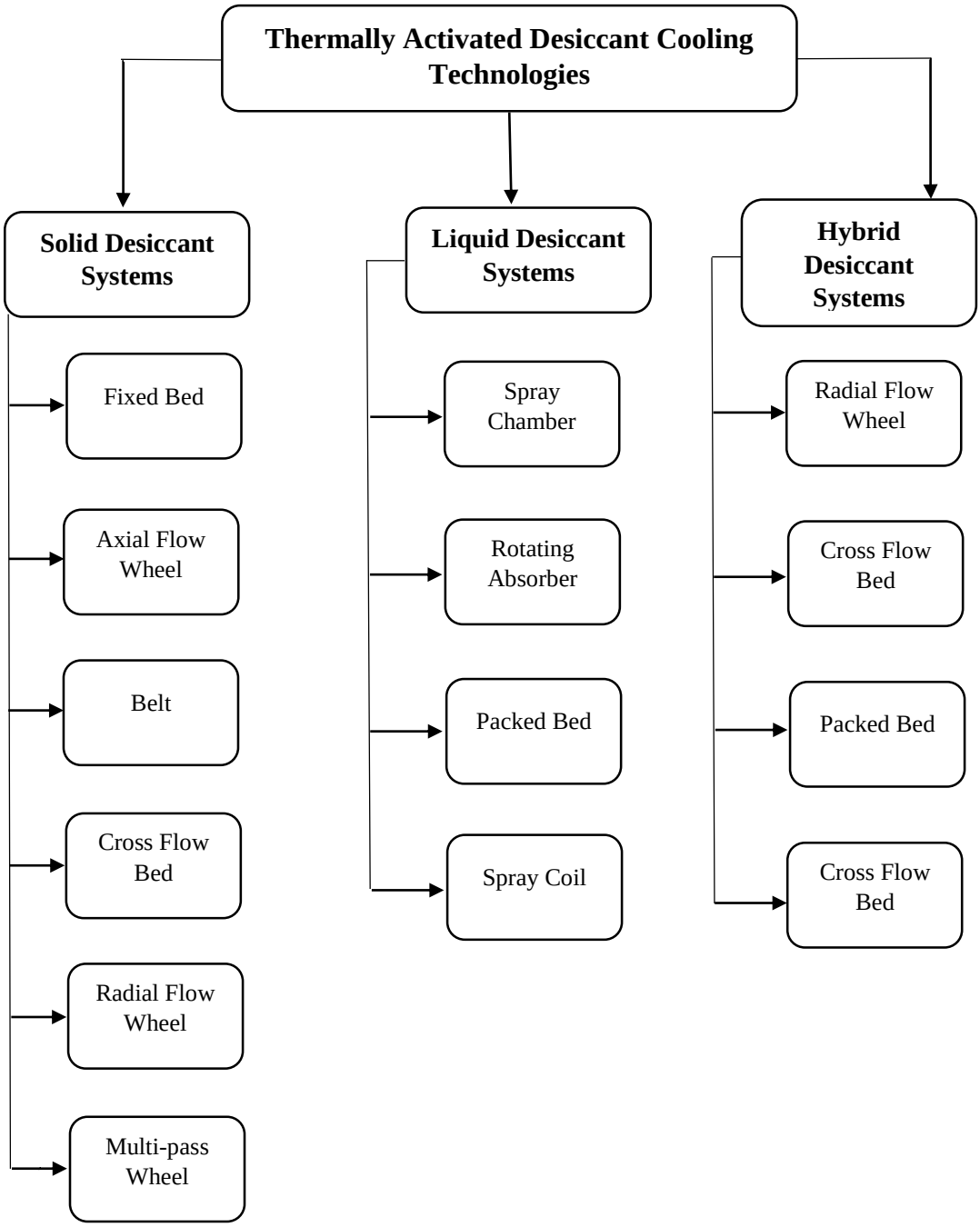

Figure 4: Different configurations for various desiccant systems [25]

In ventilation or recirculation modes, the system may work in a closed loop or in an open loop. To regenerate the desiccant, a heat supply is necessary. Low heat is adequate for regeneration at a temperature of about 60–85 °C, so renewable energies

including solar energy and waste power from traditional fossil-fuel systems can be used. The process is simple and satisfies thermal efficiency coefficient. Despite the system with fixed bed configuration cannot operate continuously, it does not have moving parts therefore operation and maintenance are easy with low costs which can be used as coolth storage.

Desiccant systems can use solid or liquid desiccants. Usually the widely used solid desiccants are active silica gel, vermiculite, titanium silicates, alumina, zeolite (natural and synthetic), molecular sieved, while lithium chloride (LiCl), lithium bromide (LiBr), try-ethylene glycol, calcium chloride ($CaCl_2$), and potassium format are common liquid desiccants. Apart from the above, organic desiccants, polymeric desiccants, compound desiccants and composite desiccants are available. The systems for desiccant devices include desiccant bed, solid tower, liquid spraying tower, falling film and several vertical beds [26]. Desiccant systems can be categorized according to the type of substance used in them as follows:

(1) Liquid desiccant assisted evaporative cooling,

(2) Solid desiccant assisted evaporative cooling [27].

In the following sections, the mentioned types of desiccants have been reviewed briefly.

2.3.2 Liquid DAEC

The liquid desiccant dehumidification system comprises a dehumidifying unit and a regenerating unit. In the dehumidifying unit, fresh liquid desiccant absorbs water to dehumidify the hot and moist process air due to the high affinity of the desiccant towards the water [28]. The moisture exchanged from the humid air to liquid desiccant solution is driven by the liquid/air vapor pressure difference. As the equilibrium vapor

pressure above the desiccant solution is lower than that of the humid air, the vapor of humid air is absorbed by the desiccant during dehumidification process. The reverse occurs in regeneration process [29]. Figure 5 shows the layout of the liquid DAEC system.

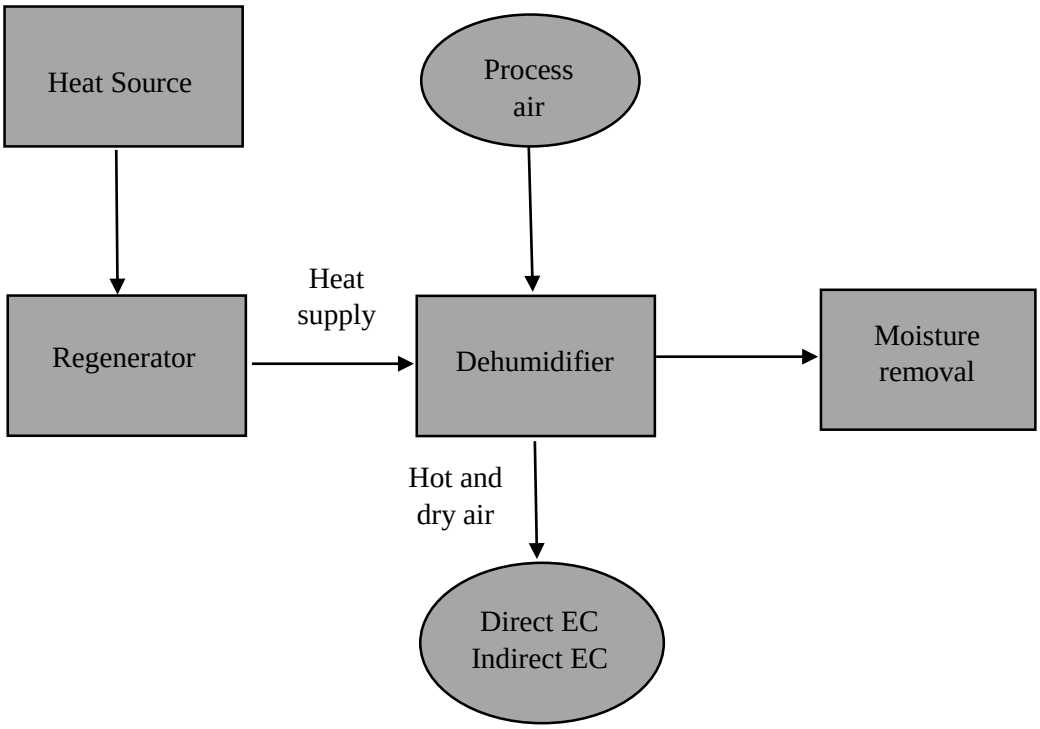

Figure 5: Principle of liquid desiccant cooling based evaporative cooler

For several DAEC systems, liquid desiccants were used and decent COP were produced [30]. LiCl, LiBr, $CaCl_2$, potassium format, and tri-ethylene glycol are typical liquid desiccants [31]. The liquid desiccant can be regenerated at a lower temperature (60–75 °C), enabling the use of solar or low grade waste heat [32].

The downside to liquid desiccant is that the dehumidification and regeneration cycle is taken out by the airflow. However, this issue is minimized or removed by a proper dehumidifier and regenerator system. In fact, the use of liquid desiccants to create dryers is easier than the use of solid desiccants. However, a liquid desiccant device is

versatile, enabling regional dehumidification to locate the regeneration area well away from the dehumidification region. The benefit of liquid desiccants is that regeneration with a high moisture reduction capability can be carried out at a lower temperature. Liquid desiccant can also absorb air contaminants from organic and inorganic sources [33]. Due to the corrosive and possible harmful features of desiccants, carryover still remains a critical issue in direct-contact liquid/air desiccant dehumidification, such as spray towers, falling film towers, packed bed towers, and ultrasonic atomization dehumidifiers. In addition, the surface wettability of liquid desiccant on plates determined the contact area of liquid and air, and thus significantly influence the heat/mass transfer efficiency. Under lower liquid flow conditions, the film is not stable and breaks up into a series of stable rivulets forming dry zones on the vertical support which severely deteriorated the dehumidification performance. Some of the main advantages and disadvantages of liquid desiccants [34] are given as follows:

Advantages:

- Low-pressure drop across the liquid desiccant makes them suitable to use with low regeneration temperatures.
- The ability to pump liquid desiccants makes the entire unit small and compact.
- Liquid desiccants can be stored and used when heat source is not available. This is advantageous when heat source is not available for regeneration.

Disadvantages;

- Liquid desiccants like LiCl, LiBr and all other salts are corrosive and can damage the desiccant system.
- Any carry-over of liquid desiccant along with supply air stream can cause significant harm to the health of the occupants.

- In order to handle large volume of liquid desiccant, large pumps are required, which draw a large amount of power.
- Desiccants of aqueous salts also face the problem of crystallization.

2.3.3 Solid DAEC

A desiccant is hygroscopic substance having high affinity to water. Solid desiccant cooling system operates on principle of adsorption of water vapor from air. In solid desiccant cooling system, the moisture in ventilated/recirculated process air is first removed by a fixed bed or rotating desiccant wheel. The temperature of this dried process air is then lowered further to the desired room conditions by use of sensible heat exchangers. To make the system working continually, amount of water vapor adsorbed by the fixed bed or rotating desiccant wheel must be driven out of the desiccant material so that it can be dried enough (regenerated) to adsorb water vapor in the next cycle. This is done by heating the desiccant material to its temperature of regeneration which is dependent upon the type of the desiccant used. Energy required for regeneration of desiccant material is supplied via regeneration heat source either by electrical heater or solar/waste heat. Rotary desiccant wheels and fixed beds are the most common desiccant dehumidifier configurations. Rotation allows continuous operation, but limits the use of the wheel because it is inconvenient to have a rotating component in some places. In contrast, a desiccant bed is flexible in positioning but cannot run continuously. Usually, more than one desiccant bed unit is used to compensate for the non-continuous drawback. One bed can be in regeneration while another is in dehumidification. Moreover, because of lack of moving part in fixed bed configuration the operational and maintenance cost is lower than rotary desiccant wheel which led to a feasible system.

Solid desiccants are extremely pore-like materials that adsorb water by various mechanisms such as chemical adsorption to pore walls, or subsequent physical layer adsorption to pores by water molecules or capillary condensation [32]. Solid desiccant material refers to material that can absorb water vapor and recycle in moisture air at relatively high temperatures. It can be divided into two main classes as: 1) porous-structural substances such as activated alumina, silica gels, zeolites, etc., are adsorbed by variations in water vapor pressure between pores in and around the desiccant content. During the adsorption processes a physical process occurs. 2) Can form solid crystalline hydrate compounds, such as LiCl, $CaCl_2$, LiBr and etc. There is also a hydration reaction inside such products. Different benefits and drawback of solid desiccants are listed as below:

Advantages:

- Solid desiccant cooling systems can be driven by low grade thermal energy, such as waste heat or renewable energy sources (i.e. solar energy, geothermic energy and etc.), thus have a large energy saving potential.
- Provide an effective and economical way for dehumidification.
- DAEC systems are less subject to corrosion when compared with liquid ones.

Drawbacks:

- Solid desiccants cause a pressure drop in the processed air when it passes through the desiccant material.
- High regeneration temperature [33].

The system principle is shown in Figure 6.

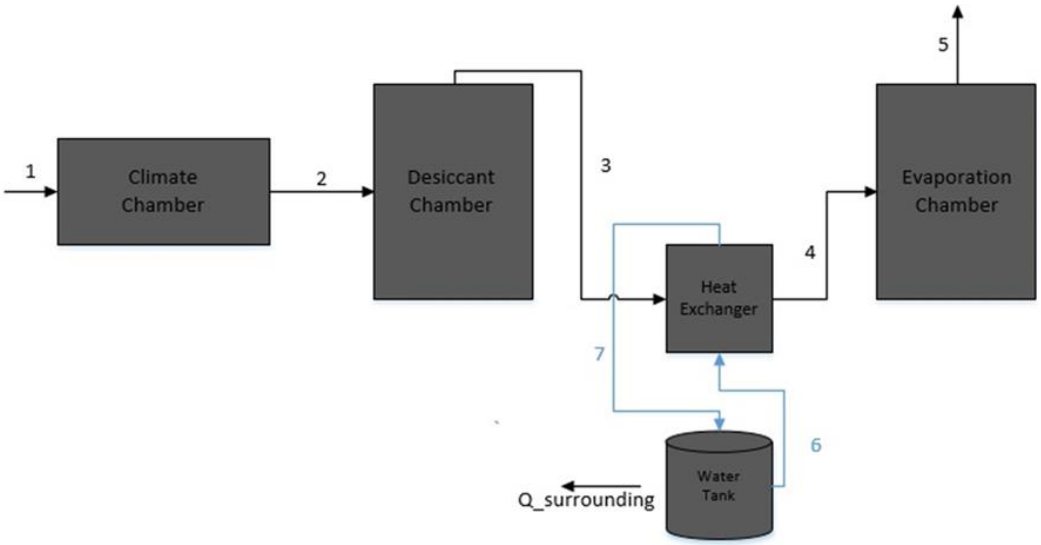

Figure 6: Principle of desiccant cooling

In solid DAEC system, desiccant material is usually impregnated with the designed wheel matrix or utilized as a fixed bed, where direct, indirect or M-cycle evaporative cooler is integrated to the desiccant unit. In this process, utilized desiccant material and ECPM are highly important, therefore, natural, low cost and environmentally friendly desiccant material and ECPMs are recently gaining attention to be employed in DAEC technology. Conventional desiccants including zeolite, silica gel and activated carbon are widely investigated due to their good water sorption properties. However, high regeneration temperature of these materials is the main obstacle for their usage in solar driven DAEC applications. Therefore, new desiccant materials need to be developed, that could be regenerated at lower temperature ranges (<80 °C). In this regard, salt based composites present an important opportunity for achieving this objective. On the other hand, several different types of commercial ECPMs were already developed including CELdek, ASPEN pad and GLASdek. Despite such ECPMs are highly efficient, their production requires energy and advanced machinery. Thereby they considerably contribute to the total investment cost of DAEC systems.

Due to these reasons, new natural materials which have high structural stability and water holding capacity also good heat and mass transfer properties are required.

2.3.4 Desiccant Materials

The desiccants are natural or synthetic substances capable of absorbing or adsorbing water vapor due the difference of water vapor pressure between the surrounding air and the desiccant surface. They are encountered in both liquid and solid states. Each of liquid and solid desiccant systems has its own advantages and shortcomings. In addition of having lower regeneration temperature and flexibility in utilization, liquid desiccant has lower pressure drop on air side. Solid desiccant is compact, less subject to corrosion and carryover. Different desiccant materials are listed in Figure 7.

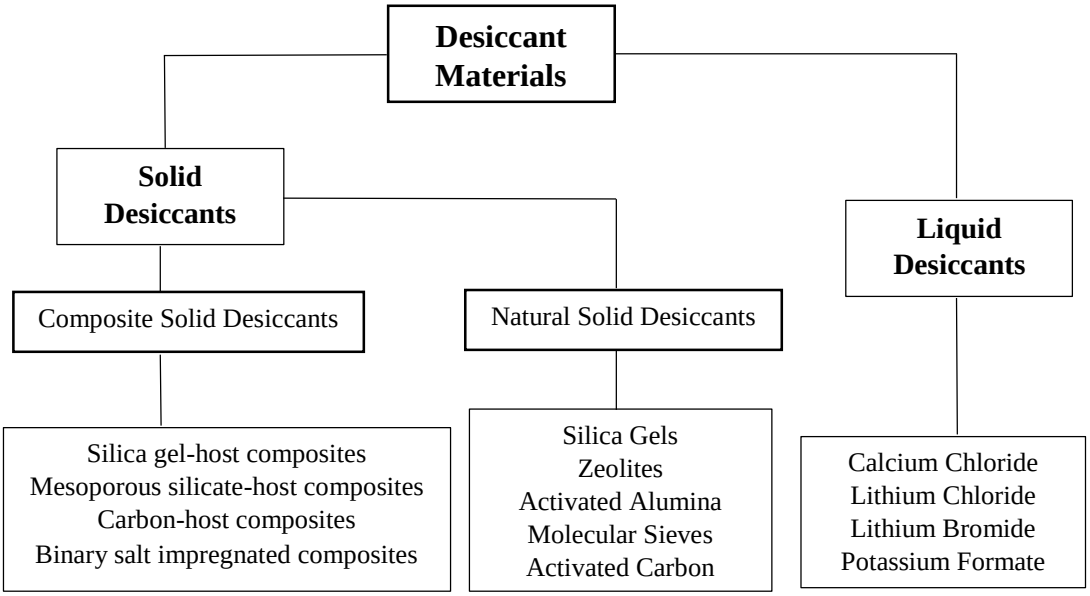

Figure 7: Classification of the desiccant materials [8]

2.4 Literature Survey

Several research on DAEC development have been performed over the last decade. In the literature, various studies have been performed on DAEC systems with the use of different desiccant materials and ECPMs. Chaudhary et al. [37] studied a solar-assisted

cooling system, which comprised a silica gel coated desiccant wheel (DW) and an indirect M-cycle evaporative cooler. Their study results showed that the outlet air temperature and thermal COP (COP_{th}) were in the range of 14 °C-22 °C and 0.65-1.17, respectively. In another study [38], a solar-driven A/C system comprising silica gel-coated concentric tube heat exchanger was fabricated and analyzed experimentally. The maximum value of dehumidification factor and cooling capacity achieved were 11.05 g/kg and 5.748 kJ/min respectively, which showed that the system was practicable. A solar-assisted hybrid desiccant cooling system was developed by Luo et al. [39]. Silica gel has been used as a desiccant material, while obtained results showed that the overall performance of the system in terms of power consumption could be enhanced by approximately 10% by integrating a solar-heated water heat exchanger in comparison to the hybrid desiccant cooling system. In different study, performance of a fixed-bed polymeric sorbent-based DAEC unit for agricultural storage applications was investigated experimentally. The results showed that the COP is highly influenced by ambient air conditions, where it raised with the increase in wet-bulb effectiveness of the EC unit [40]. In another study [41], a solid desiccant A/C system comprising silica gel was designed for an experimental room with a volume of 18 m^3. The findings revealed that the lowest temperature achieved was about 24 °C. A solar-driven DAEC system with the use of a hybrid photovoltaic thermal collector-solar air heater has been developed. System was tested in a real building and system COP was achieved as 19.8 in hot and humid ambient conditions [42]. An integrated system to regenerate the desiccant materials in fixed bed filled with silica gel for solar A/C systems was developed. The regeneration rate of the desiccant material and the average daily thermal regeneration efficiency of the system were obtained as 0.4 kg water/h m^2 and 30%, respectively [43].

In another study performed by Mehla and Yadav, a solar-powered solid desiccant A/C unit containing silica gel and phase change material (PCM) was analyzed for cooling purposes during the sunlight and sunset hours with thermal efficiency of 28.81% and 46.06%, respectively [44]. Fong and Lee were conducted year-round dynamic system simulations to investigate the impact of integrating silica gel coated DW in absorption cooling cycle. It was found that DW at high speed provided 11.5% reduction in total primary energy consumption by enabling heat recovery [45]. In another study, Heidari et al. [46] presented a DAEC system using silica gel for co-production of water and cooling. Average COP of the system was achieved as 1.53, whereas for the same operating conditions, COP for the VC system was found as 1.2. Sohani et al. [47] employed static and dynamic optimization approaches on a desiccant-enhanced indirect EC to find the best possible operating condition of that system in different climates. Study results showed that, by employing the dynamic optimization instead of static optimization the annual average COP of 50.5% could be achieved. The modelling of solar driven DAEC system for hot and humid region was investigated by Sudhakar et al., which highlighted the importance of control system and optimization for achieving better efficiency. LiCl and potassium formate were the two desiccants used in this experimental study [48]. In another research, Pandelidis et al. [49] presented a numerical study of a multi-stage desiccant A/C process designed for moderate climates. Maximum COP of the investigated system was determined as 4. A cascade system, including solar heating and poly-acrylic acid sodium salt as solid desiccant material, was developed for the air cooling process by Caliskan et al. [50]. The cooling capacity of the system reached to 9.29 kW. Furthermore, total COP (COP_t) and electrical COP (COP_e) were achieved as 1.7 and 6.66, respectively. Zhou and Reece [51] investigated a non-adiabatic polymeric DW with a concentric structure at

low regeneration temperatures. The results showed that when the inlet temperature of the process air was 35 °C, dehumidification performance of the investigated DW was very close to the ideal. A dynamic simulation-optimization of a solar-assisted desiccant cooling system integrated with a ground source heat exchanger developed by Rayegan et al. By lowering the regeneration temperature, the maximum COP of 10.2 achieved [52]. In a different study, a solar driven DAEC system using silica gel was analyzed experimentally to maintain indoor air conditions in a research lab room located in Southern Europe. Researchers suggested that investigated system could be considered as an alternative to traditional direct expansion systems [53]. In another study, Singh et al. [54] investigated coco-peat, sawdust and dried cow dung as low cost alternatives to the conventional desiccants. Performance of the selected materials was compared with silica gel. It was concluded that coco-peat and dried cow-dung could be used as potential low cost desiccant materials.

She et al. [55] developed a liquid desiccant cooler in another research and compared its efficiency with the conventional vapor pressure cooling system. The findings showed that the COP of this method was 18.8 % higher than the results obtained under the same operating conditions for the VC process. Desiccant cooling is regarded as a concurrent solution to provide energy efficient, safe and environmentally friendly cooling impact.

Liu et al. [56] have conducted a theoretical method for examining the ideal high COP and existing differences between the real and ideal working conditions of the cooled internal liquid desiccant dehumidifier powered heat pump. Nain et al. have experimentally constructed and analyzed a solar air conditioning system composed of silica gel-coated, concentrated tube heat exchanger [57]. The optimum dehumidifier

level and cooling capacity obtained was 11,05 g / kg with the ambient air temperature of 37,6 °C and a specific humidity of 23,99 g / kg, respectively. Batukray has reviewed solid desiccant-based evaporative cooling systems [58] and it has been demonstrated that DAEC works better than conventional air-conditioning systems and demonstrates relatively lower energy consumption. Jani et al. [59] gave a description of modeling the thermal cooling system, simulation and study of previous transient simulation tests. Chen et al. reviewed the physical properties of different desiccant materials and their dehumidification results [60]. Different dehumidifier forms were also tested and combined with the liquid dehumidifier method. The design of a solar hybrid desiccant air conditioning system, integrating the methods of desiccant cooling with VC A/C, was analyzed in a further research by Dong La et al. [61]. The findings revealed that such a combination functions well in significant humid areas and achieves 87 % COP_t with a solar fraction of 27.7 %.

Jia and colleague used a compound desiccant to create a high-performance desiccant cooling device, concluding that a compound desiccant would increase the overall efficiency of a desiccant wheel by 20-30 % over a silica gel desiccant wheel during practical operation. Tests also showed that the COP can achieve 1.28 which is 35% more than the silica gel desiccant wheel [62]. Guo and his colleagues analyzed microporous coordination polymers in comparison with active alumina capacity and performance, and concluded that polymeric desiccants have commercial potential. Further analysis on specific parameters of advanced desiccants is also needed in prolonged cycles in order to test the activity of microporous coordination polymers before an actual conclusion is reached [63].

Niu et al. [64] proposed a cooling ceiling-assisted heating, ventilation and air-conditioning (HVAC) system compatible with humid environment desiccant cooling and addressed energy saving potentials as the findings showed such a system would save up to 44% of energy use in contrast with the traditional AC systems. Moreover, Dai et al. [65] used a hybrid AC system of dehumidification and evaporative cooling, and air conditioning VC. Experimental tests indicated a substantial improvement of 20-30 percent in the COP of this hybrid system. In a separate analysis Goldsworthy et al. [66] optimized desiccant indirect evaporative cooling system and the findings suggested that this optimization may improve the cooling efficiency and energy savings.

Another analysis was performed by Ge et al. [67] comparing the solar-desiccant capability and conventional vapor compressors in Berlin and Shanghai under two different climatic conditions, concluded that the regeneration temperature needed in Berlin was 55 °C per day and the regeneration temperature was about 85 °C in Shanghai. Their study of feasibility reveals that complex investment payback times were 4.7 years and 7.2 years, respectively for Berlin and Shanghai.

Various experiments have examined traditional solid desiccants such as zeolite and silica gel for the desiccant cooling. In addition, some hygroscopic salts have been used in cooling systems for liquid desiccant such as LiCl, and $CaCl_2$. In comparison to the previous work, the current study and analysis explores the efficiency of the composite desiccant produced for desiccant-assisted, evaporative cooling by impregnating $CaCl_2$ in a porous host matrix (Vmc). The synthesized material for desiccant cooling systems has not previously been tested. Besides comparative work between evaporative and desiccant assisted cooling systems, significant insights were given to determine the

effect on evaporative cooling efficiency from the use of desiccants in hot and humid weather. Moreover, the real condition tests of developed solar-driven assisted evaporative cooler system performed to demonstrate the applicability of the DAEC system under hot and humid climates. Table 2 represents the summary of related studies in the literature.

Table 2: Summary of the related studies

Reference	Year	Type of study	System Performance	Advantages	Disadvantages
Pandelidis et al. [49]	2018	Numerical	COP_t of up to 4.0	System provides higher cooling capacity compared to single-stage desiccant cooler	Airflow is very humid for regeneration
Chaudhary et al. [37]	2018	Experimental	Average cooling capacity of the system was nearly 3.78 kW with average COP of 0.91	Evaporation capacity is very high	Low effectiveness of MC cooler
Luo et al. [39]	2019	Experimental	Overall performance increased by 10%. The COP of the system gradually rises with the increase in ambient temperature	Higher humidity ratios create and increase MRR values	In humid areas, large area and capacity of the solar thermal collector are required
Mahmood et al. [40]	2019	Experimental	Proved that COP_t decreases with the increase in regeneration temperature while it increases with the increase in wet-bulb effectiveness	System is suitable for different ambient conditions and various applications	COP is increased at low regeneration temperature
Saputra et al. [41]	2019	Experimental	By using DW, lowest temperature of 24 °C is achieved.	Effective humidity capacity	System requires large space area
Fan et al. [42]	2019	Numerical	The COP_e of the cooling system reached up to 19.8.	The performance of the system was increased for larger PVT-SAH systems	Energy performance of the system was affected by different weather conditions.
Mehla & Yadav [44]	2019	Experimental	The system's total thermal storage capacity varies from 1.796 kW to 1.817 kW.	The payback period of the system is 23.2 months	System requires large space area
Nain et al. [38]	2020	Experimental	The maximum value of dehumidification factor and cooling capacity achieved were 11.05 g/kg and 5.748 kJ/min, respectively.	Continuous dehumidification and cooling process	Dehumidification and cooling capacity reduce with the increase of water temperature
Present study	2020	Experimental	In DAEC mode maximum COP_e of 9.85 was achieved. Moisture removal rate was 15.27 g/min at 80 °C.	System uses low cost desiccant and ECPMs. It has simple configuration and provides high effectiveness.	Not suitable for continuous operation.

Chapter 3

DEVELOPMENT AND PERFORMANCE INVESTIGATION OF SOLID DAEC SYSTEM WITH DIFFERENT MATERIALS

The main aim of this chapter is to provide the experimentally analyzed performance of different natural, low-cost ECPMs, and composite desiccant for DAEC applications. In addition, it is proposed to perform experiments in both DAEC and direct EC modes to compare the cooling performance of both modes with the use of different ECPMs. Consequently, it is intended to evaluate the performance improvement potential by integrating desiccant material to evaporative cooling system in hot-humid climates. In order to achieve the objectives, a laboratory scale fixed-bed DAEC system was developed and utilized. The details of the system are provided in the following sections.

3.1 Proposed Design Configuration

In the study, a desiccant cooling system was developed and experimented under laboratory conditions. Figure 8 presents the 3-D view of the designed system that was generated in SolidWorks software, where arrows are displaying the path of the airflow. The temperature and relative humidity of air at various stages were measured by five sensors which are; (z_1) desiccant dehumidification unit inlet/system inlet, (z_2) desiccant dehumidification unit outlet/heat exchanger inlet, (z_3) heat exchanger outlet/evaporative cooler unit inlet, (z_4) evaporative cooler unit outlet/system outlet

and (z_5) ambient conditions. Throughout the experiments, sensors were configured to monitor the relative humidity and temperature per minute over two hours of testing.

The proposed model was a combination of three principal units; the desiccant dehumidification unit, heat exchanger unit, and evaporative cooling unit (Please see: Figure 6). A tunnel-shaped climate chamber, consisting of a centrifugal fan and electric heating coils, was used to provide the required hot air, similar to the environmental conditions at the inlet of the dehumidification unit. A household ultrasonic humidifier was also attached to the climate chamber to bring the system inlet air to the desired inlet humidity conditions. The utilized ultrasonic humidifier was equipped with a controller that allows adjusting the moisture supply rate to three different settings. The desiccant unit was designed as a solid fixed bed with material testing purposes. The desiccant material (Vmc-$CaCl_2$) was positioned inside the chamber on a tray wherein the intake air passes through the chamber. The tray has of 240 mm diameter and 100 mm height, where bottom part of it was made up of wire mesh for allowing air flow. The configuration of the desiccant tray inside the chamber is shown in Figure 8. In this study, across the desiccant bed, desiccant material absorbs the moisture of the air and reduces the humidity at the chamber outlet while increasing the temperature of the air. The hot and dry air is then moved into the air-to-water heat exchanger to eliminate the generated sorption heat and pre-cool the process air. The utilized heat exchanger is 300 mm wide, 250 mm height and 65 mm thick. It was made up of 30 pieces of copper pipes in three rows, where 88 aluminum fins were used for enhancing the heat transfer. The heat exchanger was fitted in a rectangular chamber perpendicular to the air flow, where its inlet and outlet are connected to the desiccant outlet and evaporative cooler inlet, respectively. A water tank of 3 mm galvanized sheet metal with a volume of 50 L is also integrated to the water coil of the heat exchanger. Water is circulated between

the heat exchanger and the tank to continuously remove heat from the air. The heat gained by the water from the air inside the heat exchanger is transferred to the water tank. Thereby, air temperature is sensibly reduced before EC process, which enables achieving higher cooling effectiveness.

Following the pre-cooling process in heat exchanger, the moderate-low humidity air passes to the EC system via the ducts. At this stage, air flows through the EC pad and it gets cooler as a result of water evaporation. The ECPM is placed in an identical tray and in a similar way with the desiccant material as seen in Figure 8. In the evaporative cooler, water is circulated through the waterline with a pump and sprayed over the evaporative materials (*i.e*., WoC, Pmc, Vmc, YeS, and EuF) with a nozzle to maintain consistent water evaporation. EC effect is obtained due to the cycle of evaporation, which absorbs energy mainly from incoming hot air, and partially from the water. The cool air (20-25 °C) at the system outlet then can be delivered to the conditioned environment. Due to the EC process, product air relative humidity is expected to be high (85-95%). However, it was targeted to increase the cooling capacity more than 50% with the use of desiccant in comparison with EC, for the same amount of humidity increase of air. In the desiccant chamber, once the air humidity is continually removed, the desiccant becomes saturated and loses its potential of water absorption in a period. Therefore, a regeneration process should be applied to the system to dry the desiccant material and maintain its moisture absorption potential, wherein solar energy can be used for this task. Because the developed system was investigated under laboratory conditions with the scope of analyzing the cyclic characteristics of the desiccant material, an electric sourced heating unit was located inside the climate chamber for charging purposes. The utilized electric heating unit consists of four electrical heaters (two of 0.5 kW capacity, and two of 1 kW capacity) and a heater controller to adjust

the charging supply air temperature to the set point. By this way, it was targeted to investigate the moisture desorption (dehydration) potential of Vmc-$CaCl_2$ at a temperature range of 60-80 °C, which is achievable with conventional flat plate collectors. Thereby it is proposed to address the key challenge of high regeneration temperature requirement of most conventional desiccants (i.e. zeolite and silica gel). Despite the disadvantage of unsteady nature of solar energy, development of desiccants with suitable regeneration temperature range would be high importance for future advancement of solar driven DAEC systems.

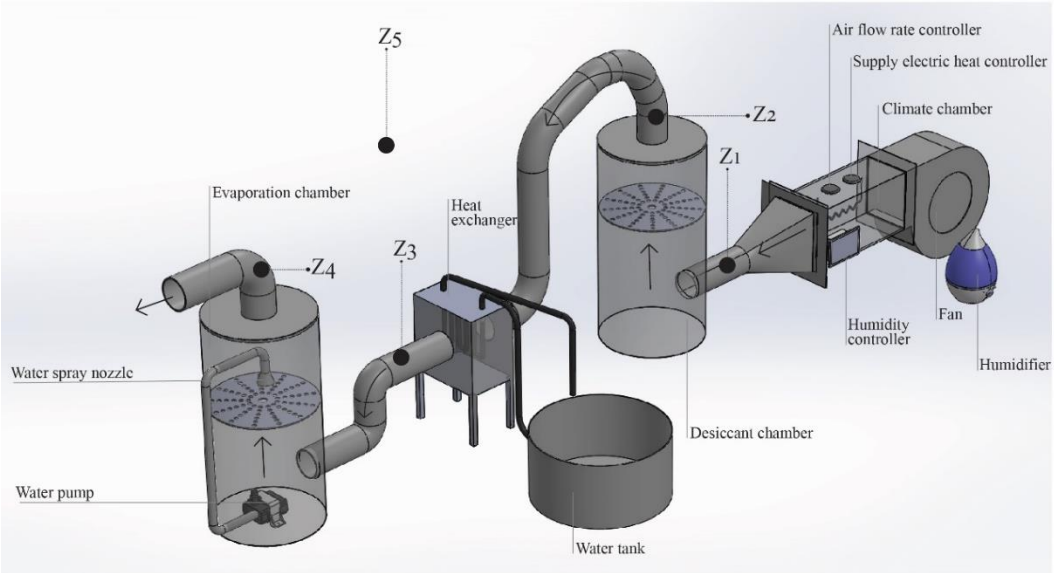

Figure 8: 3D view of the investigated desiccant assisted evaporative cooling unit

During the experiments, the sensors that have been used to record the inlet, outlet, and ambient temperature and humidity were Sensirion SHTC3 type with a typical accuracy of ±2 % (relative humidity) and ±0.2 ºC (temperature). The mass flow rate of the air was measured by a PASCO-GLX airflow meter with ±0.1m/s accuracy. The range of each measured parameter, accuracies and the percentage of errors due to the utilized measurement devices are listed in Table 3. During the experiments, airflow meter was placed at the system outlet to take into consideration the pressure loss of air across the

system components. A centrifugal fan with a maximum power of 120 Watts was used in the climate chamber to supply airflow through the system, which could be regulated by an electrical controller to manage the experiments with the appropriate airflow speed.

Table 3: Standard uncertainty, error, and measuring range of instruments

Sensor	Measured parameter	Range	Accuracy	Error
Temperature (Sensirion-SHTC3)	Temperature	0 – 130 ºC	±0.2ºC	±1.2 %
Humidity (Sensirion-SHTC3)	Relative humidity	0 – 100%	±2%	±2.5 %
Anemometer (Pasco-Xplorer)	Air velocity	2 – 6 m/s	±0.1m/s	±3.0 %

The chambers, with a radius of 250 mm and height of 1450 mm, were made by 1 mm thick double layer galvanized sheets, where 30 mm thick insulation made by glass wool was installed among the sheet layers. The used trays were placed centrally at 500 mm below the top, perpendicular to the airflow, and retain in the chambers. A submersible 25 Watt water pump was used in the evaporative cooler for pumping the water from the water tank to the top of the cooler with sufficient pressure for creating water spray on to the EC materials via the water sprinkler valve.

3.1.1 Experimental Procedure

In this research, a comparison between EC and DAEC was performed in which, Vmc-$CaCl_2$ composite is used as the desiccant material [6]. Additionally, various materials such as WoC, YeS, Pmc, EuF, and Vmc were utilized as evaporative materials, as shown in Figure 9. The system was assessed as a set of experiments under laboratory conditions for different materials in EC and DAEC modes. Also, the cyclic performance of the DAEC system in charging and discharging modes was carried out with different charging temperatures. Finally, a comparative analysis of EC and DAEC

mode operations, based on various performance parameters is presented. In the experimented system inlet temperature and relative humidity are set to ~36-38 °C and 36-38% respectively, which reflects the average summer time conditions of Mediterranean Climate (*i.e.* NC). The detailed experimental methodology of the current study is shown in Figure 10.

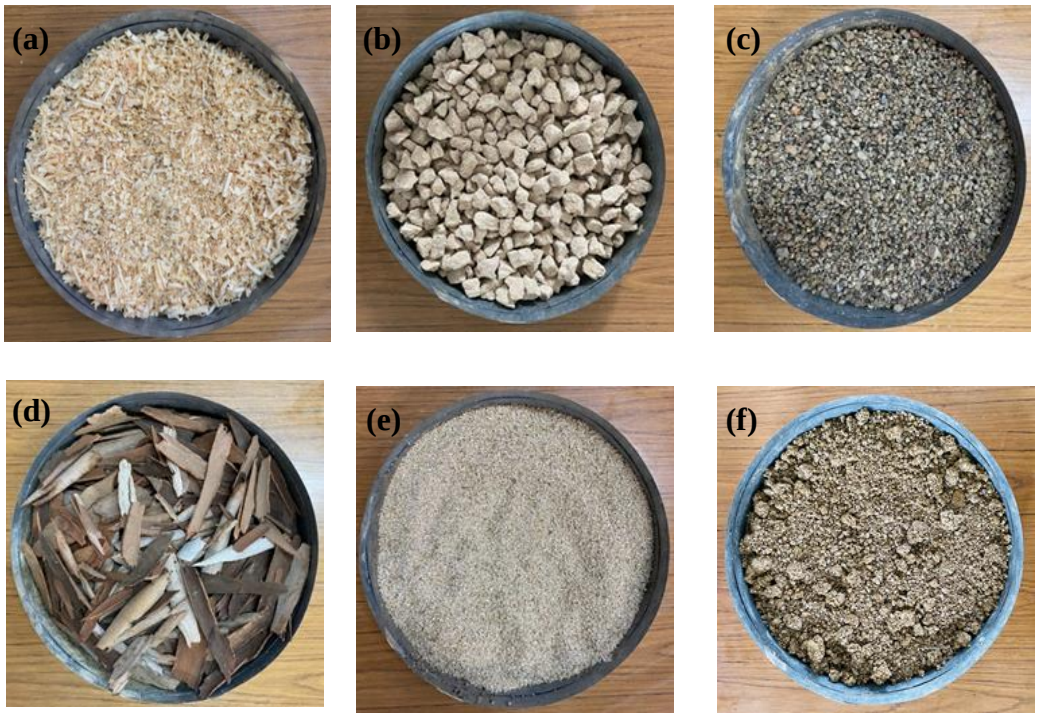

Figure 9: Various materials used in EVAP and DAEC mode (a) WoC, (b) YeS, (c) Pmc, (d) EuF, (e) Vmc, and (f) Vmc-$CaCl_2$

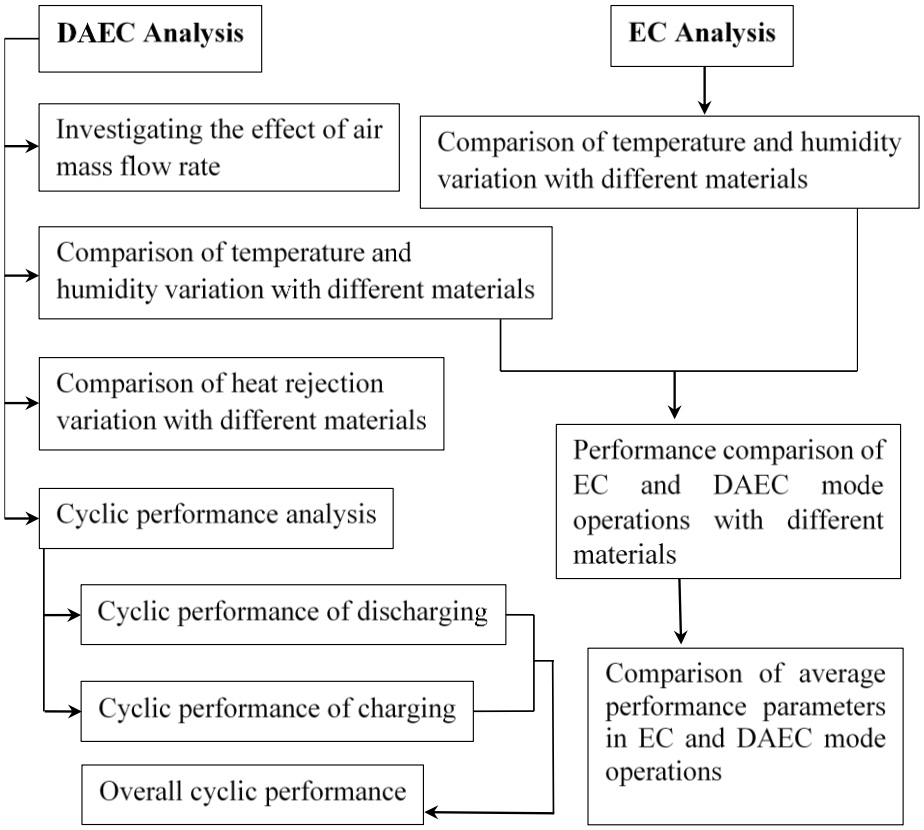

Figure 10: Flowchart of the experimental testing methodology

3.1.2 Synthesize of Vmc-Cacl$_2$ Composite Desiccant Material

The Incipient Wetness Technique (IWT) has been used for synthesizing the composite sorbent. In this study this impregnation method uses the natural wetting or liquid absorption capacity of the host matrix materials to fill the pore structure with the applied salt solution. For preparing Vmc-$CaCl_2$ composite, 43wt% saturated $CaCl_2$ salt solution was prepared. The purpose of preparing the saturated solution was to ensure that the maximum amount of desiccant is included in the synthesized composite for achieving high air dehumidification effect. More detailed information on the applied saturated $CaCl_2$ solution preparation method can be found in the research published previously [68].

The synthesis procedure applied for preparing the composite sorbent is presented in Figure 11.

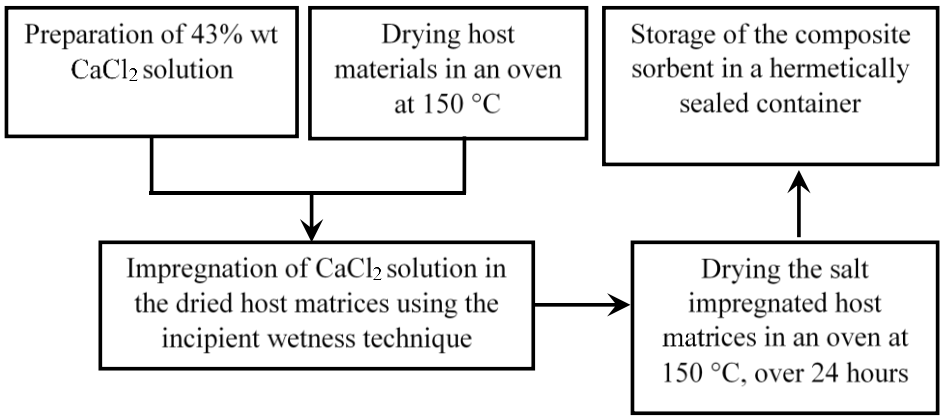

Figure 11: Flowchart of the synthesis procedure of the composite sorbent

3.1.3 Thermodynamic Analysis

The conducted experiments were used to compare the material performance in EC and DAEC modes and analyze the cyclic performance in the charging/discharging of DAEC mode. During the material performance assessment, system inlet temperature and relative humidity were set to 36-38 °C and 36-38% for simulating real summer-time weather inside the laboratory environment. Thermodynamic performance of the system was carried out based on the measured data at the sensor positions of; (z_1) desiccant dehumidification unit inlet/system inlet, (z_2) desiccant dehumidification unit outlet/heat exchanger inlet, (z_3) heat exchanger outlet/evaporative cooler unit inlet, (z_4) evaporative cooler unit outlet/system outlet and (z_5) ambient conditions. Here z_5 and z_1 represent the climate chamber inlet (ambient) and outlet conditions. It should be noted that climate chamber is not considered as part of the system in discharging operation as it is only used for increasing the air temperature and humidity to simulate the real summer conditions. However, in charging cycle, regeneration heat supplied

by the chamber (difference between z_5 and z_1) is considered in the analysis for calculating the COP_{th} of DAEC process.

In EC mode, as the desiccant material has not been used, only evaporative cooler inlet (z_3) and outlet (z_4) measurements were considered in the analysis. The temperatures and relative humidity were measured simultaneously in each state to determine the system performance.

The cooling rate obtained from the system is calculated by taking into consideration the inlet temperature, outlet temperature, and the flow rate of the processed air stream, and it is given in Equation (1) [69];

$$\dot{Q}_c = \dot{m}_a \Delta h = \dot{m}_a C_p (T_1 - T_4) \quad (1)$$

Absolute humidity is expressed as the mass of water vapor per unit mass of the dry air. Based on the measured data, absolute humidity, as a function of temperature and relative humidity, could be obtained with the Equation (2) [70];

$$w = 216.7 \left[\frac{\frac{RH}{100\%}.6.112.exp\left(\frac{17.62.T}{243.12+T}\right)}{273.15+T} \right] \quad (2)$$

The mass balance of water can be determined by consideration of the rate of water removal from the air through the desiccant dehumidification unit and the rate of water supply to the processed air across the EC unit. The water removal rate through the desiccant dehumidifier is directly related to the absolute humidity change of air across the desiccant dehumidification unit and the flow rate of the processed air [71] and can be obtained via Equation (3) and Equation (4);

$$\dot{m}_{w-r} = \dot{m}_a \, \Delta w_{1,2} \quad (3)$$

$$\dot{m}_{w-r} = \dot{m}_a (w_1 - w_2) \quad (4)$$

while the rate of water supply through the evaporative cooler is the function of the absolute humidity variation of air and flow rate of the air stream as given in Equation (5) and Equation (6);

$$\dot{m}_{w-a} = \dot{m}_a \, \Delta w_{4,3} \tag{5}$$

$$\dot{m}_{w-a} = \dot{m}_a \, (w_4 - w_3) \tag{6}$$

In the heat exchanger, the rate of energy rejected from the air is equal to the rate of energy gain by the water as obtained via Equation (7) and Equation (8);

$$\dot{m}_w \, \Delta h_w = \dot{m}_a \, \Delta h_a \tag{7}$$

$$\dot{m}_w c_p \left(T_{w,o} - T_{w,i}\right) = \dot{m}_a c_p \left(T_{a,i} - T_{a,o}\right) \tag{8}$$

During the experiments initial water temperature inside the tank was measured as ~25 °C where this temperature gradually increased depending on the rate of heat gain from the air as determined via Equation (8). The temperature variation of water inside the tank is discussed in section 3.1.3.

The wet-bulb effectiveness (ε_{wb}) is an important expression used to characterize the air saturation capacity of the developed evaporative and desiccant assisted evaporative cooling processes. It could be defined as the ratio of the actual temperature change of the air to the theoretical maximum temperature difference of air when it is fully saturated across the wet-bulb line. The wet-bulb effectiveness of DAEC and EC processes could be obtained via Equation (9) and Equation (10) respectively [72];

$$\varepsilon_{wb,DAEC} = \frac{T_1 - T_4}{T_1 - T_{wb}} \tag{9}$$

$$\varepsilon_{wb,EC} = \frac{T_3 - T_4}{T_3 - T_{wb}} \tag{10}$$

Where T_1 is the system inlet temperature, and T_4 is the system outlet temperature. All parameters are measured by the Sensirion SHTC3 type sensors except the wet-bulb temperature, which can be obtained from the Equation (11) [73];

$$T_{wb} = T.\tan^{-1}\left[0.151977.(RH\% + 8.313659)^{1/2}\right] + \tan^{-1}(T + RH\%) - \tan^{-1}(RH\% - 1.676331) + 0.00391838.(RH\%)^{3/2}\tan^{-1}(0.023101.RH\%) - 4.686035 \quad (11)$$

The dew point temperature (T_d) is defined as the temperature where the air becomes saturated as a result of the sensible cooling process (*i.e.*, without any increase in humidity content), and condensation occurs at constant pressure. It is derived by using Equation (12) [70];

$$T_d = 243.2\left[\frac{\ln\left(\frac{RH}{100\%}\right)+\left(\frac{17.62.T}{243.12+T}\right)}{17.62-\ln\left(\frac{RH}{100\%}\right)-\left(\frac{17.62.T}{243.12+T}\right)}\right] \quad (12)$$

The dew point effectiveness (ε_d) could be described as the actual temperature difference of air across the evaporative cooler to the obtainable temperature difference if it is cooled up to its dew point temperature. Dew point effectiveness for the DAEC and EC processes is determined via Equation (13) and Equation (14) respectively;

$$\varepsilon_{d,DAEC} = \frac{T_1 - T_4}{T_1 - T_d} \quad (13)$$

$$\varepsilon_{d,EC} = \frac{T_3 - T_4}{T_3 - T_d} \quad (14)$$

For DAEC performance evaluation, COP_t is an important measure. It is defined as the ratio of the cooling capacity ($\dot{Q}_c$) in discharging cycle to the total energy input ($\dot{W}_i$) to the system as given in Equation (15);

$$COP_t = \frac{\dot{Q}_c}{\dot{W}_i} \quad (15)$$

Total energy consumption of the system is obtained with Equation (16);

$$\dot{W}_i = \dot{W}_p + \dot{W}_f + \dot{W}_{eh} \quad (16)$$

Where $\dot{W}_p$ and $\dot{W}_f$ and $\dot{W}_{eh}$ represents the energy consumption of fan, pump and electric heating coils. By neglecting the heat losses, $\dot{W}_{eh}$ could be considered equal to

thermal energy gain of air ($\dot{Q}_h$) in regeneration process and it is calculated via Equation (17) and Equation (18);

$$\dot{W}_{eh} = \dot{Q}_h \tag{17}$$

$$\dot{W}_{eh} = \dot{m}_a(h_2 - h_1) \tag{18}$$

3.1.4 Uncertainty Analysis

The uncertainty analysis is important to evaluate the accuracy of the obtained experimental results. In this study, Gauss propagation law was used to determine the experimental uncertainties. The result w_R is obtained as a function of the independent variables x_1, x_2, x_3, …, x_n and w_1, w_2, w_3, …, w_n represents the uncertainties of the independent variables.

In the developed testing rig, four sensor locations were used for determining the temperature and relative humidity of the system inlet, desiccant chamber outlet, heat exchanger outlet, and EC outlet. Air mass flow rate ($\dot{m}_a$) was also measured at the outlet of the system during the experiments to minimize the pressure loss across the system. The experimental uncertainty, w_R, is expressed by the Equation (19) [74]:

$$w_R = \left[\left(\frac{\partial R}{\partial x_1}w_1\right)^2 + \left(\frac{\partial R}{\partial x_2}w_2\right)^2 + \left(\frac{\partial R}{\partial x_3}w_3\right)^2 + \cdots + \left(\frac{\partial R}{\partial x_4}w_4\right)^2\right]^{1/2} \tag{19}$$

It is obtained from the Equation (20) and Equation (21) that the wet-bulb effectiveness (ε_{wb}) is the function of T and RH measured in DAEC process, is subjected to uncertainty:

$$\varepsilon_{wb} = f(T_1, T_4, RH_1) \tag{20}$$

The total uncertainty for the calculation of the ε_{wb} is as;

$$w\varepsilon_{wb} = \left[\left(\frac{\partial \varepsilon_{wb}}{\partial T_1}w_{T_1}\right)^2 + \left(\frac{\partial \varepsilon_{wb}}{\partial T_4}w_{T_4}\right)^2 + \left(\frac{\partial \varepsilon_{wb}}{\partial RH_4}w_{RH_1}\right)^2\right]^{1/2} \tag{21}$$

where w_{T1}, w_{T4}, w_{RH1} are the instrument uncertainties of temperature sensor and relative humidity sensor are ±0.2 ℃ and ±2% respectively. The partial derivatives are the sensitivity coefficient of the ε_{wb} to each of the measured variables. In order to obtain the partial derivatives, Equation (11) is inserted in Equation (9). By this way, ε_{wb} is formulated as a function of T_1, T_4, RH_1 and then partial derivatives of ε_{wb}, based on this parameters, are obtained. The values of the sensitivity coefficients are determined as follows:

$$\frac{\partial \varepsilon_{wb}}{\partial T_1} = +0.0509 \tag{22}$$

$$\frac{\partial \varepsilon_{wb}}{\partial T_4} = -0.0419 \tag{23}$$

$$\frac{\partial \varepsilon_{wb}}{\partial RH_1} = -3.422 \tag{24}$$

where, T_1 = 37.3 °C, T_4 = 22.9 °C and RH_1 = 36.9%.

By inserting the uncertainties of temperature and humidity sensors (w_{T1}, w_{T4}, w_{RH1}) and their calculated sensitivity coefficients (Equations 22-24) in Equation 21, the random uncertainty of ε_{wb} is obtained as 0.069. Thus, uncertainty rate in ε_{wb} can be obtained with the following relation. In order to determine the maximum uncertainty of ε_{wb}, the obtained minimum value of that parameter, in the experimental analysis of DAEC is considered, which is equal to 102% as it is given in Equation (25).

$$\frac{w\varepsilon_{wb}}{\varepsilon_{wb}} \times 100 = \frac{0.069}{1.02} \times 100 = 6.83\% \tag{25}$$

3.2 Results and Discussion

The comparison between material performances in EC and DAEC modes and the cyclic performance of charging/discharging in DAEC mode were analyzed experimentally.

Tests have been conducted in two different modes; (i) direct EC and (ii) DAEC. The inlet temperature and relative humidity were kept nearly steady, at 38 ˚C and 38% respectively. For the selected inlet conditions, EC can theoretically reduce the air temperature up to a minimum of 26 °C, which is above the human comfort range. However, such inlet conditions were purposely selected in order to investigate the percentage improvement of air cooling performance with the use of desiccant in hot-humid ambient conditions.

According to the following evaluations, results are obtained for EC and DAEC modes:

1. Temperature and relative humidity variations;
2. Water consumption and cooling performance;
3. Cooling effectiveness, wet-bulb effectiveness, dew-point effectiveness, and COP of the system;
4. Cyclic performance of DAEC in charging/discharging cycles.

The coverage and the limitations of the performed experiments are listed as follows;

- In any real life application of EC and DAEC, based on the calculated cooling demand and the required air change per hour (ACH = 5-9) of the conditioned space, optimum air flow rate should be determined and kept steady. However, the present study focuses on the investigation of desiccant and ECPM performances at different air mass flow rates. Therefore, air flow rate is not kept constant and considered as a variable in the study.
- The developed DAEC system is designed at small scale with the purpose of performance evaluation of different materials. Therefore, pilot testing and performance monitoring of DAEC system in a real building is not within the scope of the performed study.

- The main concern of the study was to evaluate the material performances in EC and DEAC processes. With this purpose, in order to keep the coverage of the study focused, in all tests, inlet temperature and relative humidity of air were kept steady. Therefore, system performance analysis at different inlet air temperature and relative humidity is considered as a limitation of the present study.
- Presented study covers testing of different ECPM materials in DAEC and EC modes under different mass flow rates. Additionally, cyclic performance of the desiccant material is investigated for charging/discharging modes. Due to the large number of experiments proposed to be performed within the study, the experimental duration is limited to two hours in all tests.

3.3 DAEC Analysis

3.3.1 Effect of Air Mass Flow Rate on DAEC Performance

Temperature difference, and cooling rate variation with four different air mass flow rates ($\dot{m} = 0.03, 0.04, 0.05$ and 0.08 kg/s) over two hours of testing (for each flow rate) are shown in Figure 13. The main purpose of performing experiments at different flow rates was to investigate the impact of air flow rate on the cyclic performance of desiccant (Vmc-$CaCl_2$) material and different ECPMs.

Figure 12 demonstrates the experimentally obtained average values of DAEC process on the psychometric chart for different air mass flow rates. As it is seen from point (1) (desiccant dehumidification unit inlet) to point (2) (desiccant dehumidification unit outlet), the temperature increased from 36-38 ˚C to 43-46 ˚C range, depending on the air flow rate. The absolute humidity of air is reduced (Δw) between 4.5→2.5 (g water/kg dry air) for the increasing mass flow rate in the range of 0.03→0.08 kg/s. With nearly the same moisture content, airflow passed through the air to a water heat

exchanger at point (3), while during this passage, the temperature of the air is decreased to a range of 34.9-37.7 ˚C. As seen from the figure, for the highest mass flow rate of 0.08 kg/s, heat exchanger outlet temperature is 37.7 °C, whereas for the lowest mass flow rate it is 34.9 °C. At the EC unit outlet (4), through water evaporation, the temperature dropped considerably and minimum and maximum system outlet temperatures of 22→25 °C were achieved The absolute humidity of product air was also between 15.8→16.2 g water/kg dry air.

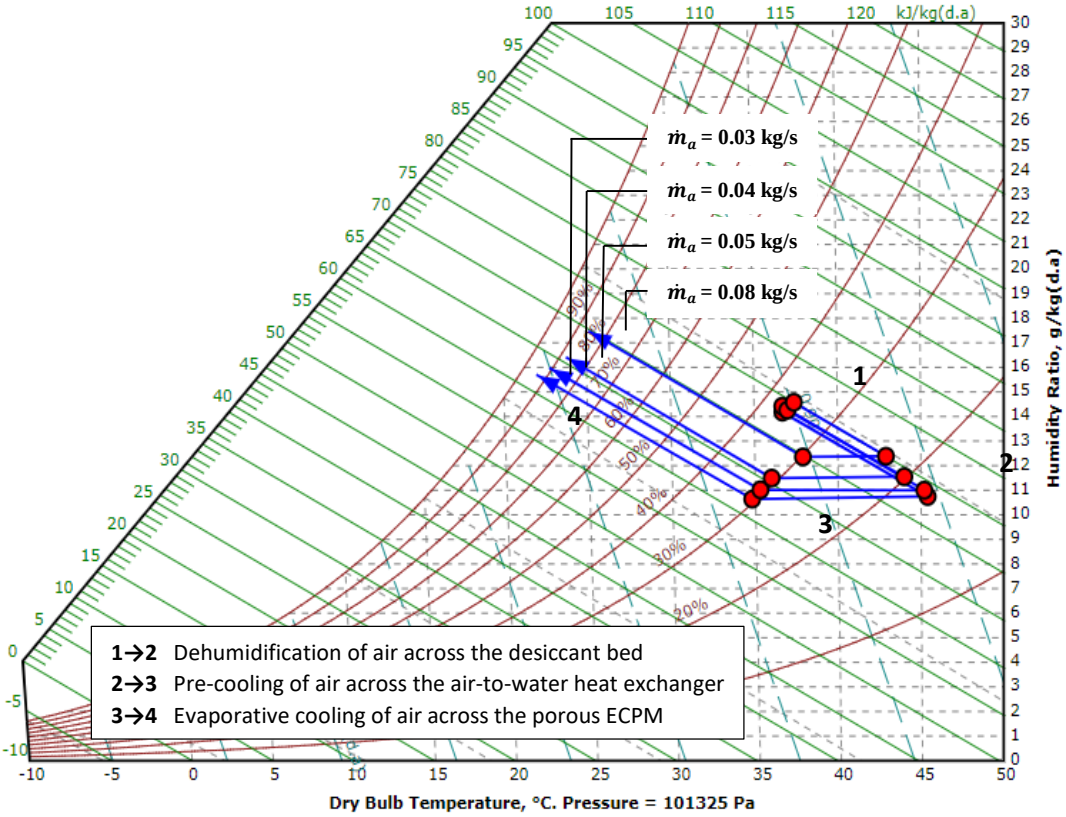

Figure 12: The psychometric process of DAEC with different air mass flow rates

According to the Figure 12, in all tests, relative humidity of the air at point (1) was between 36-38%, while after passing through the desiccant material at point (2), it experienced a fall to 18-23% range. Later at the outlet of the air to water heat exchanger (3) it increased to nearly 30%. Finally, at the outlet of the system (4) due to the

evaporation of water, the relative humidity of air reaches to a pick in the range of 88-94% with different air flow rates. Even though the obtained air cannot be directly utilized in buildings due to the high humidity, proposed system can be cascaded to achieve the same cooling affect with lower outlet relative humidity. Proposed DAEC unit could also be coupled with air-to-air heat exchangers to provide cooling effect without increasing the moisture level of the indoor environment. Alternatively, integration of DAEC unit with air sourced heat pump could be an opportunity to enhance the cooling COP of the VC based A/C units. It should be noted that the main concern of the present study is to comparatively investigate the performance of different organic materials, at different operating conditions for DEAC applications. Therefore, DAEC process design and optimization, also investigation of building indoor comfort are out of the scope of this research.

As seen in Figure 13(a), temperature difference between system inlet and outlet of the DAEC with mass flow rate of 0.08 kg/s shows the highest value of ~16 ℃. The cooling rate variation for different air mass flow rates is demonstrated in Figure 13(b). The cooling rate varied between 0.54–0.41 kW, 0.7–0.59 kW, and 0.75–0.55 kW for the air mass flow rates of 0.03, 0.04, and 0.05 kg/s, respectively. On the other hand, for 0.08 kg/s flow rate of air, cooling rate varied between 1.08-1.25 kW. Results showed that with the increasing air mass flow rate, achieved temperature drop increases, which is most likely because of the increasing rate of water evaporation with the increase in airflow rate. However, with a high mass flow rate, the desiccant material is expected to get saturated in a shorter period; therefore, at high air flow rates discharging (cooling) process could last shorter.

a) b)

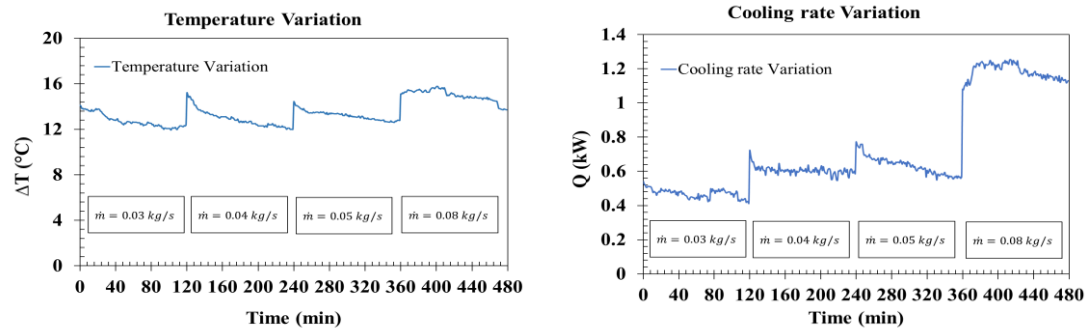

Figure 13: Effect of air mass flow rate on DAEC (a) temperature difference and (b) cooling rate

3.3.2 Comparison of Temperature Variation in DAEC Mode with Different Materials

Temperature variation of the air in DAEC tests were presented in Figure 14(a-e) for Vmc-$CaCl_2$/WoC, Vmc-$CaCl_2$/YeS, Vmc-$CaCl_2$/Pmc, Vmc-$CaCl_2$/EuF and Vmc-$Cacl_2$/Vmc, respectively. As can be seen in Figure 14(a-e), due to the sorption process in the desiccant chamber, the temperature of the air rose to 44–47 °C initially and showed a gradual drop over 2 h testing period for each material in all tests. Among all tested materials, WoC performed the most promising performance where the outlet temperature of air dropped to 23 °C initially and remained below 25 °C over the testing duration. With other evaporation materials, the outlet temperature varied between 25-28 °C.

a) b)

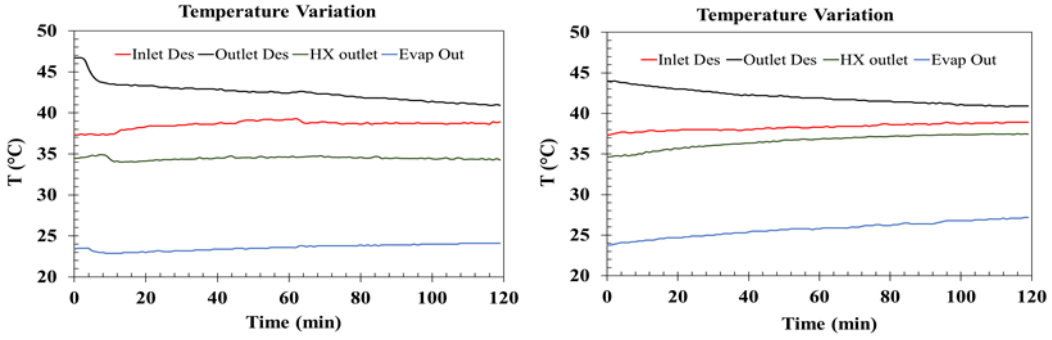

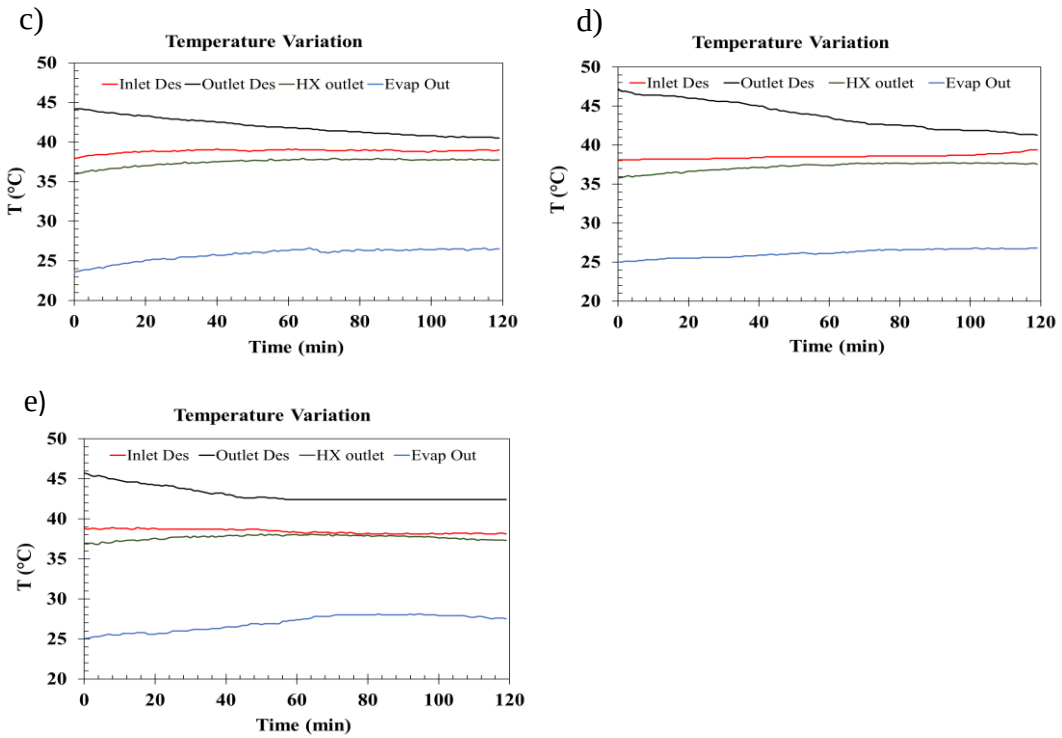

Figure 14: Temperature variation in DAEC mode for different materials (a) Vmc-$Cacl_2$/WoC, (b) Vmc-$Cacl_2$/YeS, (c) Vmc-$Cacl_2$/Pmc, (d) Vmc-$Cacl_2$/EuF and (e) Vmc-$Cacl_2$/Vmc

3.3.3 Comparison of Heat Rejection Variation in DAEC Mode with Different Materials

Pre-cooling of the air, following the moisture absorption inside the desiccant unit, is highly crucial in DAEC systems for enhancing the cooling capacity. In the investigated system, an air to water heat exchanger made up of copper pipes and aluminum fins is utilized for rejecting the generated sorption heat to a water tank. The accumulated thermal energy inside the tank is released to the surroundings after the discharging (cooling) cycle is completed; therefore, the water tank is re-used in the repeating discharge cycle as a heat sink for absorbing the sorption heat. Here it should be noted that the investigated DAEC system uses a a fixed-bed desiccant unit therefore it cannot provide continuous operation. However, it could be utilized as a storage unit to store

the energy (i.e solar energy) in the from of coolth to be used when the cooling load increases.

Figure 15 presents the heat rejection rate from the air to the water tank via the heat exchanger for various materials. As it is clear, heat rejection shows a gradual drop over two hours of testing. For different ECPMs, heat rejection rate to the water tank does not show a considerable variation as evaporative cooler is placed after the heat exchanger. The slight variations of heat rejection rate in different tests with different materials were mainly due to the initial state of the desiccant (*i.e.* any residual moisture inside the desiccant after charging), small fluctuations in inlet air conditions (temperature and relative humidity) and small differences of the intial water temperature inside the water tank in different tests. For EuF, the heat rejection varies between 0.85 kW and 0.3 kW while for WoC, YeS, Pmc, and Vmc changes in the range of 0.80→0.19 kW, 0.73→0.28 kW, 0.65→0.22 kW and 0.71→0.38 kW respectively. In the investigated DAEC unit, a water tank with 0.05 m^3 volumetric capacity is utilized. The initial water temperature inside the tank was nearly 25 °C in all experiments. As the water temperature inside the tank increased during the operation, the rate of heat rejection from the air to the water showed a decreasing trend. The average heat transfer rate to water over two hours of operation was found ~0.5 kW for all materials, and the average temperature increase of water was nearly 6 °C/hour. Testing results showed that the utilized water tank capacity is insufficient, and water tank with larger volume is required to provide steady heat rejection rate in heat exchanger without any performance drop. In Cyprus, mostly 1 m^3 thermosyphon water tanks are used for storing cold water in solar water heating systems. Therefore in real applications, where DAEC systems are integrated with solar collectors for regeneration, such water tanks could be used for rejecting the heat from the DAEC

system. In that case, due to the large size of the water tank, the heat rejection rate is expected to be constant where the rate of temperature increase of water inside the tank could be ~0.3 °C/hour per kW cooling capacity of DAEC system As a result, a steady output temperature (~22-23 °C) could be achieved at the DAEC outlet for the inlet conditions of T_{in}=38 °C and RH_{in} =38%.

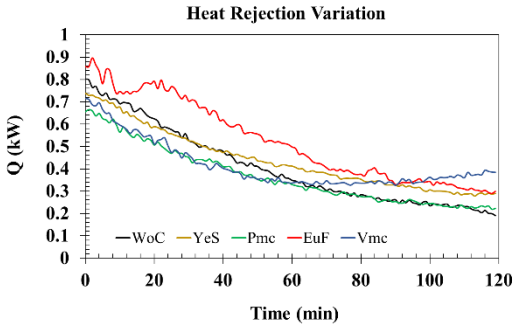

Figure 15: Heat rejection variation in DAEC mode for different materials

3.3.4 Cyclic Performance Analysis of DAEC Operational Mode

Cyclic performance of charging

In DAEC applications, mainly solar energy is utilized as the heat source, where low/medium temperature solar collectors are mostly used. Accordingly, the regeneration temperature of the desiccant material should be achievable with residential-scale solar collectors (*i.e.*, <100 °C). Furthermore, the regeneration potential of the desiccant at different temperatures should be determined for effective solar-driven DAEC design in real-life applications. For that propose, within the study, the developed DAEC system is regenerated (dehydration of desiccant material) at 60 °C, 70 °C and 80 °C under laboratory conditions and the regeneration characteristics of the desiccant material at different temperatures were evaluated (Please see: Figure 16(a)). Additionally, WoC was selected as the evaporation material as it provided the

most promising results when compared to the other candidate materials (Please see: Figure 14).

The relative humidity of three cycles in the charging mode is shown in Figure 16(b). As it is seen, with the increasing charging temperature, relative humidity shows a decreasing trend. According to the measured temperature and relative humidity at the inlet and outlet of the desiccant chamber, moisture removal rates were determined. By doing that, it is proposed to analyze the impact of the charging temperature on the regeneration potential of the desiccant material. Based on the calculated values at T_{reg} of 60 °C, 70 °C and 80 °C, moisture removal rates were found as 6.60 g/min, 7.85 g/min, and 15.27 g/min respectively. Results showed that the variation of T_{reg} between 60→70 °C increases desorption rate by 18.9%, while the change of T_{reg} in the range of 70→80 °C makes the desorption rate double. Where possible, using T_{reg}>80 °C could considerably reduce the regeneration period, therefore, increase the regeneration and cyclic efficiency.

a) b)

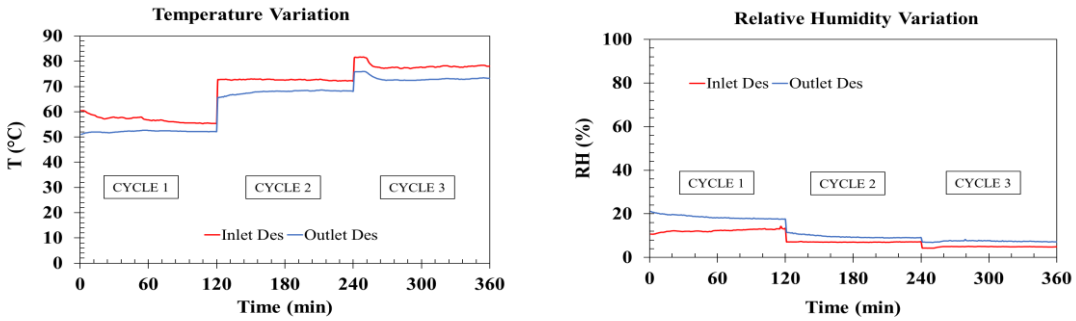

Figure 16: Cyclic performance of charging (a) temperature variation and (b) relative humidity variation

Cyclic performance of discharging

The temperature variations of air in discharging mode, for different parts of the system such as desiccant inlet, desiccant outlet, heat exchanger outlet, and evaporator outlet, are demonstrated in Figure 17(a). The inlet air temperature was nearly constant at 38 °C in all cycles, while the outlet temperature showed an increasing trend over time and rose to 22-23 °C at the end of the cycles. On the other hand, at the desiccant outlet, relative humidity initially dropped to ~20 % due to the high sorption capacity of the desiccant, whereas it was above 30% at the end of two hours of testing (Figure 17(b)). Results showed that desiccant material provides a nearly steady performance over the two hours of testing. However, in the longer term of operation, a gradual rise of the outlet temperature is expected as the desiccant material gets saturated with moisture.

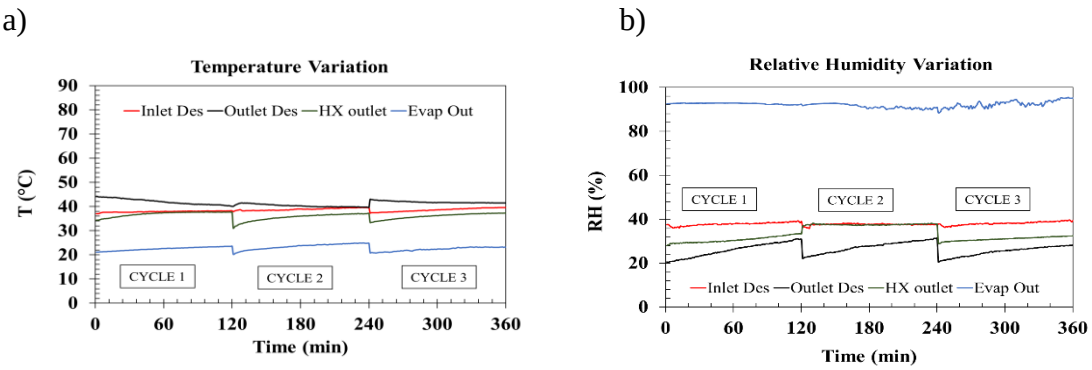

Figure 17: Cyclic performance of discharging (a) temperature variation and (b) relative humidity variation

Overall cyclic performance

The calculated rate of mass changes for the tested materials after discharging and charging cycles are illustrated in Figure 18(a), where positive and negative mass changes indicate the amount of water absorbed and desorbed, respectively. During the tests, initially, the hydrated desiccant is charged at 60 °C then the cooling (discharge) cycle is performed. After that, the desiccant is regenerated at 70 °C, and the second

cooling cycle is performed. Finally, the desiccant is charged at 80 °C, and the final cooling cycle is conducted. Between the charging and discharging processes, desiccant material is removed from the system and kept in a hermetically sealed container until the system reaches thermal equilibrium with the surroundings. Based on the obtained results, the average moisture absorption/desorption rates in three repeating cycles were found as 13.08/6.60 g/min, 18.96/7.85 g/min, and 19.82/15.27 g/min. Accordingly, the total amount of moisture absorbed/desorbed in these cycles were determined as 1569.63/792.20 g, 2275.92/941.32 g, and 2378.61/1832.58 g respectively.

Overall cyclic analysis results showed that, with the rise of T_{reg} from 60 to 70 °C, there is no substantial increase in moisture desorption rate (<20%). However, increasing the T_{reg} to 80 °C doubles the amount of moisture desorption. Therefore, in real-life applications, minimum T_{reg} of 80 °C should be applied, which is possible to achieve in hot climates (*i.e.*, Cyprus) with conventional flat plate collectors. On the other hand, total moisture absorption trends (See: Figure 18(b)) demonstrate a sharp increase between first and second discharging cycles, whereas, in the second and third cycles, the amount of moisture absorption was found in close approximation.

a)

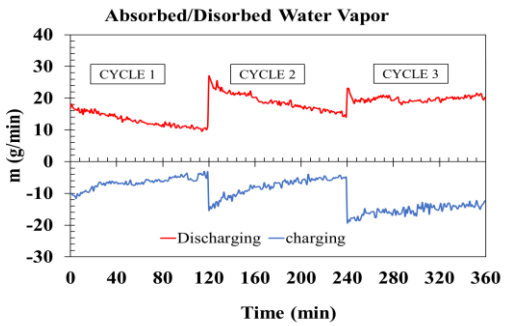

b)

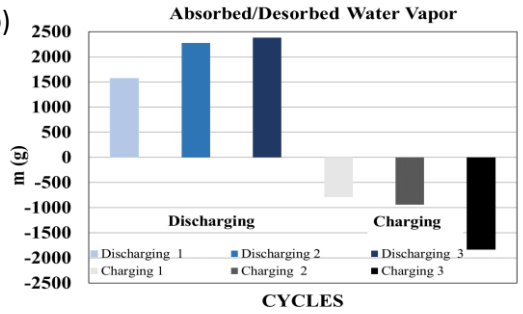

c)

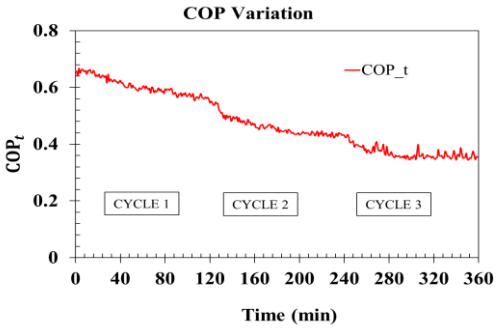

Figure 18: Overall cyclic performance (a) moisture absorption/desorption rate variation, (b) cumulative moisture absorption/desorption and (c) COP variation

In addition to the cyclic mass change of the desiccant, the COP_t of the DAEC unit in cyclic operation is presented in Figure 18(c). As seen, the first cycle with T_{reg} of 60 °C, showed the best COP_t, where it varied between 0.71→0.59. In the second and third cycles, by an increment of heat supply in charging mode, COP_t showed a decreasing trend. At T_{reg} of 70 °C and 80 °C, COP_t varied in the range of 0.55-0.43 and 0.41-0.38, respectively. Here it is important to note that; at T_{reg} of 60 °C and 70 °C, there is a gradual drop in COP_t with time, whereas, it is almost steady at T_{reg} of 80 °C. This is due to the insufficient regeneration of the desiccant at lower temperatures, thereby the reduced moisture sorption capacity of it over time. On the other hand, obtained steady COP_t at 80 °C demonstrates sufficient moisture desorption from the desiccant, where the desiccant is expected to provide similar performance over the repeating cycles at that T_{reg}. However, regenerating the material at lower temperatures could lead to a drop in COP_t in the repeating cycles.

In real applications, system could be regenerated with solar collectors, which directly heat the regeneration air. Alternatively, photovoltaic panels could be used to power an electrical heater which could be used to heat the regeneration air. In both options, similar COP_t values obtained in this study could be achieved for the DAEC system,

however conversion efficiency of solar radiation to useful heat is 4-5 times higher with solar collectors. Adding the lower investment costs of solar collectors, they could be a more suitable option to be employed for regeneration of desiccant material in DAEC applications.

3.4 Comparison of Temperature and Relative Humidity Variation in EC Mode with Different Materials

Following the conducted experiments on DAEC mode operation, desiccant material is removed, and the system is tested in EC mode for performance comparison. The outlet temperature and relative humidity variation of the air for direct EC tests were presented in Figure 19(a-b). Figure 19(a) illustrates the outlet temperature variation of air (for T_i = 38 ℃) with the use of several different evaporative materials (*i.e.*, WoC, YeS, Pmc, EuF, and Vmc). During two hours of testing, WoC showed the best performance, where the outlet temperature was nearly 27 ℃. The unfavourable performing material was determined as Pmc with an average outlet temperature of 32 ℃. In DAEC mode operation, average outlet temperatures obtained with WoC and Pmc were 23 °C and 26 °C, demonstrating the considerable performance improvement with the use of desiccant material.

a) b)

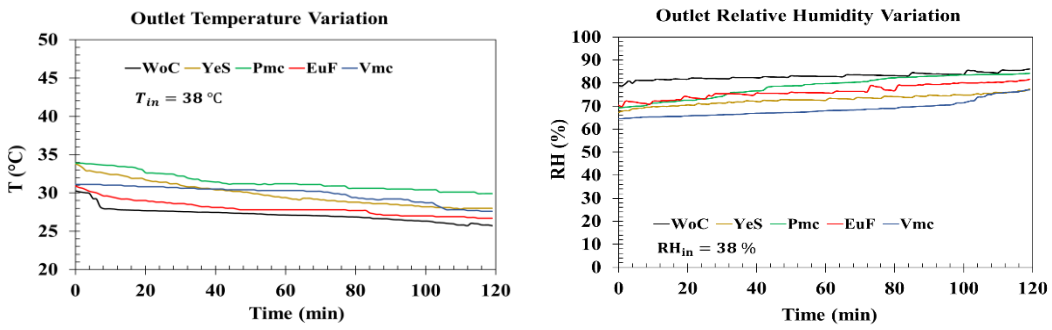

Figure 19: Comparison of various materials in EVAP mode based on (a) Outlet air temperature, (b) Outlet air relative humidity

The relative humidity variations of air in EC mode operation is presented in Figure 19(b). As seen, relative humidity ranges between 79–86%, 67–78%, 70–84%, 70–82%, and 64–77% for WoC, YeS, Pmc, EuF, and Vmc respectively, for the inlet relative humidity of 38%. According to the results, the best evaporation capacity is obtained with WoC, which resulted in the highest temperature drop of air across the evaporative cooler (Please see: Figure 19(a)).

3.5 Comparison of Material Performances in EC and DAEC Mode with Different Materials

The wet-bulb effectiveness variation of different materials in EC and DAEC modes are represented in Figure 20(a-b), respectively. As seen, in EC mode, WoC has the best wet-bulb effectiveness varying between 76-89%, while EuF is in second place, demonstrating a promising performance between 66 and 81%. Pmc provided the lowest wet-bulb effectiveness between 38 and 66%. The wet-bulb effectiveness for YeS and Vmc was nearly the same at the end of the testing at about 62-66%, whereas initially, Vmc provided nearly 20% higher effectiveness compared to YeS. The main reason is that the Vmc has better water holding capacity due to its porous nature, thereby saturates in a short time. As a result, it provides a steady performance in the EC process. On the other hand, YeS becomes saturated in a more extended period due to its rigid structure and lower porosity; thereby, it provides initially lower performance, which shows an increasing trend by the time.

In the DAEC mode, the behavior of materials is almost steady. However, the wet-bulb effectiveness values experienced a significant rise in all tests when compared to the EC mode operation. The peak wet-bulb effectiveness is obtained with WoC with a steady rate of 122%, while the worst performance referred to Vmc with an average

value of 102%. The effectiveness for Yes, Pmc and EuF has a steady alteration between 104-106% % at the end of testing. Results showed that, for different materials, a wet-bulb efficiency enhancement in the range of 26-50% was obtained in DAEC compared to EC mode operation. As sub-wet bulb temperature and effectiveness values were achieved in DAEC mode, dew-point effectiveness of EC and DAEC system were also analyzed for a more in-depth evaluation of the system performances.

The dew-point effectiveness variation of various materials in EC and DAEC mode are shown in Figure 20(c-d), respectively. As it is clear from Figure 20(c), in the EC process, WoC has the best dew-point effectiveness changing between 53-65%. After WoC, EuF experienced the best behavior with a variation between 47-58%. Yes, and Vmc showed nearly a similar alteration from 44 to 47%. Pmc demonstrated the worst behavior with dew-point effectiveness between 27-47%. In the DAEC process (Figure 20(d)), much higher dew-point effectiveness values were obtained. Vmc-$CaCl_2$/WoC couple provided steady dew-point effectiveness at 90%, where Vmc-$CaCl_2$/Pmc was the second highest with the values in the range of 88-74%. Vmc-$CaCl_2$/YeS and Vmc-CaCl2-EuF were in close approximation in the range of 82-71%. $CaCl_2$/Vmc demonstrated a relatively poor performance compared to other couples with a range of 78-64%.

The cooling rate variation of EC and DAEC modes were illustrated in Figure 20(e-f). In the EC mode, YeS and Pmc have nearly close behavior with a constant increase from 0.42 to 0.60 kW while Vmc alters around 0.62 kW. Although the cooling rate for EuF was around 0.66 kW at the beginning of the testing, it experienced a reduction to 0.60 kW at the final point. WoC provided the most exceptional cooling rate of around 0.95 kW. Similarly, in DAEC mode, the highest cooling rate of 1.24 kW achieved by

WoC, while YeS, Pmc, EuF, and Vmc had a cooling rate of around 0.90 kW after two hours of testing.

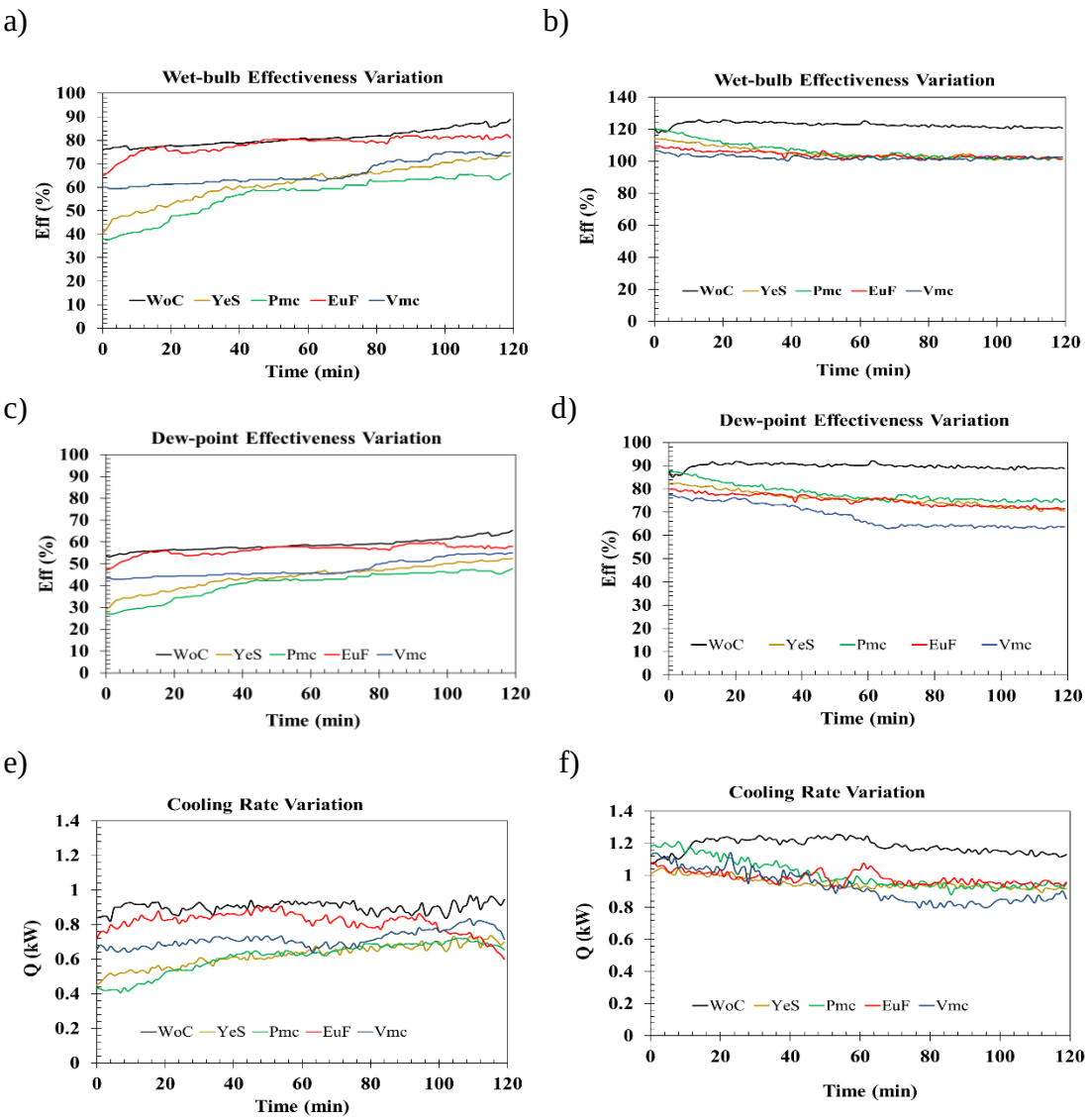

Figure 20: Variation of several performance parameters in EC and DAEC processes with the use of different ECPMs (a) EC wet-bulb effectiveness, (b) DAEC wet-bulb effectiveness, (c) EC dew-point effectiveness, (d) DAEC dew-point effectiveness, (e) EC cooling rate, and (f) DAEC cooling rate

According to the experimental results presented above, average values of the performance parameters of tested materials at a constant air mass flow rate of 0.08 kg/s were calculated and presented in Table 4. Based on the results, WoC and Pmc provided the highest and lowest ΔT_{ave} of 10.6 °C and 7.5 °C respectively. On the other hand,

best ΔT_{ave} in DAEC mode was achieved by WoC with a value of 15 °C, while the rest of the materials provided similar ΔT_{ave} values in the range of 11.8- 12.4 °C. According to the results, the achieved maximum ΔT_{ave} value of DAEC was 41.5% higher in comparison with EC mode operation. Moreover, $\varepsilon_{wb,ave}$ of DAEC and EC were found in the range of 56-81% and 102-122% respectively. Similar to ΔT_{ave}, maximum $\varepsilon_{wb,ave}$ is obtained with WoC in both operting modes. Due to the moisture absorption of desiccant and enhancement of humidification capacity of air, maximum $\varepsilon_{wb,ave}$ is increased by 50.6% in DAEC process when compared to EC. In accordance with the $\varepsilon_{wb,ave}$, a considerable improvement of $\varepsilon_{d,ave}$ is observed in DAEC process. While the $\varepsilon_{d,ave}$ in EC was between 41-59%, it varied in the range of 68-90% in DAEC process. The perentage difference between the maximum $\varepsilon_{d,ave}$ of both processes is 52.4%, which demostrates the significant impact of desiccant on the cooling performance in hot-humid climate conditions (T >35 °C, RH>35%).

The $\dot{Q}_{c,ave}$ values in DAEC process were in the range of 0.93-1.18 kW for different ECPMs. On the other hand, in EC mode operation, these parameters varied between 0.61-0.90 kW respectively. The highest values were obtained with WoC, while the percentage variation of $\dot{Q}_{c,ave}$ in DAEC and EC modes with the use of different ECPMs were 26.8% and 32.2%. This outcome indicates the considerable impact of ECPM on the performance of both processes. On the other hand, when DAEC and EC processes are compared, $\dot{Q}_{c,ave}$ was found 31.1% and higher in DAEC mode. Therefore, it could be concluded that by employing the desiccant, the cooling capacity of EC could be enhanced by >30%. This result demonstrates that DAEC could be a suitable A/C method in humid climates, where EC is not applicable due to the high moisture content of ambient air.

Table 4: Average obtained values of the performance parameters of tested materials

Operating parameter	$\Delta_{T,ave}$ (°C)		$\varepsilon_{wb,ave}$ (%)		$\varepsilon_{d,ave}$ (%)		$\dot{Q}_{c,ave}$ (kW)	
	Operating Mode							
ECPM	EC	DAEC	EC	DAEC	EC	DAEC	EC	DAEC
WoC	10.6	15.0	81	122	59	90	0.90	1.18
YeS	7.8	11.8	62	105	44	76	0.62	0.95
Pmc	7.5	12.4	56	106	41	79	0.61	1.0
Euf	10.0	12.3	78	104	56	75	0.81	0.98
Vmc	8.8	12.1	66	102	47	68	0.71	0.93

Chapter 4

DESIGN, DEVELOPMENT AND INVESTIGATION OF A SOLAR-DRIVEN DAEC SYSTEM

DAEC system can be driven by low grade thermal energy, such as renewable energy sources (i.e. solar energy), which has a large energy saving potential. Based on the available literature, none of the previously performed literature review provided in chapter 2 have been conducted on the designing of a solar-driven DAEC system using mentioned candidate materials in hot and humid climate. In this section, a potential low-cost implementation method of the investigated DAEC systems in real building applications is presented. Moreover, this chapter presents the design and assembling details of a novel solar-driven DAEC unit. The performance of the system and the experimental results were discussed in this chapter.

4.1 Design, Assembling and Thermal Analysis of Solar-Driven DAEC System

The 2-D view of the designed solar-driven DAEC unit is shown in Figure 21. The proposed concept consists of a solar water heating system, desiccant chamber, and the evaporative cooling chamber. As seen, in charging mode the water stored in the storage tank (1) flows to the flat plate solar collector. After circulation of water in the solar collector, the hot water goes to the storage tank (2) for transferring to the air to water heat exchanger (3). Meantime, the water in the heat exchanger after passing by a pump (4) sends back to the storage tank (5) to complete the cycle of the system. At point (6)

the ambient air firstly, passes through a centrifugal fan then goes to the heat exchanger (7) to gain heat and achieve desirable regeneration temperature. Lastly, the hot air enters the desiccant chamber (8) to desorbs water vapor of desiccant material and complete the regeneration process. However, in discharging mode the after passage of ambient air through centrifugal fan (6) it enters to the desiccant chamber (8) since the heat exchanger in this mode is deactivated (7). In desiccant chamber the desiccant material absorbs the moisture of air and decrease the humidity of the air while increasing the air temperature. The hot and dry air transferred to the air-to-water heat exchanger (9) to remove the generated heat of the sorption and cool the process air. Thereafter, the moderate, low humidity air goes to EC system (10) to pass through EC pad. As a consequence of water evaporation, the cool air will be the outcome of the system (14). The points (11-13) show the water circulation between the water tank and air-to-water heat exchanger by a pump.

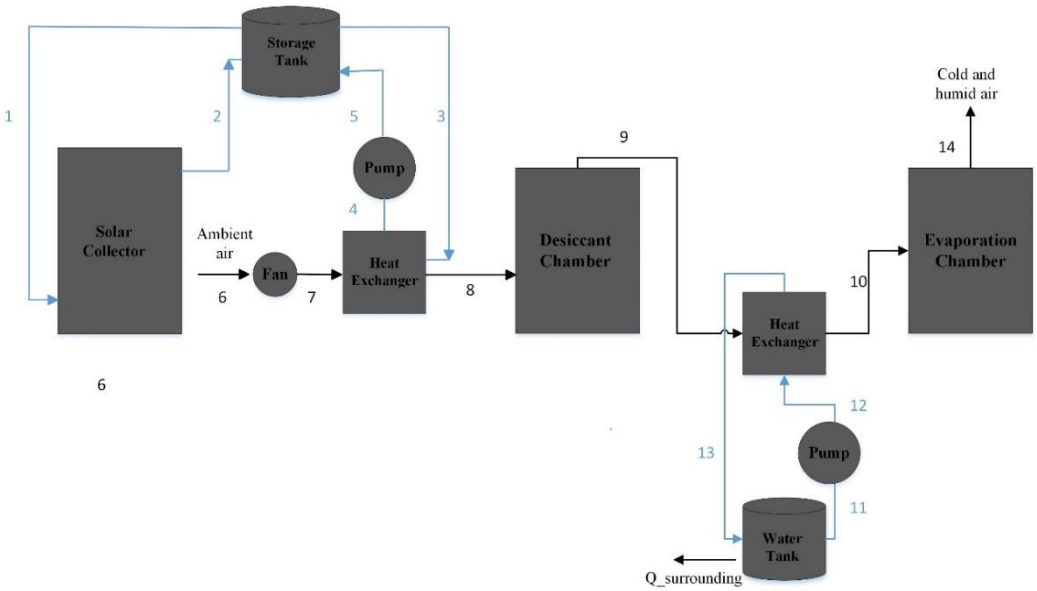

Figure 21: 2D view of the storage type solar-driven DAEC system

The proposed solar-driven DAEC unit could be used as a storage type cooler, where it is charged during day time with collector, and the cooling could be produced in the afternoon and night time to reduce the usage of vapor compression A/C thereby to reduce the associated costs and emissions. Despite the peak cooling loads occur between 12:00-15:00 hours in NC, between 15:00-24:00 hours still, the ambient temperature is above the comfort level (Please see: Figure 22(a-b)), thereby space cooling is needed within that period.

a) b)

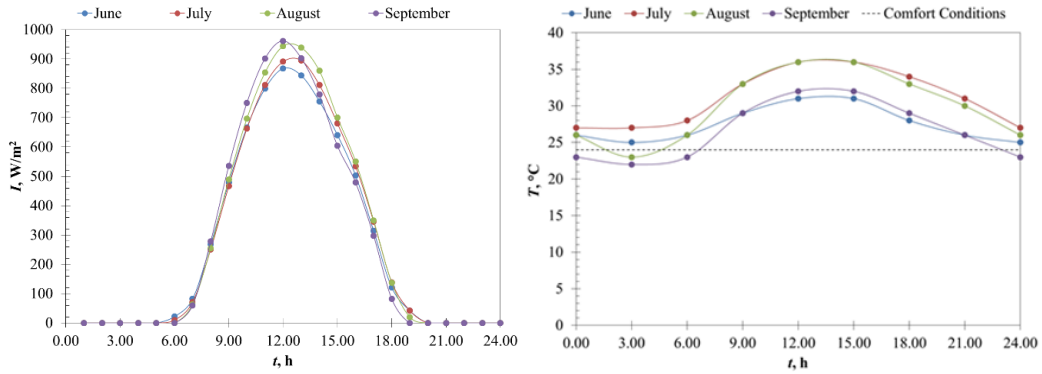

Figure 22: (a) The hourly solar intensity and (b) ambient temperature in months June, July, August, and September in NC [75-76]

In order to measure the temperature and humidity of the different parameters in charging mode, a thermometer with four channel has been used to measuring the temperature on points (1-4) with 1°C accuracy. Moreover, two SHTC3 Sensiron type sensors were installed at points (8) and (9) to measuring inlet and outlet desiccant temperature and humidity. Also one sensor was installed at point (6) to measure the ambient temperature and humidity. Finally, a PASCO-GLX airflow meter was used to measure the airflow speed at the outlet of the charging process at point (9). During the charging process the Eppley Precision Spectral Pyranometer (PSP) was used to measuring the solar intensity on the solar collector. On the other hand, in discharging

process five SHTC3 Sensiron type sensors have been installed to measure temperature and humidity of ambient condition (6), desiccant inlet (8), desiccant outlet (9), heat exchanger outlet (10), and evaporation chamber outlet (14) of the system. A PASCO-GLX airflow meter was used to measure the airflow speed at the outlet of the system (14). Also a thermometer has been used to measure the temperature of the water tank. The range of each measured parameter, its accuracies and the percentage errors due to the utilized measurement devices were listed in Table 5.

Table 5: Standard uncertainty, error, and measuring range of instruments

Sensor	Measured parameter	Range	Accuracy	Error
Temperature (Sensirion-SHTC3)	Temperature	0 – 130 ºC	±0.2ºC	±1.2 %
Humidity (Sensirion-SHTC3)	Relative humidity	0 – 100%	±2%	±2.5 %
Anemometer (Pasco-Xplorer)	Air velocity	2 – 6 m/s	±0.1m/s	±3.0 %
Temperature Data Logger (PCE)	Temperature	-100 – 1370°C	±0.5°C	0.4%
Eppley Pyranometer (PSP)	Solar intensity	0 – 2800W/m^2	±3 W/m^2	±0.5 %

4.1.1 Flat Plate Solar Collector

A flat plate solar collector was designed and assembled in order to utilize the solar thermal energy in the charging process of the solar-driven DAEC system. Because of better characteristics like light weight, high strength, proper corrosion properties, high surface reflectivity, excellent electrical, and thermal conductivities an Aluminum flat plate was used in this study. The geometrical parameters of the flat plate solar collector are given in Table 6.

Table 6: The geometrical data of the designed flat plate solar collector

Item	Symbol	Value (mm)
Length	L	1940
Height	H	940
Width	w	90

4.1.2 Experimental Measurement and Thermodynamic Analysis

The operation of the DAEC system can be described with the "charging – discharging" cyclic order. For the current study the tests were performed between 30th July and 15th August 2020. All the discharging tests were done during the evenings between 18:00 and 22:00 hence, solar heat had no effect on the discharging tests. In the discharge process, the ambient air flows to the desiccant chamber with constant air mass flow rate of 0.06 kg/s in all cycles. The air temperature after passing through the desiccant material (Vmc-$CaCl_2$) was increased, while experiencing the reduction in relative humidity. In the next stage, to reduce the temperature of an air-to-water heat exchanger was used to brings the air temperature to ambient level. In the last part the moderate low humid air was entered to the evaporation chamber where a nozzle was installed to spray water on evaporation material (WoC). As a result, cool air achieved that could be used for A/C applications.

During the charging phase, the incident solar radiation is absorbed by the flat plate solar collector. After that the solar heated water is collected in the storage tank. The hot water circulates between the hot water tank and air to water heat exchanger. Meantime, ambient air passes through the heat exchanger and heat is transferred from water to air, thereby air temperature is increased. In the next stage, the hot air passes through the wet material with air mass flow rate of 0.03 kg/s and consequently, desorbs

water from the composite sorbent and released in the air that was blown through the system by the fan. The outlet air had a higher temperature than the ambient air at the inlet. A photograph of the manufactured solar assisted DAEC system is shown in Figure 23(a-b).

The performance of the solar-driven DAEC system has been investigated by measuring the different performance parameters using the installed sensors. The thermodynamic equations discussed in Section 3.1.3 were used to calculate the thermodynamic parameters.

Figure 23: Designed solar assisted DAEC system (a) front view and (b) rear view

4.2 Material Synthesis and Experimental Methodology

Due to its availability, high sorption kinetics and low regeneration temperature, which are the key parameters for selecting a working material in solar–driven DAEC systems, Vmc-$CaCl_2$ composite was selected as the working material in testing the newly designed DAEC system. The method and procedure used for synthesizing the Vmc-

$CaCl_2$ composite has been discussed in the section 3.1.2 and Figure 11. The accuracy range and percentage error of the measurement devices is given in Table 5. The detailed experimental methodology of the study is illustrated in Figure 24.

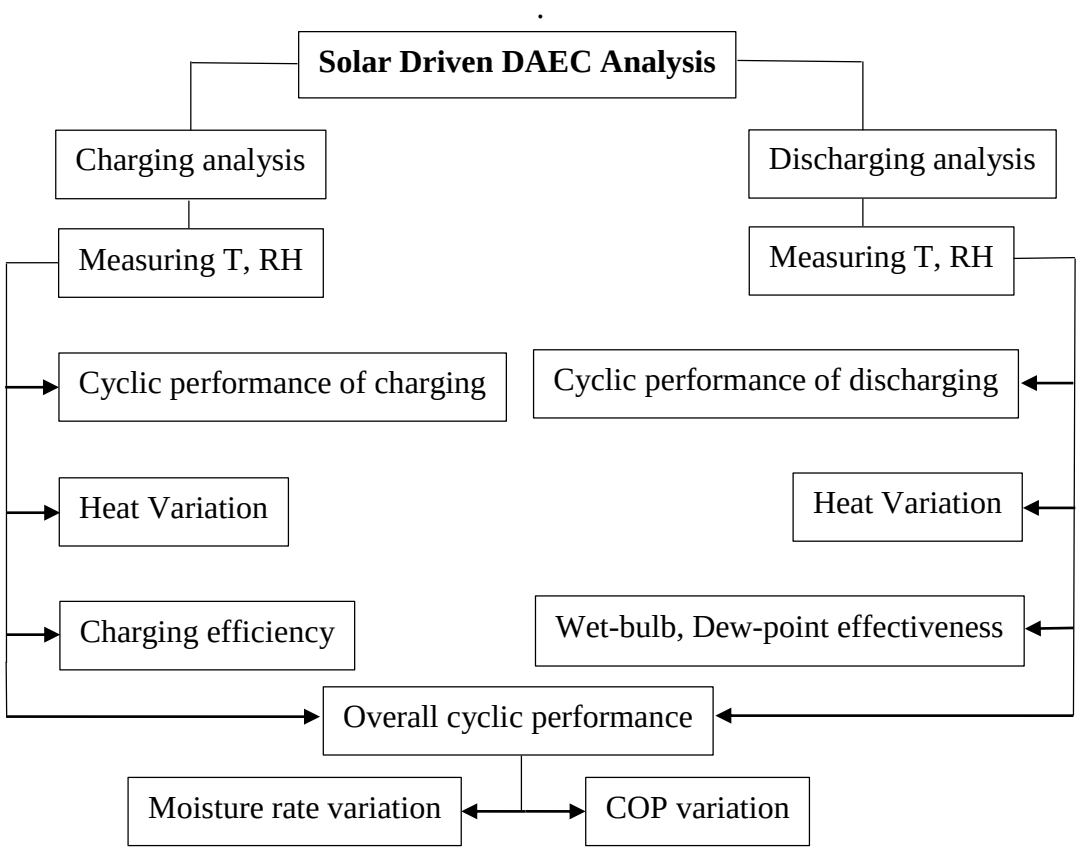

Figure 24: Flowchart of experimental testing methodology

4.3 Thermodynamic Analysis

The experiments were carried out to investigate the cyclic thermal and hygro-thermal performance of the system. During the discharging tests, system inlet (ambient) temperature was varying between 35 °C - 37 °C. The temperatures and relative humidity were measured simultaneously in each state to determine the system performance.

The cooling rate obtained from the system is calculated by taking into consideration the inlet temperature, outlet temperature, and the flow rate of the processed air stream, and it is given in Equation (26);

$$\dot{Q}_c = \dot{m}_a \Delta h = \dot{m}_a C_p (T_8 - T_{14}) \quad (26)$$

Absolute humidity indicates the water vapor content of the air. It is expressed as the mass of water vapor per unit mass of the dry air. Based on the measured data, absolute humidity, as a function of temperature and relative humidity, could be obtained with the Equation (27) [69];

$$w = 216.7 \left[\frac{\frac{RH}{100\%}.6.112.exp\left(\frac{17.62.T}{243.12+T}\right)}{273.15+T} \right] \quad (27)$$

The mass balance of water can be determined by consideration of the rate of water removal from the air through the desiccant dehumidification unit and the rate of water supply to the processed air across the EC unit. The water removal rate through the desiccant dehumidifier is directly related to the absolute humidity change of air across the desiccant dehumidification unit and the flow rate of the processed air [70] and can be obtained via Equation (28) and Equation (29);

$$\dot{m}_{w-r} = \dot{m}_a \, \Delta w_{8,9} \quad (28)$$

$$\dot{m}_{w-r} = \dot{m}_a (w_8 - w_9) \quad (29)$$

While the rate of water supply through the evaporative cooler is the function of the absolute humidity variation of air and flow rate of the air stream as given in Equation (30) and Equation (31);

$$\dot{m}_{w-a} = \dot{m}_a \, \Delta w_{14,10} \quad (30)$$

$$\dot{m}_{w-a} = \dot{m}_a \, (w_{14} - w_{10}) \quad (31)$$

In the heat exchanger, the rate of energy rejected from the air is equal to the rate of energy gain by the water as obtained via Equation (32) and Equation (33);

$$\dot{m}_w \, \Delta h_w = \dot{m}_a \, \Delta h_a \tag{32}$$

$$\dot{m}_w c_p \left(T_{w,o} - T_{w,i}\right) = \dot{m}_a c_p \left(T_{a,i} - T_{a,o}\right) \tag{33}$$

The wet-bulb effectiveness (ε_{wb}) of DAEC process could be obtained via Equation (34) [71];

$$\varepsilon_{wb} = \frac{T_8 - T_{14}}{T_8 - T_{wb}} \tag{34}$$

Where T_8 is the system inlet temperature, and T_{14} is the system outlet temperature. All parameters are measured by the Sensirion SHTC3 type sensors except the wet-bulb temperature, which can be obtained from the Equation (35) [70];

$$T_{wb} = T.\tan^{-1}\left[0.151977.\left(RH\% + 8.313659\right)^{1/2}\right] + \tan^{-1}(T + RH\%) - \tan^{-1}(RH\% - 1.676331) + 0.00391838.\left(RH\%\right)^{3/2}\tan^{-1}(0.023101.RH\%) - 4.686035 \tag{35}$$

The dew point temperature (T_d) is defined as the temperature where the air becomes saturated as a result of the sensible cooling process (*i.e.*, at constant absolute humidity), and condensation starts under constant pressure. It can be derived by using Equation (36) [70];

$$T_d = 243.2\left[\frac{\ln\left(\frac{RH}{100\%}\right) + \left(\frac{17.62.T}{243.12+T}\right)}{17.62 - \ln\left(\frac{RH}{100\%}\right) - \left(\frac{17.62.T}{243.12+T}\right)}\right] \tag{36}$$

The dew point effectiveness (ε_d) could be described as the actual temperature difference of air across the evaporative cooler to the obtainable temperature difference if it is cooled up to its dew point temperature. Dew point effectiveness is determined via Equation (37);

$$\varepsilon_d = \frac{T_8 - T_{14}}{T_8 - T_d} \tag{37}$$

In charging cycle, $Q_{solar,ava}$ represents the available solar energy on the collector surface and it could be calculated by multiplying the collector surface area (Aa) with the solar irradiance (I), as given in Equation (38);

$$Q_{solar,ava} = I.A_a \quad (38)$$

The rate of heat gain ($\dot{Q}_{solar,g}$) by the flat plate solar collector in charging cycles is calculated with the Equation (39):

$$\dot{Q}_{solar,g} = I.A_a.\eta_{collector} \quad (39)$$

Where $\eta_{collector}$ could be calculated via Equation (40):

$$\eta_{collector} = \frac{\dot{m}_w C_p (T_1 - T_2)}{A_a.I} \quad (40)$$

Electrical COP (COP_e) of the system is defined as the ratio of the total cooling output ($\dot{Q}_c.\ t_d$), to the electric work input and could be determined via Equations (41-42);

$$COP_e = \frac{\dot{Q}_c.t_{dc}}{\dot{W}_i.t_{dc} + \dot{W}_i.t_{cr}} \quad (41)$$

here t_{dc} and t_{cr} represents the discharging and charging cycle durations. The rate of electric power consumption of the system is calculated as follows;

$$\dot{W}_i = \dot{W}_p + \dot{W}_f \quad (42)$$

Where $\dot{W}_p$ and $\dot{W}_f$ represents the energy consumption of fan and pump. For DAEC performance evaluation, COP_{th} is an important measure. It is defined as the ratio of the cooling output ($\dot{Q}_c.t_{dc}$) in discharging cycle to the total amount of solar energy transferred to charging air ($\dot{Q}_{useful,Hx}.t_{cr}$) as given in Equation (43);

$$COP_{th} = \frac{\dot{Q}_c.t_{dc}}{\dot{Q}_{useful,Hx}.t_{cr}} \quad (43)$$

Similarly, COP_t is defined as the ratio of the cooling capacity ($\dot{Q}_c.t_{dc}$) in discharging cycle to the total energy input ($\dot{E}_i$) to the system as given in Equation (44);

$$COP_t = \frac{\dot{Q}_c}{\dot{E}_i} \quad (44)$$

Total energy consumption of the system is obtained with Equation (45);

$$\dot{E}_i = \left(\dot{W}_p + \dot{W}_f\right).(t_{dc}) + \left(\dot{W}_p + \dot{W}_f\right).(t_{cr}) + \dot{Q}_{useful,Hx}.(t_{cr}) \quad (45)$$

Useful rate of solar energy transferred to the charging air could be determined by obtaining the enthalpy change of air across the heat exchanger via Equation (46) where, mass flow rate of charging air is defined as $\dot{m}_a$, and enthalpy of air at inlet and outlet of heat exchanger is specified as h_7 and h_8, respectively.

$$\dot{Q}_{useful,Hx} = \dot{m}_a(h_8 - h_7) \tag{46}$$

The heat transferred from the air to the desiccant across the desiccant chamber can be found by using Equation (47):

$$\dot{Q}_{trans,des} = \dot{m}_a(h_8 - h_9) \tag{47}$$

where enthalpy at inlet and outlet of charging cycle specified as h_8 and h_9, respectively.

The charging efficiency (η_{ch}) is defined as the ratio of the heat transfer across the desiccant chamber to the solar energy gained as presented in Equation (48):

$$\eta_{ch} = \frac{\dot{Q}_{trans,des}}{\dot{Q}_{solar,g}} \tag{48}$$

The hygrothermal efficiency (η_{hyg}) is another important parameter that was analyzed in the study which is calculated by using Equation (49) as below:

$$\eta_{hyg} = \frac{m_{des}}{m_{abs}} \tag{49}$$

The total uncertainty for the calculation of the ε_{wb} can be expressed as;

$$w_R = \left[\left(\frac{\partial \varepsilon_{wb}}{\partial T_1} w_{T_1}\right)^2 + \left(\frac{\partial \varepsilon_{wb}}{\partial T_4} w_{T_4}\right)^2 + \left(\frac{\partial \varepsilon_{wb}}{\partial RH_4} w_{RH_4}\right)^2\right]^{1/2} \tag{50}$$

Total uncertainty rate affecting the εwb of the proposed system was computed by using Equations (50). The estimation implies that total uncertainty in the calculation of the εwb is found to be 6.51%.

The uncertainty rate evaluated for different parameters are presented in Table 7.

Table 7: Evaluated uncertainty for various parameters

Parameter	Uncertainty Rate (%)
$\dot{Q}_c$	4.53
$\dot{Q}_{solar,g}$	2.16
$\dot{Q}_{useful,Hx}$	5.83
$\dot{Q}_{trans,des}$	6.14
ε_{wb}	6.51
ε_d	2.41
$\eta_{collector}$	2.37
η_{ch}	5.73
η_{hyg}	2.82
COP_e	4.53
COP_{th}	5.44
COP_t	5.58

4.4 Results and Discussion

In this section, three cycles (charging/discharging) testing results of the investigated solar driven DEAC system were presented. During the experiments, temperature and relative humidity variation of air across the system components was measured. In addition, water temperature variations in different components were recorded. Accordingly, several performance parameters including solar heat gain, charging efficiency, cooling output, wet bulb/dew point effectiveness and COP of the system were analyzed.

4.4.1 Cyclic Performance of Charging

In this study, solar energy is utilized as the heat source, where low/medium temperature solar collector was used to regenerate the desiccant material. The variation of the intensity of solar radiation entering the flat plate solar collector during the charging tests is shown in Figure 25. The charging performance depends heavily on the solar radiation absorbed by the system. The solar irradiance measurements were

performed every 20 minutes. The average of the solar irradiance for the three charging cycles was 842, 822, and 789 W/m^2. Each cycle was completed in six hours.

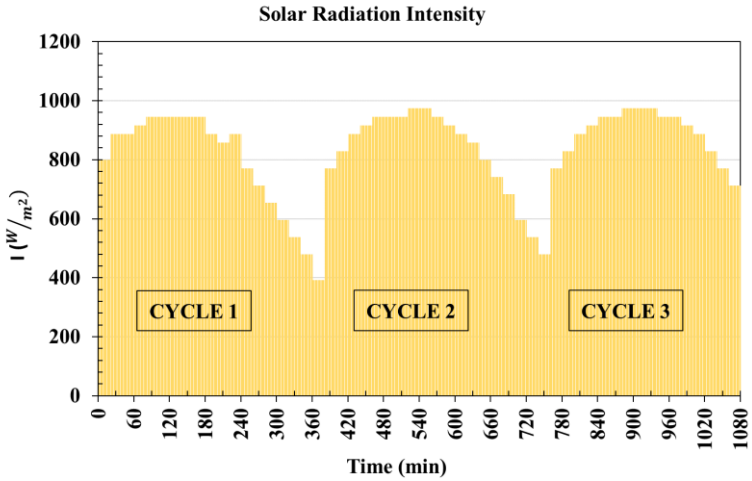

Figure 25: Intensity variation of solar radiation entering the flat plate solar collector

Temperature and relative humidity variations

The collector outlet water temperature for all the cycles was in the range of 75 – 85 ^{o}C. The temperature variation of air across the desiccant material (Vmc-$CaCl_2$) in three different cycles, with regeneration (inlet) temperatures of 57.5 °C – 66.1 °C, 54.1 °C – 60.1 °C and 46.3 °C – 55.4 °C are shown in Figure 26(a) respectively, for different testing days. In all tests, air mass flow rate of 0.03 kg/s was used based on the results obtained in the laboratory scale tests. As explained in Figure 21, the hot water goes to the air to water heat exchanger, where the ambient air flows to it. Consequently, heat is transferred from water to air and increases the temperature of the ambient air. The relative humidity of three cycles in the charging mode was presented in Figure 26(b). As it is seen, with the increasing charging temperature, relative humidity shows a decreasing trend. Based on the calculated values at regeneration temperature of 60 °C, 55 °C and 50 °C, moisture removal rates were found as 3.53 g/min, 3.48 g/min, and

3.43 g/min respectively. Results showed that the increase of regeneration temperature could increase the regeneration capacity thereby reduce the regeneration period.

a) b)

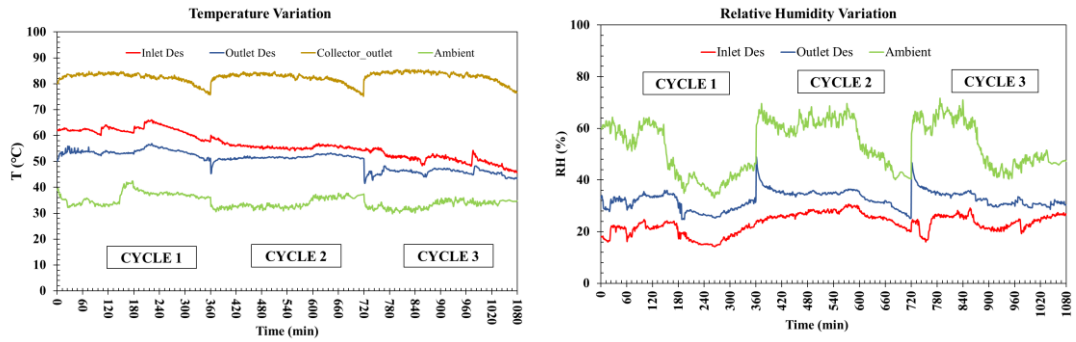

Figure 26: Cyclic performance of charging (a) temperature variation and (b) relative humidity variation

Energy Analysis

The variation of the available solar energy that radiated to the flat plate solar collector during the charging cycle is shown in Figure 27. The average of the input solar energy for the three cycles is 1.44, 1.42, and 1.38 kW, respectively.

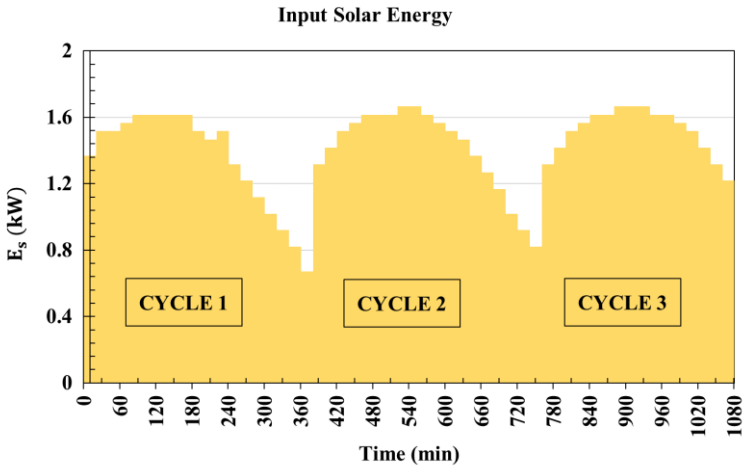

Figure 27: Variation of the input solar energy

The average values of available solar energy on collector surface ($Q_{solar,\ ava}$), the rate of heat gain of solar collector ($Q_{solar,g}$), the rate of heat transfer to the air across the heat exchanger ($Q_{useful,Hx}$) and the rate of heat transfer to the desiccant for moisture desorption ($Q_{trans,des}$) in charging cycles are presented in Figure 28. As seen from the figure, average available solar radiation on the collector surface was 1.43 kW, whereas 0.67 kW of it is gained by the collector during the experiments. Furthermore, the rate of heat transfer to the charging air was found 0.59 kW, which indicates that the heat transfer across the heat exchanger was effective. Finally, results showed that the rate of heat consumption for moisture desorption was 0.16 kW, which was lower than the desired heat transfer ratio. The low desorption heat consumption could be due to the relatively low regeneration temperature used in charging < 65 °C. Additionally, desiccant bed thickness and charging air flow rate might influence on desorption heat consumption, thereby, increasing the bed thickness and air flow rate could enhance the heat transfer rate across the desiccant bed. Such improvements could be considered in future studies.

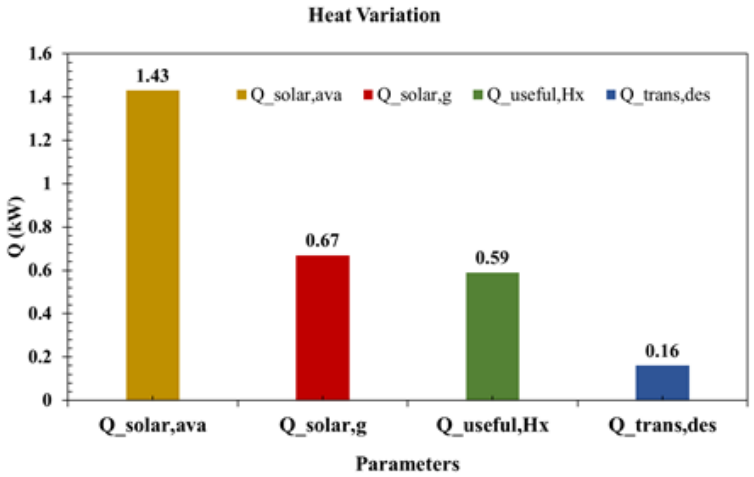

Figure 28: Average heat variation across the system

Based on the presented energy break-down across the system components, cyclic $\eta_{collector}$ and η_{ch} were calculated and presented in Figure 29. Here, $\eta_{collector}$ is defined as the ratio of $Q_{solar,g}$ to $Q_{solar,ava,}$ whereas charging efficiency is the ratio of $Q_{trans,des}$ to $Q_{solar,g}$. Accordingly, $\eta_{collector}$ and η_{ch} were found in the range of 0.51-0.46 and 0.27-0.22 respectively. For both efficiencies, a slight drop is observed over the repeating cycles. This could be mainly due to the gradually decreasing $Q_{solar,\ ava}$ over the cycles. As a result, $Q_{solar,g}$ and $Q_{trans,des}$ were decreased, which negatively influenced the $\eta_{collector}$ and η_{ch}. In addition, some residual moisture remained inside the desiccant over the repeating charging cycles might have affected the heat transfer rate in desiccant chamber. Modifications in desiccant bed configuration could be considered for enhancing the η_{ch}.

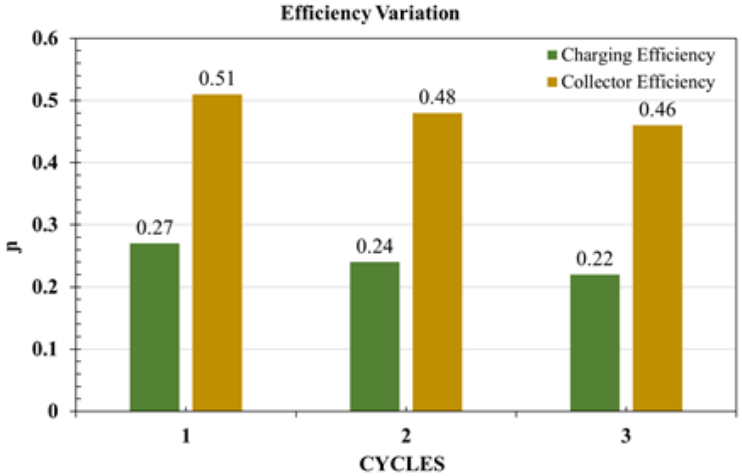

Figure 29: Collector efficiency and charging efficiency of the solar-driven DAEC system

4.4.2 Cyclic Performance of Discharging

The performance of the developed system and the characterization of the Vmc-$CaCl_2$ composite for the three discharging cycles have been discussed in this section. Each cycle was completed in four hours. The temperature variations of air in discharging mode, for different parts of the system such as desiccant inlet, desiccant outlet, heat

exchanger outlet, and evaporator outlet, are demonstrated in Figure 30(a). The inlet air temperature was varying between 32 °C and 35 °C in all cycles, while the outlet temperature showed a steady trend over time and reached to 24-26 °C at the end of the cycles. As can be seen in the figure, the temperature difference between desiccant inlet and evaporative cooling chamber outlet was about 7.4 ℃, 7.6 ℃ and 7.9 ℃ respectively. The variation of the relative humidity at various points of the system is shown in Figure 30(b). Relative humidity at the inlet desiccant was in the range of 49–65% for different cycles whereas at the outlet of the desiccant chamber it changed from 34% to 53%. The reason of this reduction is because of the water absorption of desiccant material in the desiccant chamber. The relative humidity at the outlet of the heat exchanger varying between 41% and 62%. The relative humidity of the evaporative chamber outlet with increasing trend reached to 95%. This dramatic growth is because the water was sprayed over the evaporative materials with a nozzle to maintain consistent water evaporation and absorbing the energy.

In this system an air-to-water heat exchanger was used to eliminate the generated sorption heat of the air at the outlet of the desiccant chamber and pre-cool the process air. Figure 30(c) shows the heat rejection rate from the air to the water tank via the heat exchanger. In the considered DAEC unit, a water tank with 200 L volumetric capacity is utilized. The initial water temperature inside the tank was nearly 28 °C in three cycles. As the water temperature inside the tank increased during the operation, the rate of heat rejection from the air to the water showed a decreasing trend. The average heat transfer rate to water over four hours of operation for three cycles was found as 0.29, 0.24, and 0.32 kW, respectively. By rejecting heat to the tank, the temperature of the processed air temperature decreases close to the ambient (desiccant inlet) temperature, which consequently can increase the efficiency of the system.

a)

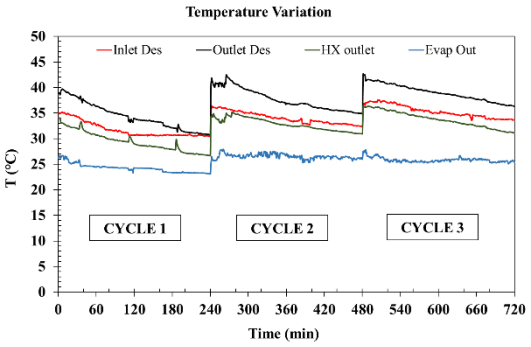

b)

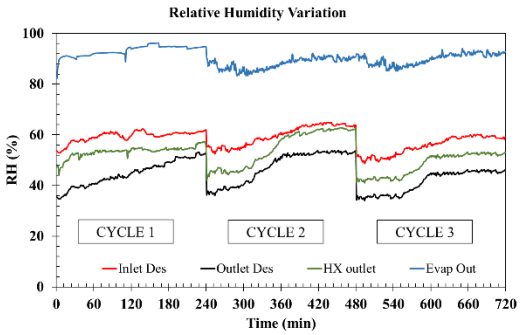

c)

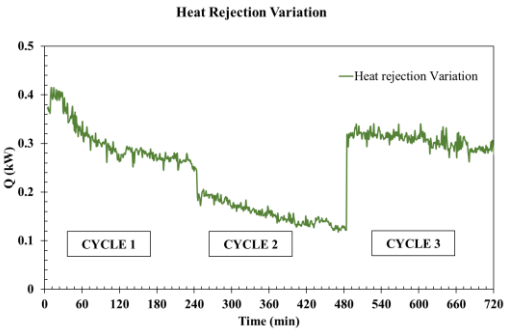

Figure 30: Cyclic performance of discharging (a) temperature variation, (b) relative humidity variation, and (c) heat rejection variation

4.4.3 Material Performance Analysis in Discharging Mode

The wet-bulb effectiveness variation in discharging mode is shown in Figure 31(a). As seen, in the discharging mode, the behavior of materials was nearly steady. However, the wet-bulb effectiveness values experienced a constant decrement in the first cycle when compared to the other cycles. The peak wet-bulb effectiveness was obtained as 134%, 131% and 130%, respectively.

The dew-point effectiveness variation in discharging mode was demonstrated in Figure 31(b). As it is clear from this figure, in the discharging process the first cycle provided dew-point effectiveness of 95%, where in the second cycle values were in the range of 85-95%. The third cycle was in the range of 84-96% which can provide cold supply air temperatures and more comfortable indoor conditions.

The cooling rate variation in the discharging mode is presented in Figure 31(c). The cycles demonstrated a similar behavior with highest cooling rate of 0.73 kW, which was achieved in the third cycle. The average Q_c values were determined as 0.45 kW, 0.47 kW and 0.57 kW respectively. The reason of higher average Q_c in third cycle was the higher temperature and lower relative humidity of ambient air during that cycle. The average ambient temperature and relative humidity were 31.7 °C, 34.0 °C, 35.2 °C and 59.4%, 57.8%, 55.6% over the repeating cycles. Accordingly, it could be stated that; beside the design and configuration of the system, the ambient conditions also significantly influence the solar driven DEAC performance. The higher ambient temperature and lower ambient relative humidity could enhance the cooling capacity as a result higher cooling performance could be achieved.

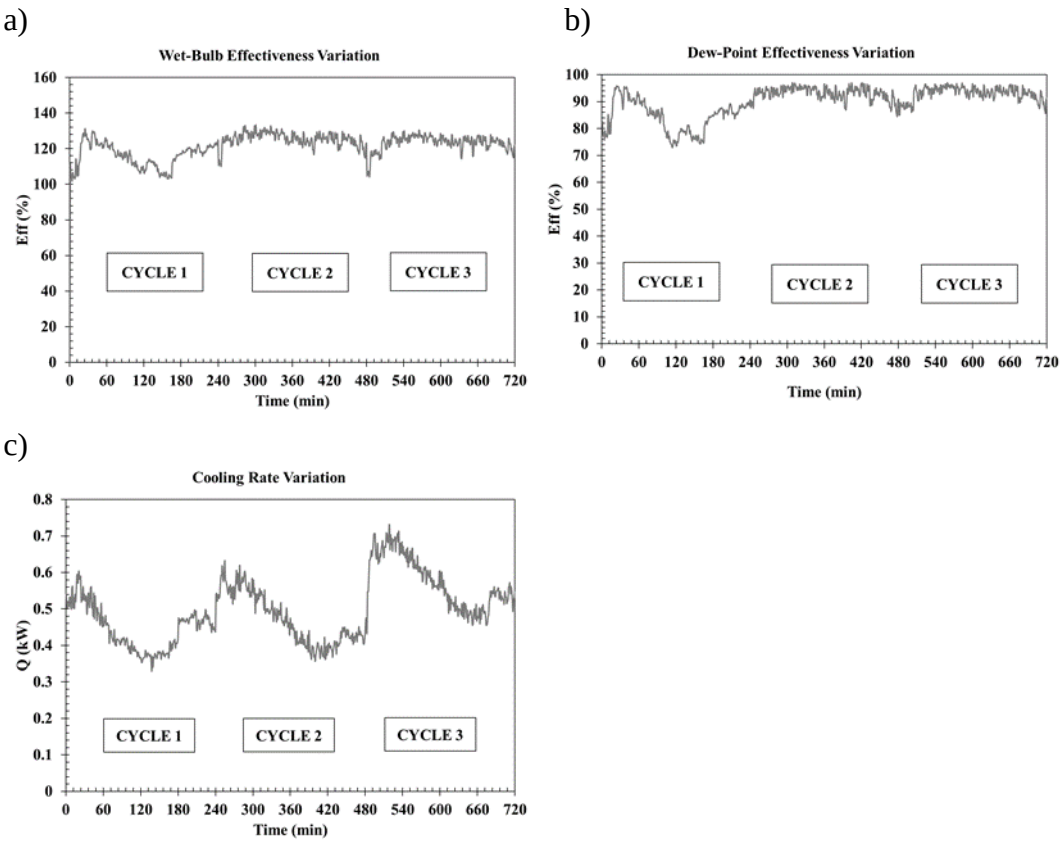

Figure 31: Variation of performance parameters in discharging process (a) discharging wet-bulb effectiveness, (b) discharging dew-point effectiveness, (c) discharging cooling rate

4.4.4 Overall Performance

The calculated rate of mass changes of the tested material after discharging and charging cycles are illustrated in Figure 32(a-b), where positive and negative mass changes indicate the amount of water absorbed and desorbed, respectively. During the tests, the hydrated desiccant was charged in three different cycles with regeneration temperature of 60 °C, 55 °C, and 50 °C, respectively. After each completed charging cycle, the cooling (discharge) cycle was performed. Between the charging and discharging processes, desiccant material was removed from the system and kept in a hermetically sealed container until the system reaches thermal equilibrium with the surroundings. Based on the obtained measurements, average moisture absorption/desorption rates in three repeating cycles were found as 9.64/4.24 g/min, 9.19/3.89 g/min, and 8.5/3.81 g/min. Accordingly, the total amount of moisture absorbed/desorbed in these cycles were determined as 2314.70/1529.13 g, 2206.12/1403.46 g, and 2041.41/1392.02 g, respectively (Please see: Figure 32(c)). Overall cyclic analysis results showed that, with the decline of T_{reg} from 60 °C to 50 °C, the amount of moisture desorption was reduced. Therefore, it is suggested to increase the T_{reg} in order to rise the cyclic efficiency of the system. Also it is recommended to use more efficient solar collector, or an auxiliary heater driven with photovoltaics although it will increase the cost of the system and effect the feasibility of the system.

a)

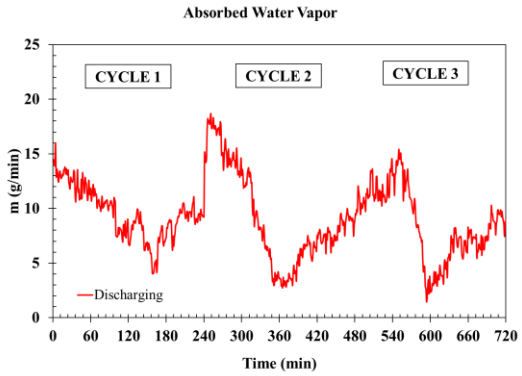

b)

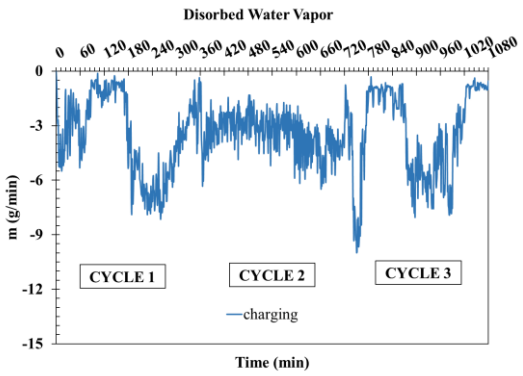

c)

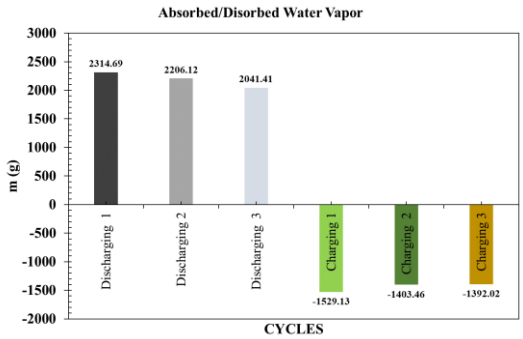

Figure 32: Overall cyclic performance (a) moisture absorption rate variation (b) moisture desorption rate variation, and (c) cumulative moisture absorption/desorption

Based on the calculated cumulative moisture adsorption/desorption as shown in Figure 32(C), the η_{hyg} for Vmc-$CaCl_2$, in three cycles were found to be 0.68, 0.66, and 0.63, respectively (see Figure 33(a)). This outcome indicates that, based on the performed experiments, at an average regeneration temperature of 56 °C, nearly 65% of the moisture could be desorbed from the salt based composite desiccant.

The obtained values of the other important performance parameters, COP_{th} and COP_t, of the solar driven DAEC unit in cyclic operation are presented in Figure 33(b). As seen from the figure, both COP_{th} and COP_t showed an increasing trend from the first to third cycles. As discussed before, higher Q_c values were obtained over the repeating cycles due to the increase in ambient temperature and decrease in ambient humidity. Additionally, $Q_{trans,Hx}$ dropped over the repeating cycles due to the decreased solar

radiation. As COP_{th} and COP_t are directly proportional with Q_c and indirectly proportional to $Q_{trans,Hx}$, both of them showed a gradual increase over the repeating cycles. Accordingly, COP_{th} varied in the range of 0.39→0.86 whereas COP_t was between 0.26→0.46. The overall average COP_{th} and COP_t were calculated as 0.6 and 0.35 respectively, which were in accordance with the previous studies in the literature.

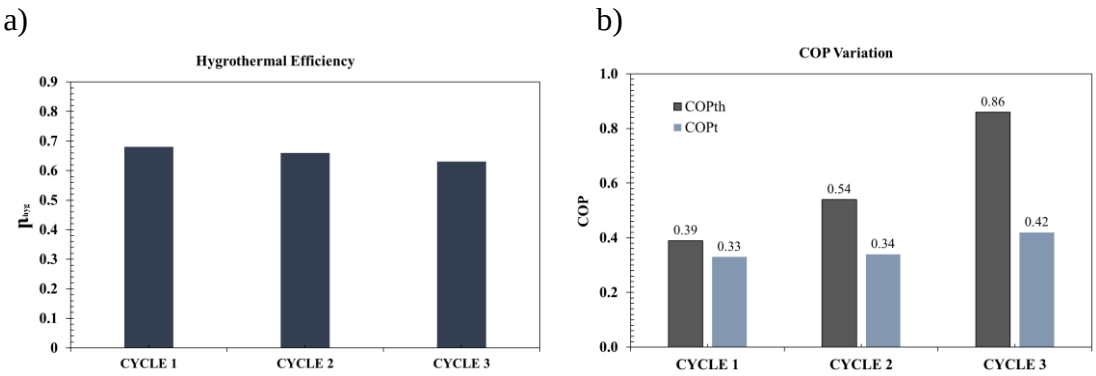

Figure 33: (a) Hygrothermal efficiency and (b) COP variation

4.4.5 Review of the previous researches

Numerous experimental and mathematical studies have been previously conducted on solar driven desiccant cooling systems. Comino et al. [77] experimentally determined the COP of a solar driven desiccant cooling system to control indoor conditions in a research lab room. The experimental results showed that the system independently adjusted the temperature and humidity of the supply air. 75% of the energy consumed by this air handling system comes from renewable sources. According to the study results, cooling COP up to 9.8 and effectiveness value up to 0.88 is obtained. Hussain et al. [78] presented numerical investigations on a solar-assisted hybrid desiccant EC system integrated with solar air collectors for hot and humid climatic conditions of Kuwait. The outcomes of this work indicated that solar-assisted hybrid desiccant EC device integrated with air collectors is capable of providing average coefficient of performance of 0.85. The role of the desiccant in a solar cooling system under hot and

humid climatic conditions was reviewed through year-round dynamic system simulation using TRNSYS [79]. the system performance of the solar cooling system with energy recovery was not sensitive to the storage tank size, and that the merit of the solar cooling system with energy recovery over the other two solar cooling systems augmented with an improvement in the thermal efficiency of the grid electricity in long term. Belguith et al. [80] carried out a performance investigation of the impact of the ambient conditions on the desiccant cooling systems with cycle COP of 1.89. Study of a novel dehumidification system based on silica gel packed beds is carried out by De Antonellis et al. [81]. Depending on bed thickness, airflow arrangement and air velocity, the humidity ratio of airflow supplied to the building can be increased from 1.5 g kg-1 to 4.8 - 5.8 g kg-1 when the indoor humidity ratio is 5.8 g kg-1 and the regeneration temperature is around 50 °C. The summary of the literature presented in Table 8.

The developed system was tested to analyze the real-life implementation performance of solar driven DAEC for coolth energy storage in hot-humid climates. The study suggests an innovative integration method of the investigated process to the existing solar water heating systems in buildings. With the suggested method, the desiccant cooling system could be charged (desiccant dehumidification) with domestic solar water heaters. As a result, coolth energy is stored within the solar driven DAEC system for later usage (i.e., night time cooling). In discharging (cooling) mode, the heat generated due to the moisture sorption could be rejected to the cold water tank, which is generally installed together with the existing solar water heaters. The proposed integration method is described the first time in the literature, and possible implementation of it in new and existing buildings could provide considerable energy and cost savings in A/C applications. Meanwhile, such applications could enhance the

utility of existing solar water heating systems installed in buildings during the summer period.

Table 8: Comparison of the previous studies on solar driven DAEC system

Reference	Year	Working material	Type of study	Air flow rate	COP
Comino et al. [77]	2020	silica gel & metal silicates	Experimental	0–1600 m^3/h	0.5
Hussain et al. [78]	2020	silica gel	Numerical	1000 kg/h	0.85
Fong & Lee [79]	2020	silica gel	Numerical	1.79 m^3/s	0.7
Belguith et al. [80]	2020	silica gel	Experimental Numerical	0.5 m^3/s	-
De Antonellis et al. [81].	2020	silica gel	Experimental	0.8 m^3/s	1.13
Present study	2021	Vmc-$CaCl_2$	Experimental	0.06 kg/s	0.86

4.5 Potential Real-Life Application of Solar Driven DAEC

In this chapter, the design and assembling details of a novel solar-driven DAEC unit with performance of the system and the experimental results were discussed. Based on the obtained promising results, a possible design of the proposed system in building is generated. It is necessary to mention that the solar water heaters are available almost in all buildings in Cyprus which are not used in summer most of the time. Therefore, integration of a cooling system with them is very attractive approach. The 3D view of the designed storage type solar-driven DAEC unit is presented in Figure 34. The proposed concept consists of a solar water heating system, desiccant chamber, and the evaporative cooling chamber. As seen from the figure, in charging mode, water from the hot water tank is circulated across the heating coil, and the air is heated. Hot air passes across the desiccant and desorbs the moisture. Moist air is then exhausted to the

environment through the exhaust outlet. In discharging mode, water circulation from the hot water tank is deactivated. Therefore, air passes across the heating coil without any heat transfer. Then it enters the desiccant chamber where the moisture is absorbed, and air humidity content is reduced. Following that, air passes across the pre-cooling heat exchanger, which is connected to the cold water storage tank. In this way, generated sorption heat is transferred to the cold water tank, and air temperature is reduced back to the ambient level. Finally, air enters the EC chamber, where its temperature is reduced to 23-24 °C. Product air is then supplied to the building. As the solar water heating system already exists in the majority of buildings, the installation costs of the system are expected to be low (1000-1500 €). Implementation of such a system could provide a low cost and sustainable opportunity for reducing the indoor temperature in buildings.

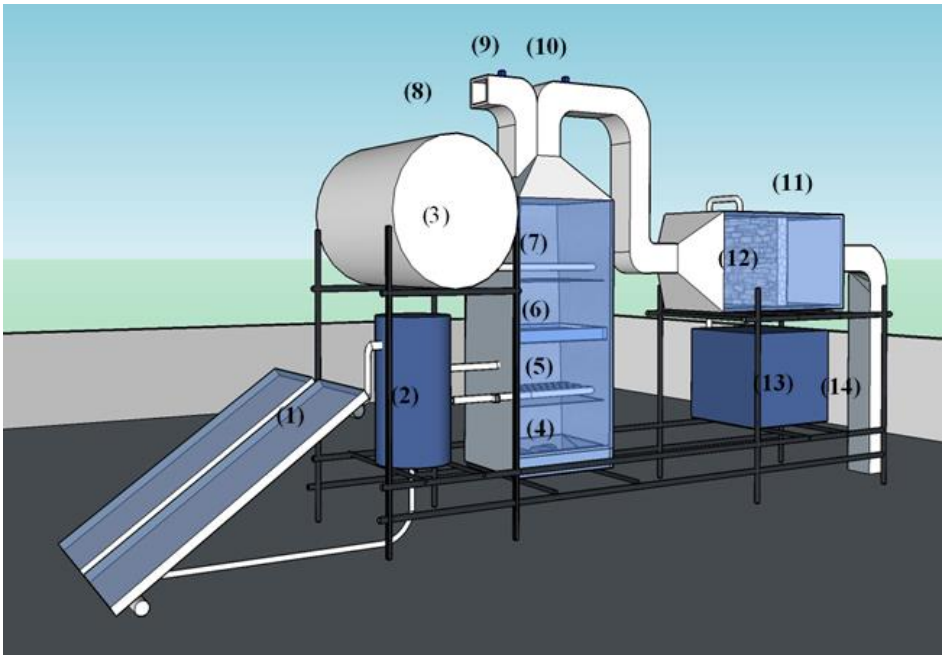

Figure 34: 3D view of the storage type solar-driven DAEC system. (1) Flat plate solar collector, (2) Hot water storage tank, (3) Cold water storage tank, (4) Fan, (5) Heating coil, (6) Desiccant material, (7) Cooling coil, (8) Charging moist air exhaust outlet, (9) Exhaust air damper, (10) Discharging line air damper, (11) EC chamber, (12) EC material, (13) Water tank, (14) Product air supply to the building

Chapter 5

NUMERICAL AND SIMULATION ANALYSIS OF THE SOLAR-DRIVEN DAEC SYSTEM

In this chapter, comprehensive analysis of the proposed solar driven DAEC configuration is performed by using TRNSYS software. TRNSYS is a general purpose program that simulates the dynamic systems for the investigation of their transient performances [82]. It is a versatile simulation tool to estimate energy analysis of simple or complex system for multi-climate and multi configurations. TESS library contains more than 150 validated component models that work using sets of differential equations. Component models are called “Type”; which are graphically connected through links which indicate the output properties of a certain component considered as input to other “Type” [83]. In the current study, the detailed transient simulations are carried out using TRNSYS version 18 for each configuration in selected climatic condition. The simulation model was developed by using validated components.

In the second section of this chapter, the economic and feasibility of the integrated solar-driven DAEC system was evaluated, and the annual cooling load of a residential building was simulated under NC climatic conditions by using DesignBuilder software. The feasibility analysis is carried out by considering the obtained DAEC system performance in previous chapters and the analysis of the conceptual building cooling load.

5.1 TRNSYS Simulation of Solar-Assisted DAEC System

The main task of the air-conditioning system in the summer, is to cool and maintain the temperature, humidity and composition of the cooled air within the narrow satisfactory limits. During the process required air temperature in the air-conditioned room is above ambient temperature. In this section, the process of solar cooling of hot and humid air by dehumidification in a fixed bed desiccant pad with solid sorption material is modeled and simulated using TRNSYS software.

The objective of this numerical analysis is to model, simulate and analyze a solar assisted desiccant based air conditioning system in cooling mode for the climatic conditions of Larnaca (34.9229° N, 33.6233° E). Since the weather data for Famagusta is not available in TRNSYS software, Larnaca, which is the closest available location to Famagusta in Cyprus, was selected as the test location. As the distance between these cities is very short, year round climatic conditions of Larnaca and Famagusta is considered as same.

The system is arranged in two different configuration schemes for discharging-charging modes and energized by a flat plate solar collector. The dynamic analysis of the systems is performed in TRNSYS which is a convenient simulation tool for conducting off-line experimentation of novel energy concepts.

Figure 35 shows the process flow diagram of the TRNSYS studio simulation for the proposed system. Hot and humid air is drawn into the desiccant chamber with the help of a fan. The air passes from desiccant chamber where silica gel is used as the desiccant material. Then the hot air flows through an air-to-water heat exchanger to transfer heat to the cooling water and at the last part this air goes to the evaporative cooling chamber.

The water is sprayed on the evaporation material (WoC) to enable water evaporation for sensible cooling of air. Then cool air is sent to the room intended for cooling. On the other hand, solar energy is used to get rid of the moisture trapped within the desiccant. Fixed bed desiccant placed in the desiccant chamber where it is heated to a higher temperature to raise its vapor pressure. For performing this mode, the hot water goes to the air-to-water heat exchanger. Meantime, the ambient air is drawn to the heat exchanger by a fan where circulation of the hot water in the heat exchanger fin tubes increases the temperature of the air. Finally, the hot air goes to the desiccant chamber to dry the material and complete the cycle.

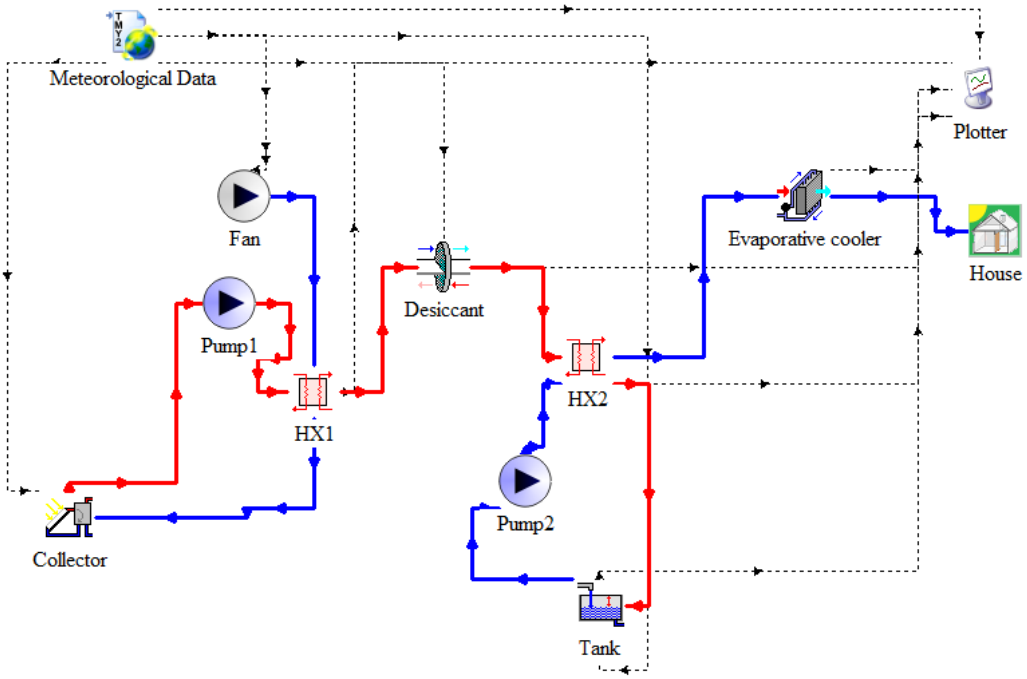

Figure 35: Schematic view of DAEC system in TRNSYS simulation studio environment.

A brief description of all the main TRNSYS components used in the modeling of solar assisted DAEC system along with their technical specifications are listed and demonstrated in Table 9.

Table 9: Type and properties of components used in the TRNSYS models

Component	Design characteristics
Desiccant pad	Type 683, F_1=0.08 F_2=0.95
Direct Evaporative Cooler	Type 506
Flat Plate Solar Collector	Type 45, Area=2 m^2, Collector slope=45°, Intercept efficiency=0.7
Heat Exchangers	Type 91, Effectiveness=0.75
Fan	Type 112, mass flow rate=0.06 kg/s
Pumps	Type 114, mass flow rate=0.02 kg/s
Weather File	Type 109
Building Zone	Type 56
Water Tank	Type 39, Volume=200 m^3
Online Plotter with File	Type 65

The weather data file for the location of Larnaca (34.9229° N, 33.6233° E) in TRNSYS type-109 is used to simulate the climatic variables. Figure 36 shows the hourly variation of available global solar radiation on the horizontal surface annually. Based on the figure, the maximum solar radiation received on summer time (June-August).

The DAEC systems are largely dependent on the desiccant material. In previous chapters, Vmc-$CaCl_2$ was selected as the desiccant material, while in the TRNSYS software this novel composite material is not available. Accordingly, silica gel was selected to model and simulate the solar assisted DAEC system which has the closest thermal behavior compared to Vmc-$CaCl_2$. Silica gel is characterized by being chemically inert, high surface area, high internal porosity, and strong adsorption capacity, widely used as dehumidifying desiccant, dehydrating agent, adsorbents,

fillers and catalyst carrier. The specifications of the silica gel are presented in Table 10.

Table 10: Characteristics of desiccant material used in the simulation [84]

Material	Density (kg/m^3)	Thermal Conductivity (W/(m°C))	Water absorption capacity (g/g)
Silica gel	700	0.234	0.40

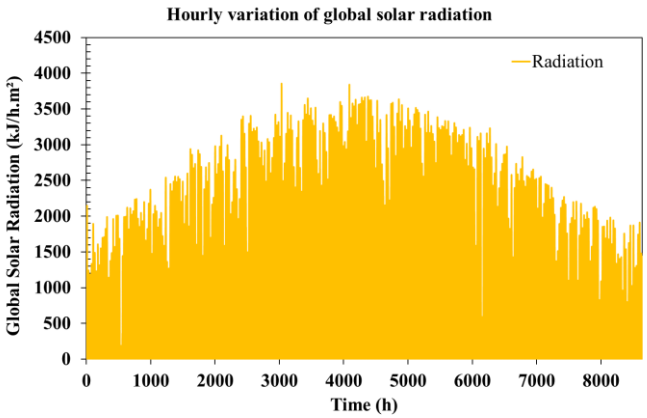

Figure 36: Hourly variation of global solar radiation on a horizontal surface

The hourly variation of ambient temperature is also depicted in Figure 37 for the whole year. According to the data maximum ambient temperature is around 37 ℃ on August.

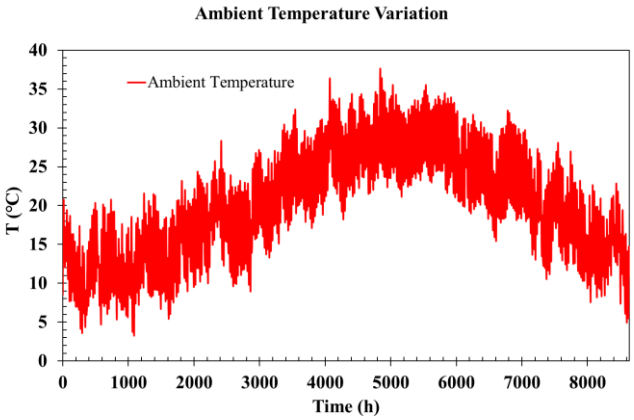

Figure 37: Hourly variation of ambient temperature over the whole year

The hourly variation of relative humidity is also demonstrated in Figure 38 for the whole year. The averaged relative humidity for the months June to August is ~67%.

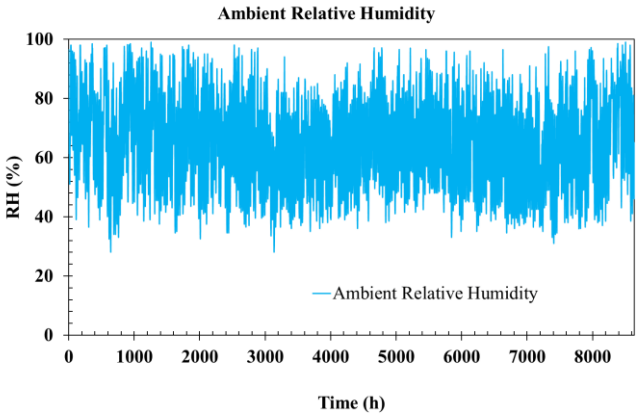

Figure 38: Hourly variation of ambient relative humidity over the whole year

5.1.1 Performance Analysis of Charging Mode

In this section, performance assessment of various parameters in charging mode in a daily base on 1st of August 2020 is performed. Since the best experimental results on real conditions of the proposed system was carried out on a same date, the said date has been defined in the TRNSYS.

Figure 39 shows the temperature variation in charging mode for silica gel. As can be seen, during six hours of testing the flat plate solar collector outlet temperature is around 72 ℃. With average regeneration temperature of ~55 ℃ desiccant moisture removal of 4.1 g/min achieved. Based on the figure, the ambient temperature is around 32 ℃.

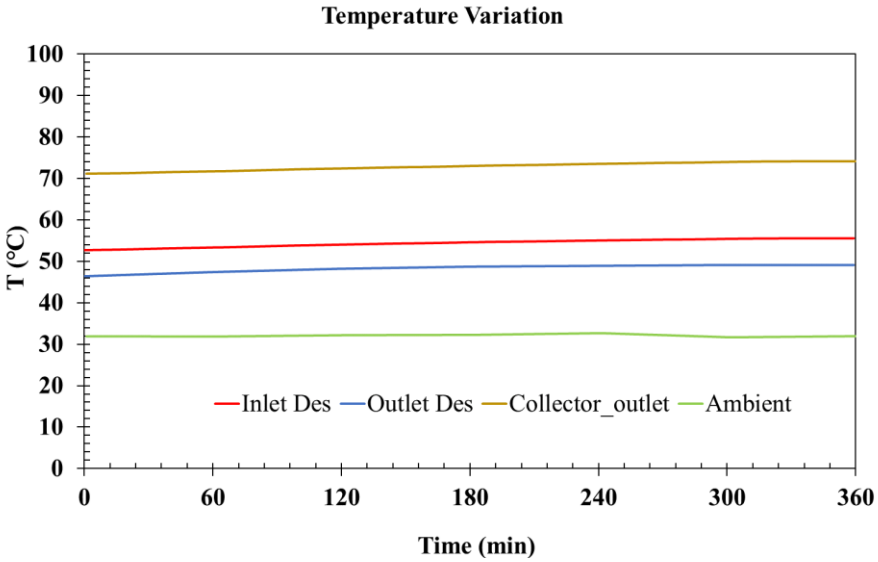

Figure 39: Temperature variation in charging mode

The relative humidity of the cycle in the charging mode is presented in Figure 40. As it is seen, with the increasing charging temperature, relative humidity shows a decreasing trend. According to the measured temperature and relative humidity at the inlet and outlet of the desiccant chamber, moisture removal rate was determined. Based on the calculated values at T_{reg} of 55 °C, cumulative moisture removal was found as 1485.43 g.

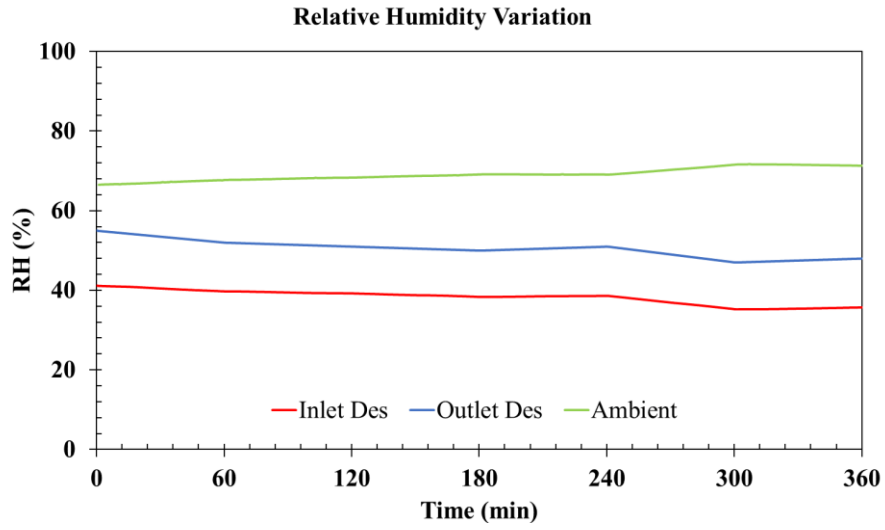

Figure 40: Relative humidity variation in charging mode

The calculated rate of mass changes of the tested material during the charging cycle is illustrated in Figure 41(a), where negative mass changes indicate the amount of water desorbed. Based on the obtained results, average moisture desorption rates in six hours testing was found as 4.12 g/min. Also the cumulative moisture removal rate in the charging mode presented in Figure 41(b). Based on the results 1485.43 g of the water vapor desorbed during six hours of testing.

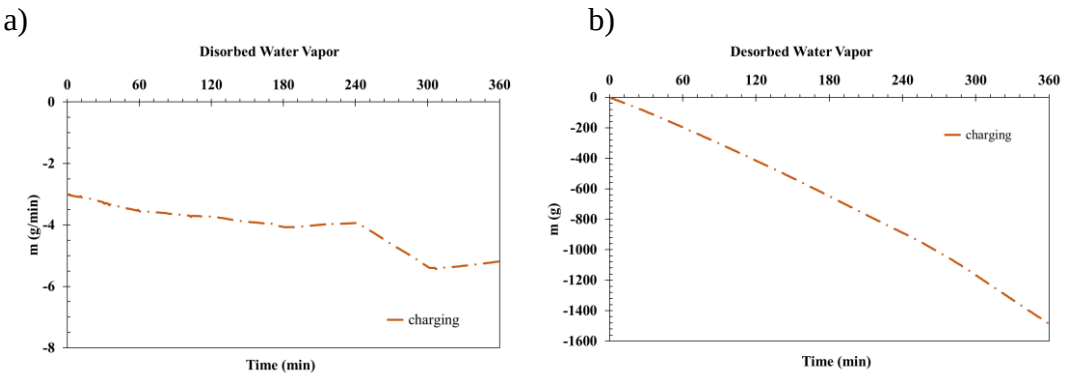

Figure 41: Moisture desorption rate variation (a) and cumulative moisture removal in charging mode (b)

5.1.2 Performance Analysis of Discharging Mode

The temperature variations of air in discharging mode, for different parts of the system such as desiccant inlet, desiccant outlet, heat exchanger outlet, evaporator outlet, and ambient are demonstrated in Figure 42. The inlet air temperature varied between 29 ℃ to 33 ℃ during the day, while the outlet temperature showed an increasing trend over time and rose to 25 ℃ after four hours of the simulation as the desiccant material gets saturated with moisture.

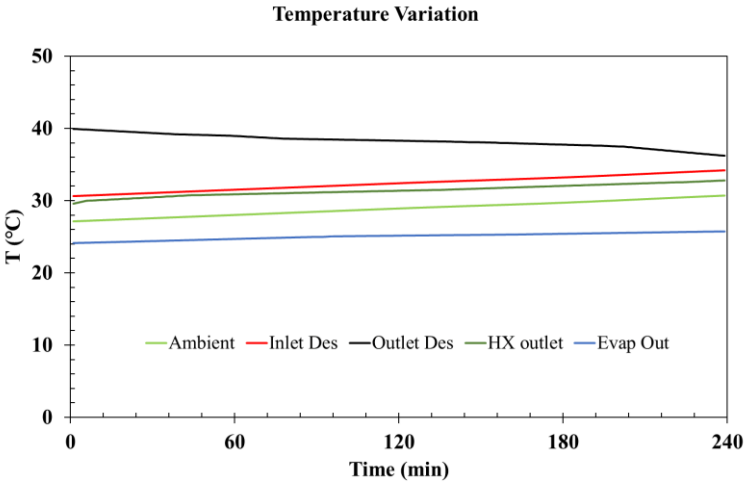

Figure 42: Temperature variation in discharging mode

The variation of the relative humidity of air in discharging mode, for various points of the system like desiccant inlet, desiccant outlet, heat exchanger outlet, evaporator outlet, and ambient is shown in Figure 43. Relative humidity at the ambient condition is changing between 54 – 73 % while inlet desiccant is in the range of 51– 68% for four hours of testing whereas the outlet relative humidity shows a constant behavior around 84%.

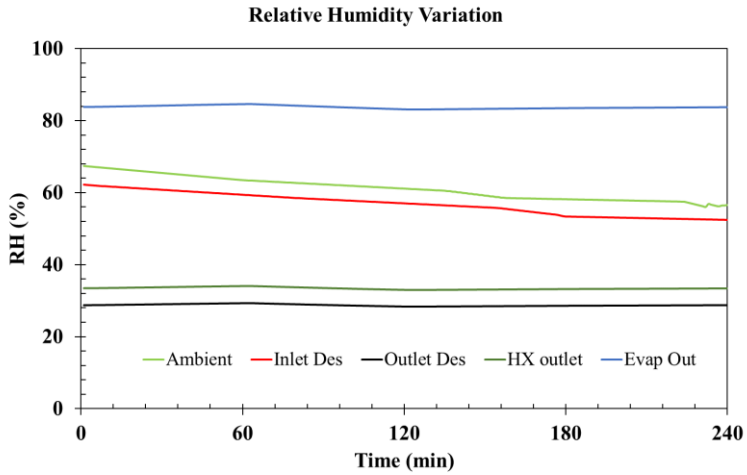

Figure 43: Relative humidity variation in discharging mode

The wet-bulb effectiveness variation in discharging mode is shown in Figure 44. The behavior of the material was almost steady. The peak wet-bulb effectiveness was obtained around 107% while the lowest value was nearly 102%.

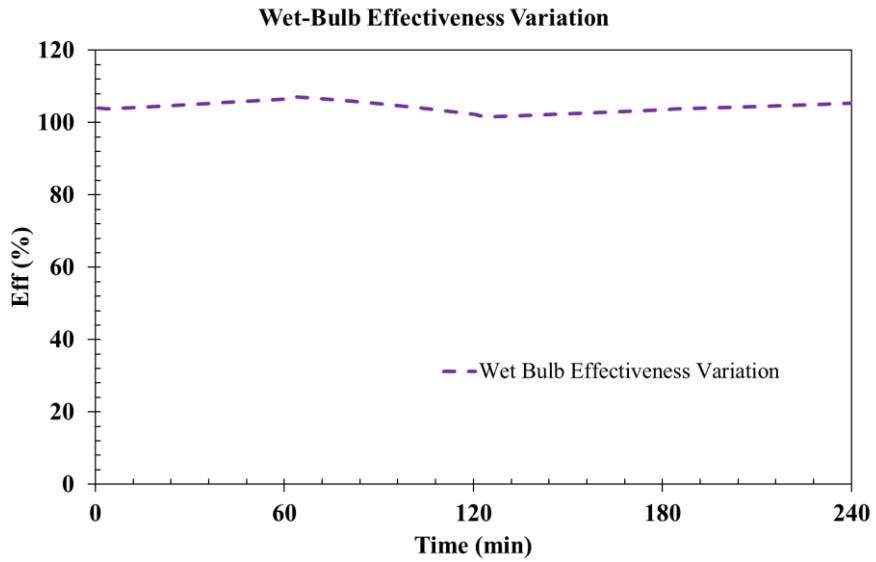

Figure 44: Wet-Bulb effectiveness variation in discharging mode

Wet bulb temperature is the lowest temperature to which air can be cooled by the evaporation of water into the air at a constant pressure and it is greater than dew point temperature. The dew-point effectiveness variation of silica gel in discharging phase was illustrated in Figure 45. As it is clear in the discharging process, the dew-point effectiveness shows a constant rise varying between 75-77% over 4 hours testing. As can be seen in Equations (9) and (13) since the wet bulb temperature is higher than the dew point temperature the wet bulb effectiveness is greater than the dew point effectiveness.

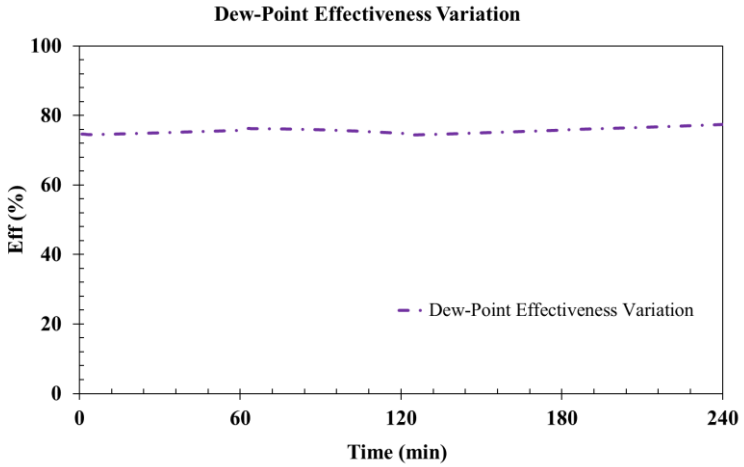

Figure 45: Dew-Point effectiveness variation in discharging mode

The cooling rate variation in discharging mode was illustrated in Figure 46 and calculated by the Equation (51):

$$\dot{Q}_c = \dot{m} C_p \left(T_{inlet,des} - T_{Evap,out} \right) \tag{51}$$

In this mode, silica gel showed a constant reduction from 0.5 to 0.4 kW with average cooling rate of 0.44 kW based on the performance of the material during four hours testing. During the real condition experiments the cooling rate of 0.49 kW achieved which validate the numerical analysis.

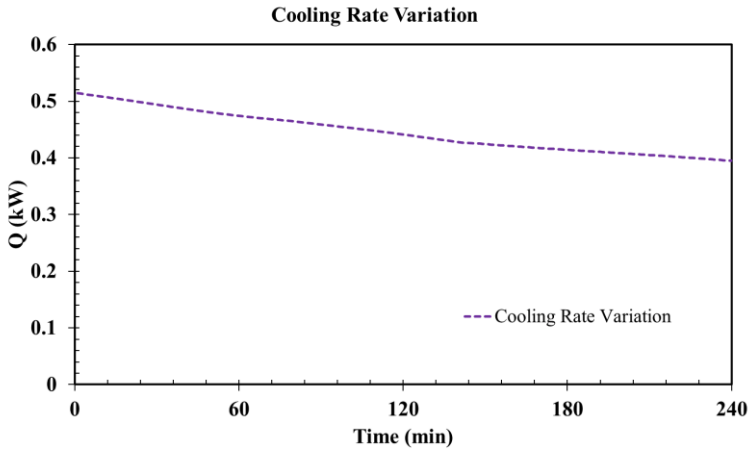

Figure 46: Cooling rate variation in discharging mode

Figure 47 shows the heat rejection rate from the air to the water tank via the heat exchanger for desiccant material. In the simulated DAEC unit, a water tank with 200 m^3 volumetric capacity is utilized. The initial water temperature inside the tank was set to 25 °C. As the water temperature inside the tank increased during the operation, the rate of heat rejection from the air to the water showed a decreasing trend. The average heat transfer rate to water over four hours of operation was found ~0.41 kW for silica gel.

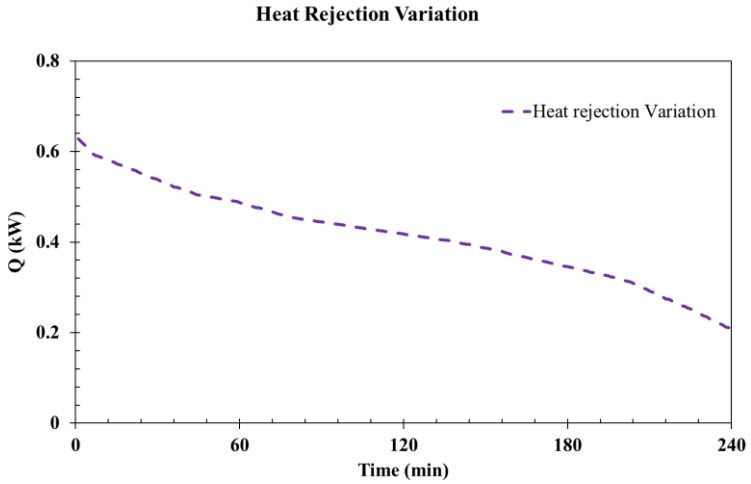

Figure 47: Heat rejection variation in DAEC mode

The calculated rate of mass changes in the tested material in discharging cycle is shown in Figure 48, where positive mass changes indicated the absorbed amount of water vapor. Based on the obtained results, average moisture absorption rates in four hours testing was achieved as 7.07 g/min. As can be seen by passing the time there is a gradual increase in water vapor absorption of silica gel since this desiccant is extremely efficient at low temperatures, but will lose some of its adsorbing capacity as temperatures begin to rise during four hours of testing.

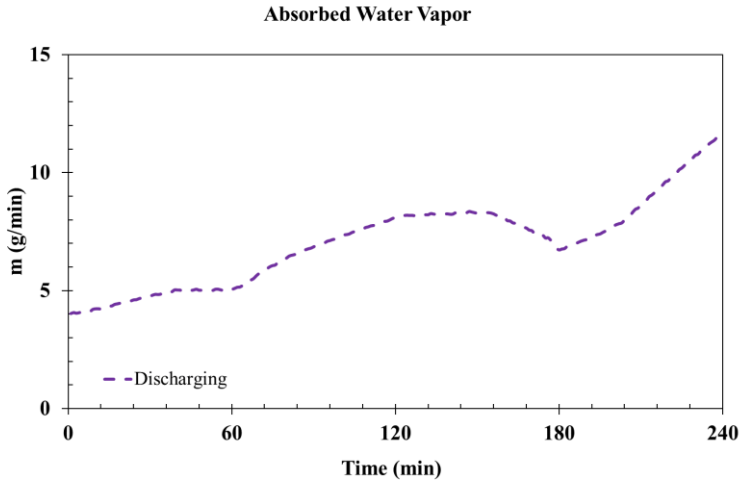

Figure 48: Moisture absorption rate variation in discharging mode

5.1.3 Overall Performance Analysis of solar driven DAEC System

The COP_t of the DAEC unit in four hours testing is shown in Figure 49. As seen, with T_{reg} of 55°C, the COP_t varied between 0.25→0.19. At T_{reg} of 55 °C, there is a gradual drop in COP_t with time. This is due to the insufficient regeneration of the desiccant at lower temperatures, thereby reduced moisture sorption capacity of it over time. As a result, regenerating the material at lower temperatures could lead to a drop in COP_t in the further cycles and it is recommended to increase the regeneration temperature. Also the COP_{th} shows a decreasing trend over four hours of testing and varied between 0.31-0.24, while reached to average value of 0.32.

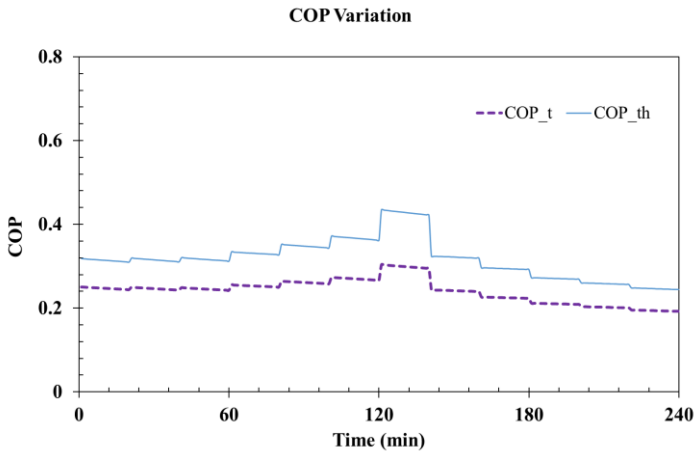

Figure 49: COP variation

The cumulative moisture absorption/desorption of the solar assisted DAEC system is shown in Figure 50. The total amount of moisture absorbed/desorbed in the test is determined as 1698.6/1485.4 g.

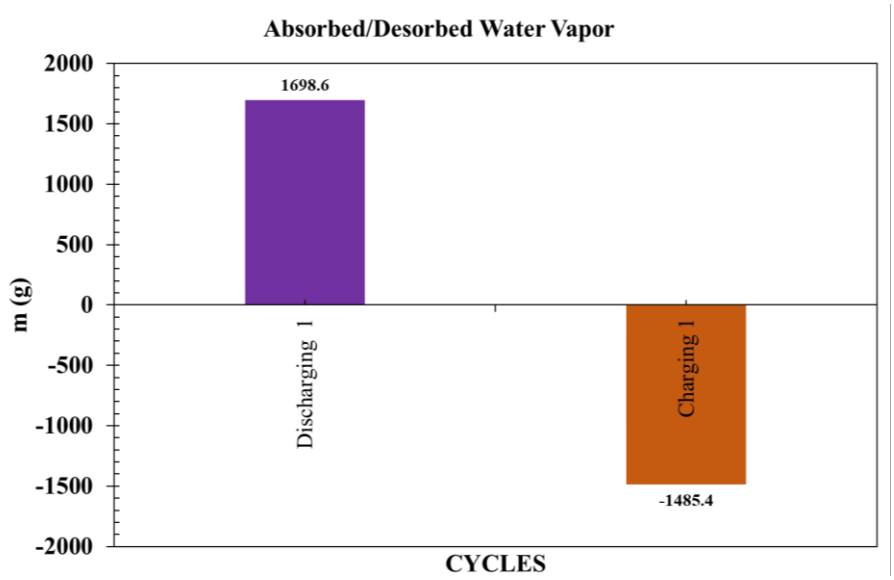

Figure 50: Cumulative moisture absorption/desorption in discharging/charging modes

5.2 Comparison of the Results

The values of the different performance parameters obtained from the experimental and numerical work for discharging and charging process are given in Tables 11 and 12, respectively. In the discharging phase, three different analysis methods performed. Based on the table the best results achieved in the lab scale test since the regeneration temperature was higher compared to real condition. In addition, during lab scale tests the duration of the experiments was limited to two hours, although in the real condition and simulation mode the time interval was increased to four hours. As it is illustrated, the real condition test shows acceptable performance with cooling rate of 0.49 kW and ΔT=8.4 ℃ compared to the simulated analysis with cooling rate of 0.44 kW and ΔT=7.4 ℃. It is important to mention that, since the mass flow rate in lab scale was

higher than the other analysis method, the greater cooling rate achieved in lab scale test. As explained before since the desiccant material that used is novel, it was not possible to define it in the TRNSYS, and because silica gel has close characteristics with Vmc-$CaCl_2$ it was employed in the simulation.

Table 11: Overall summary of the results of discharging for different case studies

Analysis method	**Material**	$\dot{m}$ **(kg/s)**	T_{in} **(°C)**	**ΔT (°C)**	Q_c **(kW)**	Q_R **(kW)**	m_{abs} **(g)**	COP_t	ε_{wb} **%**	ε_{dp} **%**
Lab scale	Vmc-$CaCl_2$	0.08	38	15.8	1.18	0.4	2274.7	0.47	122.6	89.8
Real condition	Vmc-$CaCl_2$	0.06	34	8.4	0.49	0.25	2187.4	0.27	121.6	90.2
Simulation	Silica gel	0.06	32	7.4	0.44	0.41	1698.6	0.24	104.2	75.6

As given in Table 12 three different analysis methods that studied in charging mode were summarized with same mass flow rate (0.03 kg/s). As mentioned before the experiments duration in the lab scale was around two hours which led to lower moisture desorption compared to other modes while the charging process in other methods was six hours. The hygrothermal efficiency (η_{hyg}) is another important parameter that was analyzed in the study. Based on the amount of water adsorption/desorption for various analysis methods, the simulation experiments reached to maximum hygrothermal efficiency of 87%.

Table 12: Overall summary of the results of charging for different case studies

Analysis method	Material	$\dot{m}$ (kg/s)	T_{reg} (°C)	m_{des} (g)	η_{hyg}
Lab scale	Vmc-$CaCl_2$	0.03	80	1188.7	0.52
Real condition	Vmc-$CaCl_2$	0.03	60	1441.5	0.65
Simulation	Silica gel	0.03	55	1485.4	0.87

5.3 Economic Analysis of the Solar-Driven DAEC System

In order to evaluate the economic and technical performance of the solar-driven DAEC system developed in this work, the annual cooling load of a residential building was simulated under NC climatic conditions. DesignBuilder software was used to simulate the energy consumption and environmental effects on the designed building. A schematic of the simulated building is shown in Figure 51. The simulated dwelling is a single floor building having an area of 60 m^2 and consists of a bedroom, a kitchen-living saloon, and a bathroom.

Since the weather data for Famagusta is not available in DesignBuilder software, Larnaca, which is the closest available location to Famagusta in Cyprus, was selected as the simulation geographical location. Since these cities are close to each other, year round climatic conditions of Larnaca and Famagusta is considered as same.

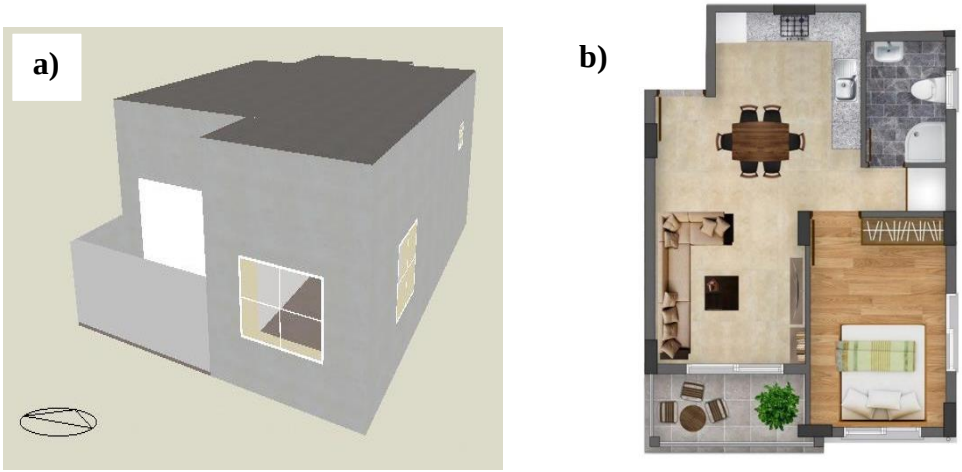

Figure 51: (a) 3-D schematic view, and (b) plan view of the simulated building

The parameters of the HVAC system that were used in the DesignBuilder software for calculating the cooling load are given in Table 13. Table 14 gives the numerical values of the rate of heat transfer of the simulated building components.

Table 13: Parameters of the HVAC system used for the building simulation

Parameter	Unit	Value
HVAC system	NA	Split no fresh
Cooling set point temperatures	ºC	Cooling → 25
COP	W/W	2.35
Air velocity for comfort calculations	m/s	0.1370
Design margin in system sizing	NA	1.25
Maximum ambient air temperature	ºC	35
Maximum ambient air humidity ratio	g/g	0.0156

Table 14: Rate of the heat transfer of building components

Surface	U ($W/m^2.K$)
Wall	0.353
Roof	0.250
Floor	0.253
Window	2.665
Door	5.429

From the simulation results, the cooling demand of the designed building achieved as 3369 kWh. Based on the assumed cooling capacity of 2 kW the system can deliver 3240 kWh which is 96% of the cooling demand of the building. The cooling period in this analysis was between 15:00-24:00.

It is found that the electrical energy required for cooling demand inside the building for cooling season (1st May-31th October) is 1378 kWh. The charging time during this simulation was between 09:00-15:00, while the discharging process analysed between 15:00-24:00.

In order to assess the potential of the proposed solar-driven DAEC system, a simplified economic feasibility analysis has been performed. The attractiveness of a solar-driven DAEC system depends on the initial investment, annual saving, discount rate, and annual maintenance cost. The proposed solar-driven DAEC system has been compared with an equivalent split unit heat pump system. The electricity tariff in NC based on the time of consumption is different and hence, US$ 0.12 [85] was considered as the average tariff in this study. In NC, the heat pump mode of a split air conditioner is generally used for cooling purposes. The equations used for determining the net present value (NPV), saving to investment ratio (SIR), simple payback period (SPP) and internal rate of return (IRR) in the economic feasibility analysis are as follows:

$$NPV = \Sigma PV_{AS} - \Sigma PV_{LCI} \quad (52)$$

where PV_{LCI} is the present value life cycle investment and PV_{AS} is the present value annual saving.

$$SIR = \frac{\Sigma PV_{AS}}{\Sigma PV_{LCI}} \quad (53)$$

$$SPP = \frac{Initial\ investment}{Annual\ saving} \quad (54)$$

IRR can be obtained when *SIR=1*, or NPV=0. (55)

A project could be considered economically feasible if SIR > 1, NPV > 0 and IRR > discount rate (See: Equations 53-55).

Table 15 gives the costs of the different components and the sorption material that were utilized in the solar-driven DAEC system developed and tested in this work. The installation of the proposed DAEC system, costs $500, which is considered as the capital investment of the project. Increasing electricity consumption for cooling usage in the building causes a decrease of the payback period and this results in a corresponding increase in the size of the solar-driven DAEC system. Based on the results of the analysis performed for a 10-years simulated duration, the usage of the solar-driven DAEC system is found to be economically feasible as compared to an A/C split unit. The values of the different economical parameters for an A/C split unit are as follow: NPV = $322, SIR = 1.3, IRR = 7% and SPP = 7.3 years while for the solar-driven DAEC system the achieved results are as: NPV = $960, SIR = 3, IRR = 31% and SPP = 3 years. As expressed before a project could be considered economically feasible if SIR > 1, NPV > 0, and IRR > discount rate. Consequently, the results indicate that the solar-driven DAEC system developed in this work is more economically feasible system.

Table 15: Cost of the components used in the solar-driven DAEC system

Item	Quantity	Cost ($)
Flat plate solar collector and frame	1	240
Heat Exchanger	2	60
Pump	3	90
Ducts and Installation	-	20
ECPM and DeM	1	50
Manufacturing cost of Desiccant and EC chamber	-	40
Total		500

The estimated economic analysis of A/C split unit and solar-driven DAEC system which are expected to be feasible can be seen in Table 16. As can be seen, the cost of A/C spilit unit for the designed building is 1200$, while the installation cost of the solar-driven DAEC is around 500$. After 10 years working period the residual value of the A/C split unit is 100$ while for the solar-driven DAEC is around 20$. By analyzing the results, it is possible to conclude that solar-driven DAEC is more feasible since the all the life cycle cost indicators are greater than the A/C split unit. The emission reductions expected from the use of each technology are also computed and listed in the table. Atikol et al. [86] indicates the power generating utilities which use fuel oil no. 6 and are assumed to operate with a thermal efficiency of 33%. The CO_2, SO_x and NO_x emissions of fuel oil no. 6 are taken as 0.263 kg/kWh, 1.47 g/kWh and 0.743 g/kWh, respectively. This project therefore has the potential to set an example and to create awareness amongst house builders in NC of the benefits of incorporating cost-effective, renewable solar energy technologies into new houses.

Table 16: Life cycle assessment of the proposed systems

Application	Installation cost ($)	Residual value ($)	Period (year)	NPV ($)	SIR	IRR (%)	SPP (year)	CO_2 (kg/year)	SO_x (g/year)	NO_x (g/year)
A/C split unit	1200	100	10	322	1.3	7	7.3	1098	6137	3102
Developed system	500	20	10	960	3	31	3	0.23	1.3	0.65

Chapter 6

CONCLUSIONS

6.1 Synthesis and Experimentation of Novel Composite Material

In this study, comparative analyses between EC and DAEC systems were performed in which, Vmc-$CaCl_2$ composite used as the DeM while, WoC, YeS, Pmc, EuF, and Vmc were employed as low cost natural ECPMs. Several performance parameters of EC and DAEC processes (temperature difference, relative humidity, water evaporation rate, cooling effectiveness, and COP) were comparatively analyzed for different materials. According to the current study results the findings are provided as follows:

- WoC was found as the most promising ECPM. In the EC mode operation, it provided an average ΔT of 10.6 °C and cooling rate of 0.90 kW. In DAEC mode, Vmc-$CaCl_2$/WoC was the leading DeM/ECPM couple with an average ΔT of 15 °C and cooling rate of 1.18 kW.
- With the use of WoC as an ECPM, obtained ΔT_{ave}, $\varepsilon_{wb,ave}$, $\varepsilon_{d,ave}$ and $\dot{Q}_{c,ave}$ in DAEC mode were found 41.5%, 50.6%, 52.5% and 31.3% higher than EC, respectively. This outcome indicates that; DAEC could be a suitable A/C method in hot-humid climates (RH>35 % and T>35 °C), where efficiency of EC remains low due to the high moisture content of ambient air.
- To investigate the cyclic behavior of Vmc-$CaCl_2$/WoC couple at different regeneration temperatures, three consequent charging/discharging cycles were performed. For regeneration temperatures of 60 °C, 70 °C and 80 °C,

absorption/desorption rates were found as 1569.63 / 792.20 g, 2275.92 / 941.32 g, and 2378.61 / 1832.58 g respectively.

- The performed analysis also showed that Vmc-$CaCl_2$ is an efficient material because of its rapid reaction, high equilibrium moisture content (~1 kg/kg), and high moisture desorption rate at T_{reg}=80 °C. Furthermore, the Vmc-$CaCl_2$ composite can be a promising material in further DAEC designs due to its low cost (0.45 $ /kg), its low critical RH (RH_{cr} = 32%) and its environmental friendly behaviour.

In terms of cyclic performance of DAEC process, it was found that the system operating with mass flow rate of 0.08 kg/s can provide thermal COP of 0.65.

6.2 Design and Development of a Solar-Driven DAEC System

The new solar-driven DAEC system was developed for the current work and its performance was examined under NC climatic conditions. Based on the analysis results, the important findings are concluded as follows:

- Three discharging- charging cycles utilizing Vmc-$CaCl_2$ as the DeM, and WoC as the ECPM were conducted in the developed solar-driven DAEC system. Over six hours of charging at T_{reg} = 60 – 50 °C and $\dot{m}$= 0.03 kg/s, in charging mode operation, it provided an average moisture desorption of 3.9 g/min.

  Over four hours of discharging at T_i = 32 – 35 °C and $\dot{m}$= 0.06 kg/s, in DAEC mode, Vmc-CaCl2/WoC reached to average ΔT of 8.4 °C and $\dot{Q}_{c,ave}$ of 0.49 kW.
- In the DAEC mode average $\varepsilon_{wb,ave}$, $\varepsilon_{d,ave}$ of 121.6% and 90.2%, were obtained respectively.

- To investigate the cyclic behaviour of Vmc-$CaCl_2$/WoC couple at different regeneration temperatures, three sequential charging/discharging cycles were performed in real conditions. For regeneration temperatures of 60 °C, 55 °C and 50 °C, the total amount of moisture absorbed/desorbed in these cycles were achieved as 2314.70 / 1529.13 g, 2206.12 / 1403.46 g, and 2041.41 / 1392.02 g, respectively. In addition, the average COP_t was found as 0.27.

6.3 Numerical and Simulation Analysis of a Solar-Driven DAEC System

Firstly, a solar driven desiccant based air conditioning system in ventilation mode in two different configuration schemes for discharging-charging modes was modelled, simulated and analysed for the climatic conditions of Larnaca using TRNSYS software. According to the obtained results, conclusions are presented as:

- A discharging- charging cycle utilizing silica gel as the DeM, and WoC as the ECPM was conducted in the developed solar-assisted DAEC system. Over six hours of charging at T_{reg} = 55 °C and $\dot{m}$= 0.03 kg/s, in charging mode operation, it provided an average moisture desorption of 4.1 g/min.
- Over four hours of discharging at T_i = 32 °C and $\dot{m}$= 0.06 kg/s, in discharging mode, silica gel/WoC reached to average ΔT of 7.4 °C and $\dot{Q}_{c,ave}$ of 0.44 kW.
- In the discharging mode average $\varepsilon_{wb,ave}$, $\varepsilon_{d,ave}$ of 104.2% and 75.6%, achieved respectively.
- For regeneration temperatures of 55 °C the total amount of moisture absorbed/desorbed in the cycle was achieved as 1698.6 / 1485.4 g.
- The average COP_t of the simulated system was found as 0.24.

In addition, an economic feasibility comparison between the developed DAEC system and a typical A/C split unit was performed for a house simulated in the DesignBuilder software package. The annual cooling load of a residential building with a surface area of 60 m^2 was simulated using the DesignBuilder software. An economic feasibility comparison between the proposed solar-driven DAEC system and an A/C split unit used in the simulated house was performed. Based on the assumed cooling capacity of 2 kW the system can deliver 3240 kWh which is 96% of the cooling demand of the building.

It is found that the electrical energy required for cooling demand inside the building for cooling season (1st May-31th October) is 1378 kWh. The charging time during this simulation was between 09:00-15:00, while the discharging process analysed between 15:00-24:00. According to the economic feasibility analysis, the following values were obtained: NPV = $960, SIR = 3, IRR = 31% and SPP = 3 years. A project could be considered economically feasible if SIR > 1, NPV > 0, and IRR > discount rate. Moreover, based on the performed LCA, the developed system produces 0.23 kg/year CO_2, which shows that it is environmentally friendly and economically feasible for using in residential buildings in NC.

6.4 Future Work and Recommendations

Based on the performed analyses and obtained results of the current study, future work suggestions and recommendations are as follows:

- Synthesis can be performed with new composites with a lower regeneration temperature and strong physical stability.
- A new solar-driven DAEC system can be developed with higher charging capacity, cooling load and temperature difference.

- Real-life pilot projects for the dissemination of solar-driven DAEC system and industrial waste heat recovery with thermochemical materials can be developed.
- Coupling of DAEC system to other conventional cooling systems for improving the energetic performance of the whole system can be performed.
- Importance and requirement of exergy analysis for improving the system performance should be considered.

REFERENCES

[1] American Society of Heating, Refrigerating and Air-Conditioning Engineers, Inc (2004). *Thermal Environmental Conditions for Human Occupancy*. ANSI/ASHRAE Standard 55-2004.

[2] Thu, K., Mitra, S., Saha, B. B., & Murthy, S. S. (2018). Thermodynamic feasibility evaluation of hybrid dehumidification–mechanical vapour compression systems. *Applied Energy*, *213*, 31-44.

[3] Jaradat, M. (2019). Thermochemical Energy Storage in Low Flow Liquid Desiccant Regenerator. *International Energy Journal*, *19*(1).

[4] Liu, X., Xie, Y., Zhang, T., Chen, L., & Cong, L. (2018). Experimental investigation of a counter-flow heat pump driven liquid desiccant dehumidification system. *Energy and Buildings*, *179*, 223-238.

[5] Liang, J. D., Huang, B. H., Chiang, Y. C., & Chen, S. L. (2020). Experimental investigation of a liquid desiccant dehumidification system integrated with shallow geothermal energy. *Energy*, *191*, 116452.

[6] Aydin, D., Charidi, M., & Khosravi, N. (2019). Synthesis and experimental investigation of V-CaCl2 composite desiccant for performance enhancement in evaporative cooling applications. *Proceedings of the Institution of Mechanical Engineers, Part E: Journal of Process Mechanical Engineering*, 0954408919889287.

[7] Rafique, M. M., Gandhidasan, P., Rehman, S., & Al-Hadhrami, L. M. (2015). A review on desiccant based evaporative cooling systems. *Renewable and Sustainable Energy Reviews*, *45*, 145-159.

[8] Misha, S., Mat, S., Ruslan, M. H., & Sopian, K. (2012). Review of solid/liquid desiccant in the drying applications and its regeneration methods. *Renewable and Sustainable Energy Reviews*, *16*(7), 4686-4707.

[9] Gandhidasan, P. (2004). A simplified model for air dehumidification with liquid desiccant. *Solar energy*, *76*(4), 409-416.

[10] Zheng, X., Ge, T. S., & Wang, R. Z. (2014). Recent progress on desiccant materials for solid desiccant cooling systems. *Energy*, *74*, 280-294.

[11] Henning, H. M. (2007). Solar assisted air conditioning of buildings–an overview. *Applied thermal engineering*, *27*(10), 1734-1749.

[12] Collier Jr, R. K. (1989). Desiccant properties and their effect on cooling system performance. *ASHRAE transactions*, *95*, 823-827.

[13] Zheng, X., Ge, T. S., & Wang, R. Z. (2014). Recent progress on desiccant materials for solid desiccant cooling systems. *Energy*, *74*, 280-294.

[14] Camargo, J. R., Ebinuma, C. D., & Cardoso, S. (2003). A mathematical model for direct evaporative cooling air conditioning system. *Revista de Engenharia Térmica*, *2*(2), 30-34.

[15] Heidarinejad, G., Bozorgmehr, M., Delfani, S., & Esmaeelian, J. (2009). Experimental investigation of two-stage indirect/direct evaporative cooling system in various climatic conditions. *Building and Environment*, *44*(10), 2073-2079.

[16] Sodha, M. S., Ashutosh, S., Kumar, A., & Sharma, A. K. (1986). Thermal performance of an evaporatively cooled multi-storey building. *Building and Environment*, *21*(2), 71-79.

[17] Porumb, B., Ungureşan, P., Tutunaru, L. F., Şerban, A., & Bălan, M. (2016). A review of indirect evaporative cooling technology. *Energy Procedia*, *85*, 461-471.

[18] Camargo, J. R., Ebinuma, C. D., & Cardoso, S. (2002). A mathematical model for direct and indirect evaporative cooling air conditioning systems. In *Proceedings of the 9th Brazilian congress of thermal engineering and sciences, CONEM*.

[19] Evaporative Cooling System, Indirect Direct Evaporative Cooling Systems. (n.d.). Retrieved from http://ategroup.com/hmx/why-evaporative/.

[20] Warke, D. A., & Deshmukh, S. J. (2017). Experimental analysis of cellulose cooling pads used in evaporative coolers. *Int. J. Energy Sci. Eng.*, *3*(4), 37-43.

[21] Vala, K. V., Kumpavat, M. T., & Nema, A. (2016). Comparative performance evaluation of evaporative cooling local pad materials with commercial pads. *International Journal of Engineering Trends and Technology*, *39*(4), 198-203.

[22] Doğramacı, P. A., & Aydın, D. (2020). Comparative experimental investigation of novel organic materials for direct evaporative cooling applications in hot-dry climate. *Journal of Building Engineering*, *30*, 101240.

[23] Kanoglu, M., Dincer, I., & Rosen, M. A. (2007). Exergy analysis of psychrometric processes for HVAC&R applications. *ASHRAE Transactions*, *113*(2), 172-181.

[24] Daou, K., Wang, R. Z., & Xia, Z. Z. (2006). Desiccant cooling air conditioning: a review. *Renewable and Sustainable Energy Reviews*, *10*(2), 55-77.

[25] Enteria, N., & Mizutani, K. (2011). The role of the thermally activated desiccant cooling technologies in the issue of energy and environment. *Renewable and Sustainable Energy Reviews*, *15*(4), 2095-2122.

[26] Baniyounes, A. M., Ghadi, Y. Y., Rasul, M. G., & Khan, M. M. K. (2013). An overview of solar assisted air conditioning in Queensland's subtropical regions, Australia. *Renewable and Sustainable Energy Reviews*, *26*, 781-804.

[27] Sahlot, M., & Riffat, S. B. (2016). Desiccant cooling systems: a review. *International Journal of Low-Carbon Technologies*, *11*(4), 489-505.

[28] Reddy, S., Priya, S. S., Carollo, A. J., & Kumar, S. H. (2020). TRNSYS simulation for solar-assisted liquid desiccant evaporative cooling. *International Journal of Ambient Energy*, *41*(1), 105-111.

[29] Qi, R., Dong, C., & Zhang, L. Z. (2020). A review of liquid desiccant air dehumidification: from system to material manipulations. *Energy and Buildings*, 109897.

[30] Koronaki, I. P., Christodoulaki, R. I., Papaefthimiou, V. D., & Rogdakis, E. D. (2013). Thermodynamic analysis of a counter flow adiabatic dehumidifier with different liquid desiccant materials. *Applied Thermal Engineering*, *50*(1), 361-373.

[31] Mei, L., & Dai, Y. J. (2008). A technical review on use of liquid-desiccant dehumidification for air-conditioning application. *Renewable and Sustainable Energy Reviews*, *12*(3), 662-689.

[32] Sultan, M., El-Sharkawy, I. I., Miyazaki, T., Saha, B. B., & Koyama, S. (2015). An overview of solid desiccant dehumidification and air conditioning systems. *Renewable and Sustainable Energy Reviews*, *46*, 16-29.

[33] Gandhidasan, P. (2004). A simplified model for air dehumidification with liquid desiccant. *Solar energy*, *76*(4), 409-416.

[34] Baniyounes, A. M., Ghadi, Y. Y., Rasul, M. G., & Khan, M. M. K. (2013). An overview of solar assisted air conditioning in Queensland's subtropical regions, Australia. *Renewable and Sustainable Energy Reviews*, *26*, 781-804.

[35] Singh, R. P., Mishra, V. K., & Das, R. K. (2018, August). Desiccant materials for air conditioning applications-A review. In *IOP Conference Series: Materials Science and Engineering* (Vol. 404, No. 1, p. 012005). IOP Publishing.

[36] Zheng, X., Ge, T. S., & Wang, R. Z. (2014). Recent progress on desiccant materials for solid desiccant cooling systems. *Energy*, *74*, 280-294.

[37] Chaudhary, G. Q., Ali, M., Sheikh, N. A., & Khushnood, S. (2018). Integration of solar assisted solid desiccant cooling system with efficient evaporative cooling technique for separate load handling. Applied Thermal Engineering, 140, 696-706.

[38] Nain, S., Kajal, S., & Parinam, A. (2020). Thermal performance of desiccant-based solar air-conditioning system with silica gel coating. *Environment, Development and Sustainability*, *22*(1), 281-296.

[39] Luo, W. J., Faridah, D., Fasya, F. R., Chen, Y. S., Mulki, F. H., & Adilah, U. N. (2019). Performance Enhancement of Hybrid Solid Desiccant Cooling Systems by Integrating Solar Water Collectors in Taiwan. *Energies*, *12*(18), 3470.

[40] Mahmood, M. H., Sultan, M., & Miyazaki, T. (2019). Solid desiccant dehumidification-based air-conditioning system for agricultural storage application: Theory and experiments. *Proceedings of the Institution of Mechanical Engineers, Part A: Journal of Power and Energy*, 0957650919869503.

[41] Saputra, D. A., Saputra, N. A., Susanti, L., Fithri, P., & Putra, D. I. (2019, August). Design of solid desiccant air conditioning system. In *IOP Conference Series: Materials Science and Engineering* (Vol. 602, No. 1, p. 012077). IOP Publishing.

[42] Fan, W., Kokogiannakis, G., & Ma, Z. (2019). Integrative modelling and optimisation of a desiccant cooling system coupled with a photovoltaic thermal-solar air heater. *Solar Energy*, *193*, 929-947.

[43] Avargani, V. M., Karimi, R., & Gheinani, T. T. (2019). Mathematical modeling of an integrated system for regeneration of solid desiccants using a solar parabolic dish concentrator. *International Journal of Heat and Mass Transfer*, *142*, 118479.

[44] Mehla, N., & Yadav, A. (2019). An experimental investigation on solar powered solid desiccant air conditioning (SPSDAC) based on regenerative evaporative cooling system with PCM unit. *International Journal of Ambient Energy*, 1-12.

[45] Fong, K. F., & Lee, C. K. (2020). Solar desiccant cooling system for hot and humid region–A new perspective and investigation. *Solar Energy*, *195*, 677-684.

[46] Heidari, A., Roshandel, R., & Vakiloroaya, V. (2019). An innovative solar assisted desiccant-based evaporative cooling system for co-production of water and cooling in hot and humid climates. *Energy conversion and Management*, *185*, 396-409.

[47] Sohani, A., Sayyaadi, H., & Azimi, M. (2019). Employing static and dynamic optimization approaches on a desiccant-enhanced indirect evaporative cooling system. *Energy Conversion and Management*, *199*, 112017.

[48] Sudhakar, K., Jenkins, M. S., Mangal, S., & Priya, S. S. (2019). Modelling of a solar desiccant cooling system using a TRNSYS-MATLAB co-simulator: A review. *Journal of Building Engineering*, *24*, 100749.

[49] Pandelidis, D., Pacak, A., Cichoń, A., Anisimov, S., Drąg, P., Vager, B., & Vasilijev, V. (2018). Multi-stage desiccant cooling system for moderate climate. *Energy Conversion and Management*, *177*, 77-90.

[50] Caliskan, H., Hong, H., & Jang, J. K. (2019). Thermodynamic assessments of the novel cascade air cooling system including solar heating and desiccant cooling units. *Energy Conversion and Management*, *199*, 112013.

[51] Zhou, X., & Reece, R. (2019). Experimental investigation for a non-adiabatic desiccant wheel with a concentric structure at low regeneration temperatures. *Energy Conversion and Management*, *201*, 112165.

[52] Rayegan, S., Motaghian, S., Heidarinejad, G., Pasdarshahri, H., Ahmadi, P., & Rosen, M. A. (2020). Dynamic simulation and multi-objective optimization of a solar-assisted desiccant cooling system integrated with ground source renewable energy. *Applied Thermal Engineering*, 115210.

[53] Comino, F., González, J. C., Navas-Martos, F. J., & de Adana, M. R. (2020). Experimental energy performance assessment of a solar desiccant cooling system in Southern Europe climates. *Applied Thermal Engineering*, *165*, 114579.

[54] Singh, A., Kumar, S., Dev, R. (2019). Studies on cocopeat, sawdust and dried cow dung as desiccant for evaporative cooling system. *Renewable Energy*, *142*, 295-303.

[55] She, X., Yin, Y., & Zhang, X. Thermodynamic analysis of a novel energy-efficient refrigeration system subcooled by liquid desiccant dehumidification and evaporation. *Energy Conversion and Management* 2014; *78*: 286-296.

[56] Liu, J., Liu, X., & Zhang, T. (2020). Performance of heat pump driven internally cooled liquid desiccant dehumidification system. Energy Conversion and Management, 205, 112447.

[57] Nain, S., Kajal, S., & Parinam, A. (2020). Thermal performance of desiccant-based solar air-conditioning system with silica gel coating. *Environment, Development and Sustainability*, *22*(1), 281-296.

[58] Batukray, J. D. (2019). An overview on desiccant assisted evaporative cooling in hot and humid climates. *Algerian Journal of Engineering and Technology*, *1*(1), 32-38.

[59] Jani, D. B., Bhabhor, K., Dadi, M., Doshi, S., Jotaniya, P. V., Ravat, H., & Bhatt, K. (2019). A review on use of TRNSYS as simulation tool in performance

prediction of desiccant cooling cycle. *Journal of Thermal Analysis and Calorimetry*, 1-21.

[60] Chen, X., Riffat, S., Hongyu, B., Zheng, X., & Reay, D. (2019). Recent Progress in Liquid Desiccant Dehumidification and Air-conditioning: A Review. *Energy and Built Environment*.

[61] La, D., Dai, Y., Li, Y., Ge, T., & Wang, R. (2011). Case study and theoretical analysis of a solar driven two-stage rotary desiccant cooling system assisted by vapor compression air-conditioning. *Solar energy*, *85*(11), 2997-3009.

[62] Jia, C. X., Dai, Y. J., Wu, J. Y., & Wang, R. Z. (2007). Use of compound desiccant to develop high performance desiccant cooling system. *International Journal of Refrigeration*, *30*(2), 345-353.

[63] Guo, P., Wong-Foy, A. G., & Matzger, A. J. (2014). Microporous coordination polymers as efficient sorbents for air dehumidification. *Langmuir*, *30*(8), 1921-1925.

[64] Niu, J. L., Zhang, L. Z., & Zuo, H. G. (2002). Energy savings potential of chilled-ceiling combined with desiccant cooling in hot and humid climates. *Energy and Buildings*, *34*(5), 487-495.

[65] Dai, Y. J., Wang, R. Z., Zhang, H. F., & Yu, J. D. (2001). Use of liquid desiccant cooling to improve the performance of vapor compression air conditioning. *Applied Thermal Engineering*, *21*(12), 1185-1202.

[66] Goldsworthy, M., & White, S. (2011). Optimization of a desiccant cooling system design with indirect evaporative cooler. *International Journal of refrigeration*, *34*(1), 148-158.

[67] Ge, T. S., Ziegler, F., Wang, R. Z., & Wang, H. (2010). Performance comparison between a solar driven rotary desiccant cooling system and conventional vapor compression system (performance study of desiccant cooling). *Applied Thermal Engineering*, *30*(6-7), 724-731.

[68] Casey, S. P., Elvins, J., Riffat, S., & Robinson, A. (2014). Salt impregnated desiccant matrices for 'open'thermochemical energy storage—selection, synthesis and characterisation of candidate materials. *Energy and buildings*, *84*, 412-425.

[69] Cengel, Y. A., & Boles, M. A. (2007). *Thermodynamics: An Engineering Approach 6th Editon (SI Units)*. The McGraw-Hill Companies, Inc., New York.

[70] The Sensirion Company: Basic Principles on Physics of Water Vapor, The Sensirion Company, Staefa, Switzerland, 2009. (2020, February 25). Retrieved fromhttps://www.sos.sk/a_info/resource/c/sensirion/Sensirion_Introduction_to_Relative_Humidity_V2.pdf.

[71] Cao, Z., Tester, J. W., Sparks, K. A., & Trout, B. L. (2001). Molecular computations using robust hydrocarbon− water potentials for predicting gas hydrate phase equilibria. *The Journal of Physical Chemistry B*, *105*(44), 10950-10960.

[72] Sonntag, R. E., Van Wylen, G. J., & Borgnakke, C. (2008). *Fundamentals of thermodynamics*. Wiley.

[73] Stull, R. (2011). Wet-bulb temperature from relative humidity and air temperature. *Journal of applied meteorology and climatology*, *50*(11), 2267-2269.

[74] Buker, M. S., Mempouo, B., & Riffat, S. B. (2014). Performance evaluation and techno-economic analysis of a novel building integrated PV/T roof collector: An experimental validation. *Energy and Buildings*, *76*, 164-175.

[75] World weather online information (2020, March 6). Retrieved from https://www.worldweatheronline.com/nicosia-weather-history/nicosia/cy.aspx.

[76] Photovoltaic geographical information system (2020, March 6). Retrieved from https://re.jrc.ec.europa.eu/pvg_tools/en/tools.html#MR.

[77] Comino, F., González, J. C., Navas-Martos, F. J., & de Adana, M. R. (2020). Experimental energy performance assessment of a solar desiccant cooling system in Southern Europe climates. *Applied Thermal Engineering*, *165*, 114579.

[78] Hussain, S., Kalendar, A., Rafique, M. Z., & Oosthuizen, P. (2020). Numerical investigations of solar-assisted hybrid desiccant evaporative cooling system for hot and humid climate. *Advances in Mechanical Engineering*, *12*(6), 1687814020934999.

[79] Fong, K. F., & Lee, C. K. (2020). Solar desiccant cooling system for hot and humid region–A new perspective and investigation. *Solar Energy*, *195*, 677-684.

[80] Belguith, S., Meddeb, Z., & Slama, R. B. (2021). Performance analysis of desiccant cooling systems in a hot and dry climate. *Euro-Mediterranean Journal for Environmental Integration*, *6*(1), 1-11.

[81] De Antonellis, S., Colombo, L., Freni, A., & Joppolo, C. (2021). Feasibility study of a desiccant packed bed system for air humidification. *Energy*, *214*, 119002.

[82] Ahmad, W., Ali, M., Sheikh, N. A., & Akhtar, J. (2020). Effect of efficient multi-stage indirect evaporative cooling on performance of solar assisted desiccant air conditioning in different climatic zones. *Heat and Mass Transfer*, *56*(9), 2725-2741.

[83] Ahamed, M. S., Guo, H., & Tanino, K. (2020). Modeling heating demands in a Chinese-style solar greenhouse using the transient building energy simulation model TRNSYS. *Journal of Building Engineering*, *29*, 101114.

[84] Sharafian, A., Fayazmanesh, K., McCague, C., & Bahrami, M. (2014). Thermal conductivity and contact resistance of mesoporous silica gel adsorbents bound with polyvinylpyrrolidone in contact with a metallic substrate for adsorption cooling system applications. *International journal of heat and mass transfer*, *79*, 64-71.

[85] Kibtek (2020, November 25). Retrieved from https://www.kibtek.com/

[86] Atikol, U., Abbasoglu, S., & Nowzari, R. (2013). A feasibility integrated approach in the promotion of solar house design. *International journal of energy research*, *37*(5), 378-388.

APPENDIX

TRNSYS CODES

SUBROUTINE TYPE683 (TIME,XIN,OUT,T,DTDT,PAR,INFO,ICNTRL,*)

This subroutine models a rotary desiccant dehumidifier containing nominal silica gel and whose performance is based on equations for f1-f2 potentials developed by Jurinak. The model determines the regeneration temerature at ambient humidity ratio which will dehumidify exactly to the supply humidity ratio. The process stream outlet temperature is also determined.

SAMPLE INPUT AND OUTPUT VALUES

PARAMETERS	SAMPLE VALUES
PAR (1) ETAF1 DEHUMIDIFIER EFFECTIVENESS 1	0.08
PAR (2) ETAF2 DEHUMIDIFIER EFFECTIVENESS 2	0.95
INPUTS	
XIN (1) TEMP (1) PROCESS AIR INLET TEMPERATURE	25.0
XIN (2) W (1) PROCESS AIR INLET HUMIDITY RATIO (1) WDEH	0.012
XIN (3) MSYS PROCESS AIR MASS FLOW RATE	450.0
XIN (4) W (3) REGENERATION AIR INLET HUMIDITY RATIO (3) WREG	0.012
XIN (5) MREG REGENERATION AIR MASS FLOW RATE	1.0
XIN (6) W (2) DEHUMIDIFIER SET POINT HUMIDITY RATIO (2)	0.009
XIN (7) TA AMBIENT TEMPERATURE	18.0
XIN (8) ION HUMIDIFIER CONTROL SIGNAL	1.0
OUTPUTS	
OUT (1) TDEH PROCESS AIR OUTLET TEMPERATURE	24.5
OUT (2) WDEH PROCESS AIR OUTLET HUMIDITY RATIO	0.0125
OUT (3) MSYS PROCESS AIR FLOW RATE	450.0
OUT (4) TREG REQUIRED REGENERATION TEMPERATURE (3)	18.0
OUT (5) xxxx REGENERATION AIR OUTLET TEMPERATURE	24.5
OUT (6) WREG REGENERATION AIR OUTLET HUMIDITY RATIO	0.0125
OUT (7) MREG REGENERATION AIR FLOW RATE	1.0
OUT (8) TEMP (4) TEMPERATURE	18.0
OUT (9) W (4) HUMIDITY	0.02

STATE INFORMATION

(1) refers to the process air inlet state

(2) refers to the process air outlet state

(3) refers to the regeneration air inlet state

(4) refers to the regeneration air outlet state

```
!export this subroutine for its use in external DLLs.
!DEC$ATTRIBUTES DLLEXPORT :: TYPE683
ACCESS TRNSYS FUNCTIONS
        USE TrnsysFunctions
        USE TrnsysConstants
IMPLICIT NONE !force explicit declaration of all variables
TRNSYS DECLARATIONS
DOUBLE PRECISION XIN,OUT,TIME,PAR,T,DTDT,TIME0,TFINAL,DELT
    INTEGER*4 INFO (15),NP,NI,NO,ND,IUNIT,ITYPE,ICNTRL
    CHARACTER*3 OCHECK,YCHECK
SET THE MAXIMUM NUMBER OF PARAMETERS (NP), INPUTS (NI),
OUTPUTS (NO), AND DERIVATIVES (ND)
THAT MAY BE SUPPLIED FOR THIS TYPE
PARAMETER (NP=2,NI=8,NO=7,ND=0)
```

```
REQUIRED TRNSYS DIMENSIONS
DIMENSION XIN(NI),OUT(NO),PAR(NP),YCHECK(NI),OCHECK(NO)
COMMON BLOCKS
!none used by this component
LOCAL VARIABLE DECLARATIONS
CHARACTER (LEN=maxMessageLength) MSG1,MSG2
DIMENSION TEMP (4),W (4)
DOUBLE PRECISION ETAF1,ETAF2,F1,F2,A1,A2,A3,TEMP,ZZ,W,B1,B2,B3,H,
&  HFG,CPA,CPV,ION,TA,TDEH,WDEH,TREG,WREG,F11,F21,F12I  ,F23I  ,F13
,F23, & F12,F22,F22I,WOLD,FNW,DFNW,WNEW,TMIX,WMIX
INTEGER I
DOUBLE PRECISION MSYS,MREG
DATA STATEMENTS
DATA A1/2865/,A2/4.344/,A3/0.8624/   !data for F1 potential of silica gel
DATA B1/6360/,B2/1.127/,B3/0.07969/  !data for F2 potential of silica gel
DATA ZZ/1.490/,CPA/1.0/,CPV/1.805/
DATA HFG/2501./
DATA YCHECK/'TE1','DM1','MF1','DM1','MF1','DM1','TE1','DM1'/
DATA OCHECK/'TE1','DM1','MF1','TE1','TE1','DM1','MF1'/
DATA MSG1/'Regeneration temperature did not converge.'/
DATA MSG2/'Humidity ratio did not converge.'/
DEFINE FUNCTIONS USED BY THIS COMPONENT
F1 (I) = -A1/((TEMP(I)+273.15)**ZZ)+A2*(W(I)**A3)
F2 (I) = ((TEMP(I)+273.15)**ZZ)/B1 - B2*(W(I)**B3)
H (I) = CPA*TEMP(I) + W(I)*(HFG + CPV*TEMP(I))
GET GLOBAL TRNSYS SIMULATION VARIABLES
TIME0=getSimulationStartTime()
TFINAL=getSimulationStopTime()
DELT=getSimulationTimeStep()
SET THE VERSION INFORMATION FOR TRNSYS
IF (INFO(7).EQ.-2) THEN
INFO(12)=16
RETURN 1
ENDIF
PERFORM LAST CALL MANIPULATIONS
IF (INFO (8).EQ.-1) RETURN 1 !none are required for this TYPE
PERFORM FIRST CALL MANIPULATIONS
IF (INFO(7).EQ.-1) THEN
!retrieve unit and type number for this component from the INFO array
IUNIT=INFO(1)
ITYPE=INFO(2)
!set some info array variables to tell the trnsys engine how this type is to work
INFO(6)=NO   !reserve space in the OUT array using INFO(6)
INFO(9)=1    !set the way in which this component is to be called
INFO(10)=0   !set required number of spots in the single precision storage structure
!call the type check subroutine to compare what this type requires with what is in the
input file.
CALL TYPECK(1,INFO,NI,NP,ND)
!call the input-output check subroutine to set the correct input and output units.
CALL RCHECK(INFO,YCHECK,OCHECK)
```

```
!return to the calling program
RETURN 1
ENDIF
PERFORM INITIAL TIMESTEP MANIPULATIONS
IF (TIME.LT.(TIME0+DELT/2.)) THEN
!set the UNIT number for future calls
IUNIT=INFO(1)
ITYPE=INFO(2)
!read parameter values
ETAF1 = PAR(1)
ETAF2 = PAR(2)
!check the parameters for problems and RETURN if any are found
IF((ETAF1.LT.0.).OR.(ETAF1.GT.1.)) CALL TYPECK(-4,INFO,0,1,0)
IF((ETAF2.LT.0.).OR.(ETAF2.GT.1.)) CALL TYPECK(-4,INFO,0,2,0)
!perform any required calculations, set the outputs to the input initial values.
OUT(1:NO)=0.d0  !zero output initial values
RETURN 1        !the first timestep is for initialization - exit.
ENDIF
PERFORM POST CONVERGENCE MANIPULATIONS
IF(INFO(13).GT.0) RETURN 1
RE-READ THE PARAMETERS IF ANOTHER UNIT OF THIS TYPE HAS BEEN
CALLED SINCE THE LAST
TIME THEY WERE READ IN
IF(INFO(1).NE.IUNIT) THEN
!reset the unit number
IUNIT=INFO (1)
ITYPE=INFO (2)
!read the parameter values
ETAF1 = PAR (1)
ETAF2 = PAR (2)
ENDIF
RETRIEVE THE CURRENT VALUES OF THE INPUTS TO THIS MODEL FROM
THE XIN ARRAY
TEMP (1) = XIN (1)         !process air inlet temperature
W (1)       = XIN (2)         !process air inlet humidity ratio
MSYS       = XIN (3)         !process air mass flow rate
W (3)       = XIN (4)         !regeneration air humidity ratio
MREG       = XIN (5)         !regeneration air mass flowrate
W (2)       = XIN (6)         !humidifier set point humidity ratio
TA           = XIN (7)         !ambient temperature
ION          = XIN (8)         !control signal
IF ((ION .EQ. 0.).OR.(W(1).LT.W(2))) THEN  !the dehumidifier is OFF, set outputs
to inputs and exit
TDEH     = TEMP (1)
WDEH     = W (1)
TREG     = TA
WREG     = W (3)
TEMP (4) = TREG
W(4)     = WREG
GO TO 100
```

```
ELSE
CONTINUE
ENDIF
F11 = F1 (1)  !calculate F1 potential for process air inlet condition
F21 = F2 (1)  !calculate F2 potential for process air inlet condition
F12I= F11
TEMP (2)= (A1 / (A2 * W(2) ** A3 - F12I)) ** (1./ZZ) - 273.15 !the F1 potential equations solved for T.
F22I = F2 (2)
F23I = F22I
TEMP (3)= (B1*(F23I + B2 * W(3) ** B3)) ** (1. / ZZ) - 273.15 !the F2 potential equations solved for T.
GO TO 40
30    TEMP(3)= TEMP(3) + 0.10
IF (TEMP(3) .LT. 150.) GO TO 40
CALL MESSAGES(-1,MSG1,'fatal',IUNIT,ITYPE)
GO TO 99
40    F13= F1 (3)  !calculate F1 potential for regeneration air inlet state
F23= F2 (3)  !calculate F2 potential for regeneration air inlet state
F12= F11 + ETAF1 * (F13 - F11) !modify the F1 potential (process air outlet) for effectiveness effects
F22= F21 + ETAF2 * (F23 - F21) !modify the F2 potential (process air outlet) for effectiveness effects
THE FOLLOWING LOOP GUESSES NEW HUMIDITY RATIOS UNTIL THE STEP SIZE GETS TO WITHIN A CERTAIN TOLERANCE
WOLD= 0.005 !humidity ratio initial guess value
DO I=1,25
FNW= B1*(F22 + B2*(WOLD ** B3)) + A1/(F12 - A2*(WOLD ** A3))
DFNW= B1 * B2 * B3 * (WOLD ** (B3 - 1.)) + A1 * A2 * A3 *
& (WOLD ** (A3 - 1.)) / ((F12 - A2 * (WOLD ** A3)) ** 2)
WNEW= WOLD - FNW/DFNW
IF (WNEW.LE.0.0) WNEW= WOLD * .5
IF (ABS((WNEW - WOLD) / WOLD).LT. .01) GO TO 50  !if the tolerance is met, test the current humidity ratio guess
WOLD = WNEW
ENDDO
CALL MESSAGES(-1,MSG2,'fatal',IUNIT,ITYPE)
99    RETURN 1
TEST WHETHER THE NEW HUMIDITY RATIO IS WITHIN A TOLERANCE OF THE DESIRED HUMIDITY RATIO
50     IF (ABS((WNEW - W(2)) / W(2)) .GT. 0.01) GO TO 30 !if not, guess a new regeneration temperature
THE GUESSED WNEW IS OKAY - COMPUTE THE REQUIRED REGENERATION TEMPERATURE
TEMP (2)= (A1 / (A2 * W(2) ** A3 - F12)) ** (1. / ZZ) - 273.15
TEMP (4)= (MSYS*(H(1)-H(2)-HFG*(W(1)-W(2)))+MREG*(H(3)-HFG*W(3)))/ &
(MSYS*CPV*(W(1)-W(2))+MREG*(CPA+CPV*W(3)))
W (4)=(MSYS*(W(1)-W(2))+MREG*W(3)) / (MREG) !perform energy balance to determine w (4)
TMIX=TEMP (1)     !temperature of inlet process air set to TMIX but not used
```

```
WMIX=W (1)          !humidity ratio of inlet process air set to WMIX but not used
TDEH=TEMP (2)     !temperature of outlet process air
WDEH=W (2)         !humidity ratio of outlet process air
TREG=TEMP (3)     !required temperature of inlet regeneration air
WREG=W (3)         !humidity ratio of inlet regeneration air
SET THE OUTPUTS
100   CONTINUE
OUT (1) = TDEH  !process air outlet temperature
OUT (2) = WDEH  !process air outlet humidity ratio
OUT (3) = MSYS  !process air mass flow rate
OUT (4) = TREG  !required temperature of regeneration air
OUT (5) = TEMP (4)  !regeneration air outlet temperature
OUT (6) = W (4)  !regeneration air outlet humidity ratio
OUT (7) = MREG  !regeneration air mass flow rate
RETURN TO TRNSYS KERNAL
RETURN       1
END
SUBROUTINE TYPE506 (TIME,XIN,OUT,T,DTDT,PAR,INFO,ICNTRL,*)
DESCRIPTION: THIS SUBROUTINE MODELS AN EVAPORATIVE COOLING
DEVICE FOR TRNSYS.
AIR CONDITION AND THE SATURATION EFFICIENCY AND THE MODEL
CALCULATES THE OUTLET AIR CONDITIONS.
TRNSYS DECLARATIONS
IMPLICIT NONE
DOUBLE PRECISION XIN,OUT,TIME,PAR,T,DTDT
INTEGER*4 INFO (15),NP,NI,NOUT,ND,IUNIT,ITYPE,ICNTRL
CHARACTER*3 YCHECK,OCHECK
USER DECLARATIONS
PARAMETER (NP=2,NI=8,NOUT=7,ND=0)
REQUIRED TRNSYS DIMENSIONS
DIMENSION XIN(NI),OUT(NOUT),PAR(NP),YCHECK(NI),OCHECK(NOUT),
1   T(ND),DTDT(ND)
DECLARATIONS AND DEFINITIONS FOR THE USER-VARIABLES
DOUBLE PRECISION TIME0,TFINAL,DELT
DOUBLE                                                    PRECISION
T_AIR_IN,W_AIR_IN,RH_AIR_IN,H_AIR_IN,WB_AIR_IN,
1T_AIR_OUT,W_AIR_OUT,RH_AIR_OUT,H_AIR_OUT,WB_AIR_OUT,FLOW_
AIR,
1Q_PARASITICS,POWER,P_AIR_IN,P_AIR_OUT,GAMMA,SAT_EFFICIENCY,
1   PSYDAT(9),Q_AIR,WB_DEPRESSION,DP_AIR
INTEGER MODE,PSYCHMODE,STATUS
GET GLOBAL TRNSYS SIMULATION VARIABLES
TIME0=getSimulationStartTime()
TFINAL=getSimulationStopTime()
DELT=getSimulationTimeStep()
SET THE VERSION INFORMATION FOR TRNSYS
IF(INFO(7).EQ.-2) THEN
INFO(12)=16
RETURN 1
ENDIF
```

```
DO ALL THE VERY LAST CALL OF THE SIMULATION MANIPULATIONS HERE
IF (INFO(8).EQ.-1) THEN
RETURN 1
ENDIF
PERFORM ANY "AFTER-ITERATION" MANIPULATIONS THAT ARE REQUIRED
IF(INFO(13).GT.0) THEN
RETURN 1
ENDIF
DO ALL THE VERY FIRST CALL OF THE SIMULATION MANIPULATIONS HERE
IF (INFO(7).EQ.-1) THEN
RETRIEVE THE UNIT NUMBER AND TYPE NUMBER FOR THIS COMPONENT FROM THE INFO ARRAY
IUNIT=INFO(1)
ITYPE=INFO(2)
SET SOME INFO ARRAY VARIABLES TO TELL THE TRNSYS ENGINE HOW THIS TYPE IS TO WORK
INFO(6)=NOUT
INFO(9)=1
INFO(10)=0
CALL THE TYPE CHECK SUBROUTINE TO COMPARE WHAT THIS COMPONENT REQUIRES TO WHAT IS SUPPLIED
CALL TYPECK(1,INFO,NI,NP,ND)
SET THE YCHECK AND OCHECK ARRAYS TO CONTAIN THE CORRECT VARIABLE TYPES FOR THE INPUTS AND OUTPUTS
DATA YCHECK/'TE1','DM1','PC1','MF1','PR4','PR4','CF1','DM1'/ DATA OCHECK/'TE1','DM1','PC1','MF1','PR4','PW1','PW1'/
CALL THE RCHECK SUBROUTINE TO SET THE CORRECT INPUT AND OUTPUT TYPES FOR THIS COMPONENT
CALL RCHECK(INFO,YCHECK,OCHECK)
RETURN TO THE CALLING PROGRAM
RETURN 1
ENDIF
DO ALL OF THE INITIAL TIMESTEP MANIPULATIONS HERE - THERE ARE NO ITERATIONS AT THE INTIAL TIME
IF (TIME.LT.(TIME0+DELT/2.D0)) THEN
SET THE UNIT NUMBER FOR FUTURE CALLS
IUNIT=INFO(1)
ITYPE=INFO(2)
READ IN THE VALUES OF THE PARAMETERS IN SEQUENTIAL ORDER
MODE=JFIX(PAR(1)+0.5)              !1=W, 2=RH
Q_PARASITICS=PAR(2)                !KJ/H - PARASITIC ENERGY DRAW FOR DEVICE WHEN OPERATING
CHECK THE PARAMETERS FOR PROBLEMS AND RETURN FROM THE SUBROUTINE IF AN ERROR IS FOUND
IF((MODE.LT.1).OR.(MODE.GT.2)) CALL TYPECK(-4,INFO,0,1,0)
IF(Q_PARASITICS.LT.0.) CALL TYPECK(-4,INFO,0,2,0)
```

```
PERFORM ANY REQUIRED CALCULATIONS TO SET THE INITIAL VALUES
OF THE OUTPUTS HERE
OUT (1)=XIN(1)
OUT (2)=XIN(2)
OUT (3)=XIN(3)
OUT (4)=0.
OUT (5)=XIN(5)
OUT (6:7)=0.
RETURN TO THE CALLING PROGRAM
RETURN 1
ENDIF
*** ITS AN ITERATIVE CALL TO THIS COMPONENT ***
RE-READ THE PARAMETERS IF ANOTHER UNIT OF THIS TYPE HAS BEEN
CALLED
IF(INFO(1).NE.IUNIT) THEN
RESET THE UNIT NUMBER
IUNIT=INFO (1)
ITYPE=INFO (2)
READ IN THE VALUES OF THE PARAMETERS IN SEQUENTIAL ORDER
MODE=JFIX(PAR(1)+0.5)
Q_PARASITICS=PAR(2)
ENDIF
RETRIEVE THE CURRENT VALUES OF THE INPUTS TO THIS MODEL FROM
THE XIN ARRAY IN SEQUENTIAL ORDER
T_AIR_IN=XIN  (1)                    !C
W_AIR_IN=XIN (2)                     !-
RH_AIR_IN=XIN (3)/100.               !PERCENTAGE
FLOW_AIR=XIN (4)                     !KG/H OF DRY AIR
P_AIR_IN=XIN (5)                     !PERCENTAGE
DP_AIR=XIN (6)                       !ATM
GAMMA=XIN (7)                        !ON/OFF CONTROL SIGNAL
SAT_EFFICIENCY=XIN (8)               !FRACTION
CHECK THE INPUTS FOR PROBLEMS
IF(W_AIR_IN.LT.0.) CALL TYPECK(-3,INFO,2,0,0)
IF(RH_AIR_IN.LT.0.) CALL TYPECK(-3,INFO,3,0,0)
IF(RH_AIR_IN.GT.1.) CALL TYPECK(-3,INFO,3,0,0)
IF(FLOW_AIR.LT.0.) CALL TYPECK(-3,INFO,4,0,0)
IF(P_AIR_IN.LT.0.) CALL TYPECK(-3,INFO,5,0,0)
IF(DP_AIR.LT.0.) CALL TYPECK(-3,INFO,6,0,0)
IF(DP_AIR.GE.P_AIR_IN) CALL TYPECK(-3,INFO,6,0,0)
IF(SAT_EFFICIENCY.LT.0.) CALL TYPECK(-3,INFO,8,0,0)
IF(SAT_EFFICIENCY.GT.1.) CALL TYPECK(-3,INFO,8,0,0)
IF(ErrorFound()) RETURN 1
PERFORM ALL THE CALCULATION HERE FOR THIS MODEL.
SET THE CORRECT INLET STATE
IF(MODE.EQ.1) THEN
PSYCHMODE=4
ELSE
PSYCHMODE=2
ENDIF
```

```
SET THE STATE OF THE INLET AIR STREAM
PSYDAT (1)=P_AIR_IN
PSYDAT (2)=T_AIR_IN
PSYDAT (4)=RH_AIR_IN
PSYDAT (6)=W_AIR_IN
CALL
PSYCHROMETRICS(TIME,INFO,1,PSYCHMODE,1,PSYDAT,0,STATUS,*10)
CALL LINKCK('TYPE 506','PSYCHROMETRICS',1,506)
10    IF(ErrorFound()) RETURN 1
T_AIR_IN=PSYDAT(2)
WB_AIR_IN=PSYDAT(3)
RH_AIR_IN=PSYDAT(4)
W_AIR_IN=PSYDAT(6)
H_AIR_IN=PSYDAT(7)
DEVICE IS NOT CURRENTLY OPERATING
IF((GAMMA.LT.0.5).OR.(FLOW_AIR.LE.0.)) THEN
P_AIR_OUT=P_AIR_IN-DP_AIR
H_AIR_OUT=H_AIR_IN
W_AIR_OUT=W_AIR_IN
PSYDAT(1)=P_AIR_OUT
PSYDAT(2)=T_AIR_OUT
PSYDAT(4)=RH_AIR_OUT
PSYDAT(6)=W_AIR_OUT
CALL PSYCHROMETRICS(TIME,INFO,1,7,0,PSYDAT,0,STATUS,*20)
20      IF(ErrorFound()) RETURN 1
T_AIR_OUT=PSYDAT(2)
RH_AIR_OUT=PSYDAT(4)
W_AIR_OUT=PSYDAT(6)
H_AIR_OUT=PSYDAT(7)
POWER=0.
Q_AIR=FLOW_AIR*(H_AIR_IN-H_AIR_OUT)
ELSE
CALCULATE THE CURRENT WET BULB DEPRESSION
WB_DEPRESSION=T_AIR_IN-WB_AIR_IN
CALCULATE THE NEW AIR OUTLET CONDITIONS
P_AIR_OUT=P_AIR_IN-DP_AIR
T_AIR_OUT=T_AIR_IN-SAT_EFFICIENCY*WB_DEPRESSION
WB_AIR_OUT=WB_AIR_IN
CALL THE PSYCH ROUTINE TO GET THE OUTLET AIR CONDITIONS
PSYDAT (1)=P_AIR_OUT
PSYDAT (2)=T_AIR_OUT
PSYDAT (3)=WB_AIR_OUT
CALL PSYCHROMETRICS(TIME,INFO,1,1,1,PSYDAT,1,STATUS,*30)
30      IF(ErrorFound()) RETURN 1
T_AIR_OUT=PSYDAT(2)
RH_AIR_OUT=PSYDAT(4)
W_AIR_OUT=PSYDAT(6)
H_AIR_OUT=PSYDAT(7)
CALCULATE THE HEAT TRANSFER QUANTITIES
POWER=Q_PARASITICS
```

```
Q_AIR=FLOW_AIR*(H_AIR_IN-H_AIR_OUT)
ENDIF
SET THE OUTPUTS FROM THIS MODEL IN SEQUENTIAL ORDER AND GET OUT
OUT (1)=T_AIR_OUT
OUT (2)=W_AIR_OUT
OUT (3)=RH_AIR_OUT*100.
OUT (4)=FLOW_AIR
OUT (5)=P_AIR_OUT
OUT (6)=POWER
OUT (7)=Q_AIR
RETURN 1
EVERYTHING IS DONE - RETURN FROM THIS SUBROUTINE AND MOVE ON
RETURN 1
END
SUBROUTINE TYPE45(TIME,XIN,OUT,TT,DTDT,PAR,INFO,ICNTRL,*)
THERMOSYPHON SYSTEM - THE THERMOSYPHON SYSTEM CONSISTS OF A FLAT-PLATE
COLLECTOR, A STRATIFIED STORAGE TANK (EITHER VERTICAL OR HORIZONTAL), A
THIS ROUTINE CALLS A MODIFIED VERSION OF TYPE38- STORAGE TANK AND THE PIPE SUBROUTINE.
TRNSYS acess functions (allow to acess TIME etc.)
USE TrnsysConstants
USE TrnsysFunctions
!export this subroutine for its use in external DLLs.
!DEC$ATTRIBUTES DLLEXPORT :: TYPE45
TRNSYS DECLARATIONS
IMPLICIT NONE
DOUBLE PRECISION XIN !THE ARRAY FROM WHICH THE INPUTS TO THIS TYPE WILL BE RETRIEVED
DOUBLE PRECISION OUT !THE ARRAY WHICH WILL BE USED TO STORE THE OUTPUTS FROM THIS TYPE
DOUBLE PRECISION TIME !THE CURRENT SIMULATION TIME - YOU MAY USE THIS VARIABLE BUT DO NOT SET IT!
DOUBLE PRECISION PAR !THE ARRAY FROM WHICH THE PARAMETERS FOR THIS TYPE WILL BE RETRIEVED
DOUBLE PRECISION STORED !THE STORAGE ARRAY FOR HOLDING VARIABLES FROM TIMESTEP TO TIMESTEP
DOUBLE PRECISION T !AN ARRAY CONTAINING THE RESULTS FROM THE DIFFERENTIAL EQUATION SOLVER
DOUBLE PRECISION DTDT !AN ARRAY CONTAINING THE DERIVATIVES TO BE PASSED TO THE DIFF.EQ. SOLVER
INTEGER*4 INFO(15) !THE INFO ARRAY STORES AND PASSES VALUABLE INFORMATION TO AND FROM THIS TYPE
INTEGER*4 NOMAX !VARIABLES FOR THE MAXIMUM NUMBER OUTPUTS
INTEGER*4 NP,NI,NOUT,ND !VARIABLES FOR THE MAXIMUM NUMBER OF PARAMETERS,INPUTS,OUTPUTS AND DERIVATIVES
```

```
INTEGER*4 NPAR,NIN,NDER !VARIABLES FOR THE CORRECT NUMBER OF PARAMETERS,INPUTS,OUTPUTS AND DERIVATIVES
INTEGER*4 IUNIT,ITYPE !THE UNIT NUMBER AND TYPE NUMBER FOR THIS COMPONENT
INTEGER*4 ICNTRL !AN ARRAY FOR HOLDING VALUES OF CONTROL FUNCTIONS WITH THE NEW SOLVER
INTEGER*4 NSTORED !THE NUMBER OF VARIABLES THAT WILL BE PASSED INTO AND OUT OF STORAGE
CHARACTER*3 OCHECK !AN ARRAY TO BE FILLED WITH THE CORRECT VARIABLE TYPES FOR THE OUTPUTS
CHARACTER*3 YCHECK !AN ARRAY TO BE FILLED WITH THE CORRECT VARIABLE TYPES FOR THE INPUTS
USER DECLARATIONS - SET THE MAXIMUM NUMBER OF PARAMETERS (NP), INPUTS (NI),
OUTPUTS (NOUT), AND DERIVATIVES (ND) THAT MAY BE SUPPLIED FOR THIS TYPE
PARAMETER (NP=39,NI=10,NOMAX=20,NOUT=12,ND=0,NSTORED=0)
REQUIRED TRNSYS DIMENSIONS
DIMENSION XIN(NI),OUT(NOMAX),PAR(NP),YCHECK(NI),
1   OCHECK(NOUT),STORED(NSTORED),T(ND),DTDT(ND)
INTEGER NITEMS
DOUBLE PRECISION TIN,TOUT, TCONV, SG, VI, TAUALF, THETA,
& AC, FRTAN, FRUL, GTEST, B0, SLOPE, LUDATA, NDATA, DR, DH, LH,
& H2, H5, D1, L1, NB1, U1, D2, L2, NB2, U2, HIN, CP, RHO,
& H4, FPUL, RTEST, FSKY, FGND, EFFSKY, EFFGND, TASKY, TANGND,
& LR, DX, UA1, UA2, S1, S2, GT, GH, GD, RHOG,NR,TAGND, N,TT,
& TA, QU, G, TABEAM, GDT, TABAR, FRTA, S, GLAST, GLOW,
& GHIGH, FC, FO, FNOT, HI, HC, HO, HNOT, TO, FLAST, F, FHIGH,
& PI, EP, A, B, GRAV, VIS, FLOW, HT, DF, GABS, FI,XDATA,YDATA,
& TI, CTIN, X, Y, TC, RATIO, UIN, UOUT, TBAR, U, RN, DEV, DRH,
& XKIN, XKOUT, FTOT, HTOT, IWARN,
& TIME0,
& DELT,
& TIMEF
INTEGER NUMX, ILOOP2, I, NX, IC
LOGICAL FIRST,REV
INTEGER*4 INFO7
DIMENSION TIN(6),TOUT(NOUT),NUMX(1),XDATA(1),YDATA(1)
DATA PI/3.14151927/,EP/.1/,IUNIT/0/
DATA A/1./,B/0./,GRAV/9.8/,VIS/.1/
DATA YCHECK /'IR1','IR1','IR1','DG1','DM1','TE1','TE1','MF1','TE1'
1         ,'CF1'/
DATA OCHECK /'TE1','PW1','TE1','MF1','TE1','MF1','PW1','PW1','EN1'
1         ,'PW1','PW1','TE1'/
FUNCTIONS
TCONV(T)=(T-B)/A
SG(T)=1.00026-4.05E-06*TCONV(T)**2-3.906E-05*TCONV(T)
VI(T)=VIS/(2.1482*(TCONV(T)-8.435+
.   SQRT(8078.4+(TCONV(T)-8.435)**2))-120.)
TAUALF(THETA)=1.-B0*(1./DMAX1(0.5,COS(THETA*PI/180.))-1.)
```

```
(1.-B0)*(DMAX1(60.,THETA)-60.)/30.
GET GLOBAL TRNSYS SIMULATION VARIABLES
TIME0 = getSimulationStartTime()
DELT  = getSimulationTimeStep()
TIMEF = getSimulationStopTime()
SET THE VERSION INFORMATION FOR TRNSYS
IF(INFO(7).EQ.-2) THEN
INFO(12)=16
RETURN 1
ENDIF
DO ALL THE VERY LAST CALL OF THE SIMULATION MANIPULATIONS HERE
IF (INFO(8).EQ.-1) THEN
RETURN 1
ENDIF
PERFORM ANY POST-CONVERGENCE MANIPULATIONS THAT ARE REQUIRED HERE
IF (INFO(13).GT.0) THEN
RETURN 1
ENDIF
PERFORM FIRST CALL MANIPULATIONS
IF (INFO(7).EQ.-1) THEN
!retrieve unit and type number for this component from the INFO array
IUNIT=INFO(1)
ITYPE=INFO(2)
!set some info array variables to tell the trnsys engine how this type is to work
INFO(6)  = NOUT !reserve space in the OUT array using INFO(6)
INFO(9)  = 1     !set the way in which this component is to be called
INFO(10) = 0     !set required number of spots in the single precision storage structure
!reserve space in the double precision storage structure
!call the type check subroutine to compare what this type requires with what is in the input file.
CALL TYPECK(1,INFO,NI,NP,ND)
!call the input-output check subroutine to set the correct input and output units.
CALL RCHECK(INFO,YCHECK,OCHECK)
!return to the calling program
RETURN 1
ENDIF
PERFORM INITIAL TIMESTEP MANIPULATIONS
IF (TIME.LT.(TIME0+DELT/2.d0)) THEN
!set the UNIT number for future calls
IUNIT=INFO(1)
ITYPE=INFO(2)
!read the first four parameter values - there are other parameters used directly in the
!code without first being set to local variables.
!check the parameters for problems and RETURN if any are found
AC    = PAR(1)
FRTAN  = PAR(2)
FRUL   = DMAX1(PAR(3),1.E-06)
GTEST  = PAR(4)
```

```
B0     = PAR(5)
SLOPE  = PAR(6)
LUDATA = JFIX(PAR(7)+SIGN(0.5,PAR(7))+0.1)
NDATA  = JFIX(PAR(8)+.1)
IF(LUDATA.LT.0) NR=NDATA
DR     = PAR(9)
DH     = PAR(10)
LH     = PAR(11)
NX     = JFIX(PAR(12)+0.1)
H2     = PAR(13)
H5     = PAR(14)
D1     = PAR(15)
L1     = PAR(16)
NB1    = PAR(17)
U1     = PAR(18)
D2     = PAR(19)
L2     = PAR(20)
NB2    = PAR(21)
U2     = PAR(22)
HIN    = PAR(26)
CP     = PAR(27)
RHO    = PAR(28)
!set the initial values of the stored variables
!INITIALIZE TYPE38
CALL TYPE38(TIME,TIN,TOUT,TT,DTDT,PAR,INFO,ICNTRL)
!set the outputs to appropriate initial values.
OUT(1) = PAR(33)  !Initial temperature  ->Temperature to tank
OUT(2) = 0.d0             !Useful energy from collector
OUT(3) = PAR(33)  !Initial temperature  ->Temperature to collector
OUT(4) = XIN(8)       !Load flow rate       ->Flow rate to collector
OUT(5) = PAR(33)  !Initial temperature  ->Temperature to load
OUT(6) = XIN(8)       !Flow rate to load
OUT(7:11) = 0.D0  !Energy flows
OUT(12)= PAR(33)  !Initial temperature  ->Average tank temperature
RETURN 1        !the first timestep is for initialization - exit.
ENDIF
THIS IS AN ITERATIVE CALL TO THIS COMPONENT ***
RE-READ THE PARAMETERS IF ANOTHER UNIT OF THIS TYPE HAS BEEN
CALLED SINCE THE LAST
TIME THEY WERE READ IN
IF(INFO(1).NE.IUNIT) THEN
!recall the UNIT and TYPE number
IUNIT = INFO(1)
ITYPE = INFO(2)
!read parameter values
AC     = PAR(1)
FRTAN  = PAR(2)
FRUL   = DMAX1(PAR(3),1.E-06)
GTEST  = PAR(4)
B0     = PAR(5)
```

```
SLOPE  = PAR(6)
LUDATA = JFIX(PAR(7)+SIGN(0.5,PAR(7))+0.1)
NDATA  = JFIX(PAR(8)+.1)
IF(LUDATA.LT.0) NR=NDATA
DR     = PAR(9)
DH     = PAR(10)
LH     = PAR(11)
NX     = JFIX(PAR(12)+0.1)
H2     = PAR(13)
H5     = PAR(14)
D1     = PAR(15)
L1     = PAR(16)
NB1    = PAR(17)
U1     = PAR(18)
D2     = PAR(19)
L2     = PAR(20)
NB2    = PAR(21)
U2     = PAR(22)
HIN    = PAR(26)
CP     = PAR(27)
RHO    = PAR(28)
ENDIF
GET THE VALUES OF THE INPUTS TO THIS COMPONENT
INPUTS
GT     = XIN(1)
GH     = XIN(2)
GD     = XIN(3)
THETA  = XIN(4)
RHOG   = XIN(5)
TA     = XIN(6)
TIN(3) = XIN(7)
TIN(4) = XIN(8)
TIN(5) = XIN(9)
TIN(6) = XIN(10)
PRELIMINARIES
H4     = H5+HIN
FPUL   = -GTEST*CP*DLOG(1.-FRUL/GTEST/CP)
RTEST  = GTEST*CP*(1.-EXP(-FPUL/GTEST/CP))
FSKY   = (1.+COS(SLOPE*PI/180.))/2.
FGND   = (1.-COS(SLOPE*PI/180.))/2.
EFFSKY = 59.98-0.1388*SLOPE+0.001497*SLOPE*SLOPE
EFFGND = 90.-0.5788*SLOPE+0.002693*SLOPE*SLOPE
TASKY  = TAUALF(EFFSKY)
TAGND  = TAUALF(EFFGND)
LR     = H2/SIN(SLOPE*PI/180.)
DX     = LR/REAL(NX)
UA1    = U1*PI*D1*L1
UA2    = U2*PI*D2*L2
IF(LUDATA.GE.0) GOTO 1
S1=0
```

```
S2=0
DO 6 N=1,NR
S1=S1+(NR-N+1)
6     S2=S2+(NR-N+1)**2
S1=S1/NR**2
S2=S2/NR**2
1     ILOOP2=0
IC=-1
IF(GT.GT.0.) GO TO 5
NO RADIATION
IC=0
TIN(1)=TA
TIN(2)=0.
!     CALL V15TYPE38(TIME,TIN,TOUT,TT,DTDT,PAR,INFO,ICNTRL,*44)
CALL TYPE38(TIME,TIN,TOUT,TT,DTDT,PAR,INFO,ICNTRL,*44)
CALL LINKCK('TYPE45','TYPE38',1,99)
44    CONTINUE
IF(TOUT(1).LT.TA) GO TO 5
QU=0.
G=0.
GO TO 100
 DETERMINE INCIDENCE ANGLE MODIFIER
5     TABEAM  = TAUALF(THETA)
GDT     = FSKY*GD+RHOG*FGND*GH
IF(GT .GT. 0.) THEN
TABAR                                                                    =((GT-
GDT)*TABEAM+GD*FSKY*TASKY+RHOG*GH*FGND*TAGND)/GT
ENDIF
FRTA    = FRTAN*TABAR
S       = GT*FRTA/FRUL
 INITIALIZATIONS
IF(INFO(7).EQ.-1) OUT(20)=1.
GLAST=OUT(20)
GLOW=-5000.
GHIGH=5000.
IF(GLAST.LE.0) GLAST=1.
G=GLAST
FIRST=.TRUE.
GO TO 50
10    IF(INFO(7).EQ.-1) GO TO 100
FLAST=F
FIRST=.FALSE.
G=GLAST+1.
GO TO 50
 ITERATION LOOP
20    IF(F.LT.0) GO TO 21
IF(G.GT.GHIGH)GO TO 22
FHIGH=F
GHIGH=G
GO TO 22
```

```
21    IF(G.LT.GLOW) GO TO 22
FLOW=F
GLOW=G
SECANT METHOD SOLUTION
22     IF(.NOT.REV.OR.GLOW.GE.0) GO TO 24
FLOW=HNOT-HT-FNOT
GLOW=0.
24    DF=(F-FLAST)/(G-GLAST)
GLAST=G
G=G-F/DF
FLAST=F
 APPLY REGULI FALSI IF NEXT FLOW IS OUTSIDE LIMITS
NEED LIMITS ON BOTH SIDES OF SOLUTION
IF(GHIGH.EQ.5000.OR.GLOW.EQ.-5000) GO TO 50
IF(G.GT.GHIGH .OR. G.LT.GLOW)
G=GHIGH-FHIGH/((FHIGH-FLOW)/(GHIGH-GLOW))
 THERMOSYPHON LOOP CALCULATIONS
50    IC=IC+1
FLOW DIRECTION
REV=.FALSE.
IF(G.LT.0.) REV=.TRUE.
GABS=ABS(G)
IF(GABS.GT.0. .AND. .NOT.(FIRST)) GO TO 55
NO FLOW OR FIRST ITERATION
FI=0.
FC=0
NUMX(1)=NDATA
XDATA(1)=0.
YDATA(1)=FC
IF(LUDATA.GE.0) THEN
CALL DATA(LUDATA,1,NUMX,1,XDATA,YDATA,INFO,*46)
CALL LINKCK('TYPE45','DATA  ',1,99)
ENDIF
46    CONTINUE
FC=YDATA(1)*RHO*GRAV
FO=0.
FNOT=FC
HI=SG(TA)*H5*GRAV*RHO
HC=SG(TA+S)*H2*GRAV*RHO
HO=SG(TA)*(H4-H2)*GRAV*RHO
HNOT=HC+HO-HI
IF(FIRST .AND. GABS.GT.0.) GO TO 55
TO=TA
QU=0.
GO TO 75
56    ILOOP2=1
 COLLECTOR INLET PIPE
55    TI=TOUT(1)
CALL PIPE(GABS*AC,TI,RHO,CP,UA1,D1,L1,H5,TA,FI,HI,TO,1,NB1,DH)
```

```
COLLECTOR
THERMAL HEAD AND OUTLET TEMPERATURE
CTIN=TO
TI=TO
HC=0.
DO 60 I=1,NX
X=DX*(I-1)+DX/2.
Y=DMIN1(50.,FPUL*X/LR/GABS/CP)
TC=(TI-TA-S)*EXP(-Y)+TA+S
60    HC=HC+SG(TC)*DX*H2/LR*RHO*GRAV
Y=DMIN1(50.,FPUL/GABS/CP)
RATIO=GABS*CP*(1.-EXP(-Y))/RTEST
QU=RATIO*AC*(FRTA*GT-FRUL*(TI-TA))
TO=QU/GABS/AC/CP+TI
IF(LUDATA.GE.0) GO TO 92
FRICTION HEAD
HEADERS
UIN=GABS*AC/3600./(RHO*SG(TI)*PI*DH**2/4.)
UOUT=GABS*AC/3600./(RHO*SG(TO)*PI*DH**2/4.)
FC=(S1*32.*LH/DH**2*(-UIN*VI(TI)+UOUT*VI(TO))+S2*RHO/2.*
.(UIN**2*SG(TI)+UOUT**2*SG(TO)))/2.
RISERS
TBAR=(TI+TO)/2.
U=GABS*AC/NR/3600./(RHO*SG(TBAR)*PI*DR**2/4.)
RN=U*DR*RHO*SG(TBAR)/VI(TBAR)
DEVELOPING FLOW FACTOR
DEV=1+.038/(LR/RN/DR)**.964
FC=FC+32./RN*LR*U**2*RHO*SG(TBAR)/DR*DEV
DRH=(DR/DH)**2
XKIN=(-.3259*DRH**2-.1784*DRH+.5)*DRH**2
XKOUT=.667*DRH**2-2.667*DRH+2.
FC=FC+(XKIN+XKOUT)*U**2*RHO*SG(TBAR)/2.
GO TO 93
NUMX(1) = NDATA
XDATA(1)=GABS*AC
YDATA(1)=FC
92    CALL DATA(LUDATA,1,NUMX,1,XDATA,YDATA,INFO,*48)
CALL LINKCK('TYPE45','DATA  ',1,99)
48    CONTINUE
FC=YDATA(1)*RHO*GRAV
OUTLET PIPE
93    TI=TO
CALL PIPE(GABS*AC,TI,RHO,CP,UA2,D2,L2,
H4-H2,TA,FO,HO,TO,2,NB2,DH)
 TANK
75    TIN(1)=TO
TIN(2)=DMAX1(G*AC,0.)
INFO7 = JFIX(INFO(7))
IF(INFO7.GT.-1 .AND. IC.GT.0) INFO(7)=MAX0(INFO7,IC)
!     CALL V15TYPE38(TIME,TIN,TOUT,TT,DTDT,PAR,INFO,ICNTRL,*52)
```

```
CALL TYPE38(TIME,TIN,TOUT,TT,DTDT,PAR,INFO,ICNTRL,*52)
CALL LINKCK('TYPE45','TYPE38',1,99)
52    CONTINUE
INFO(7)=INFO7
HT=TOUT(11)
TOTAL HEAD
TERMINATE ITERATION IF NETT THERMOSYPHON HEAD <2PA WHEN G=0
IF(REV .AND. (HNOT-HT).GE.(FNOT-2.)) GO TO 100
FTOT=FI+FC+FO
HTOT=HC+HO-HI-HT
F=FTOT+HTOT
IF(REV) F=HNOT-HT-FTOT
IF(FIRST) GO TO 10
IF(GLAST.LE.0.AND.ILOOP2.EQ.0) GO TO 56
ILOOP2=0
 CHECK CONVERGENCE
IF(ABS(F).GT..01*DMAX1(FTOT,ABS(HTOT),100.) .AND.
.    ABS(G-GLAST).GT.EP .AND. IC.LT.30) GO TO 20
IF(IC.EQ.30) THEN
IWARN=IWARN+1
ENDIF
1000  FORMAT(//2X,19H***** WARNING *****,/5X,4HUNIT,1X,I3,1X,
.   4HTYPE,1X,I3,/5X,19HFLOW ITERATION LOOP,
.   19H FAILED TO CONVERGE,/5X,8HAT TIME=,F10.4)
 SET OUTPUTS
OUTPUTS WERE SET IN SUBROUTINE TANK, SAVE LAST VALUE OF G
100   OUT(1)=TIN(1)
OUT(2)=0
IF(.NOT.(REV)) OUT(2)=DMAX1(QU,0.D0)
DO 125 I=3,12
125   OUT(I)=TOUT(I-2)
OUT(18)=TABAR
OUT(19)=0.
IF(OUT(2).GT.0.) OUT(19)=RATIO
OUT(20)=G
RETURN 1
END
SUBROUTINE PIPE(FLW,TI,RHO,CP,UA,D,L,H,TA,FH,TH,TO,IEND,NB,DH)
IMPLICIT NONE
DOUBLE PRECISION FLW,TI,RHO,CP,UA,D,L,H,TA,FH,TH,TO,NB,DH,
    & A,B,GRAV,VCONV,PI,T,X,Y,TBAR,R,V,DDH,K,LE,TCONV,SG,VI
INTEGER IEND
DATA A/1./,B/0./GRAV/9.8/,VCONV/360./
DATA PI/3.1415927/
LOCAL FUNCTIONS
TCONV(T)=(T-B)/A
SG(T)=1.00026-4.05E-06*TCONV(T)**2-3.906E-05*TCONV(T)
VI(T)=VCONV/(2.1482*(TCONV(T)-8.435+
.   SQRT(8078.4+(TCONV(T)-8.435)**2))-120.)
```

```
THERMAL HEAD
X=DMIN1(50.,UA/CP/FLW)
Y=EXP(-X)
TO=TA+(TI-TA)*Y
TBAR=TI
IF(X.GT.0.) TBAR=TA+(TI-TA)*(1.-Y)/X
TH=SG(TBAR)*H*GRAV*RHO
PIPE FRICTION
R=4.*FLW/D/PI/VI(TBAR)
V=4.*FLW/PI/D/D/RHO/SG(TBAR)/3600.
FH=64./R
IF(R.GT.2000.) FH=0.032
DEVELOPING FLOW CORRECTION
FH=FH*(1.+.038/(L/(D*R))**.964)
 OTHER FRICTION
DDH=(D/DH)**2
IF(IEND.EQ.2) GO TO 10
ENTRY FROM TANK TO PIPE
K=.5
ENTRY FROM PIPE TO COLLECTOR HEADER
IF(D.LT.DH) K=K+.667*DDH*DDH-2.667*DDH+2.
IF(D.GT.DH)K=K-.3259/DDH/DDH-.1784/DDH+.5
GO TO 20
EXIT FROM PIPE TO TANK
10    K=1
EXIT FROM HEADER TO RETURN PIPE TO TANK
IF(D.LT.DH)K=K+(-.3259*DDH*DDH-.1784*DDH+.5)*DDH*DDH
IF(D.GT.DH)K=K+(.667/DDH/DDH-2.667/DDH+2.)*DDH*DDH
BENDS
20    LE=L
IF(R.LE.2000)LE=L+NB*30.*D
IF(R.GT.2000)K=K+NB*1
FH=(FH*LE/D+K)*(V**2/2.*SG(TBAR)*RHO)
 RETURN
END
SUBROUTINE TYPE91 (TIME,XIN,OUT,T,DTDT,PAR,INFO,ICNTRL,*)
THIS ROUTINE SIMULATES A SENSIBLE HEAT EXCHANGER, GIVING OUTLET TEMPERATURES AND FLOWRATES OF HOT AND COLD STREAMS. THE CONSTANT HEAT EXCHANGER EFFECTIVENESS MUST BE SUPPLIED AS A PARAMETER.
!export this subroutine for its use in external DLLs.
!DEC$ATTRIBUTES DLLEXPORT :: TYPE91
USE STATEMENTS
USE TrnsysFunctions
IMPLICIT NONE !force explicit declaration of local variables
TRNSYS DECLARATIONS
DOUBLE PRECISION XIN,OUT,TIME,PAR,T,DTDT,TIME0,TFINAL,DELT
INTEGER*4 INFO(15),NP,NI,NO,ND,IUNIT,ITYPE,ICNTRL
CHARACTER*3 OCHECK,YCHECK
```